

Article

Provision of Desalinated Irrigation Water by the Desalination of Groundwater within a Saline Aquifer

David D. J. Antia

DCA Consultants Ltd., Haughend Farm, Bridge of Earn Road, Dunning, Perthshire PH2 9BX, UK; dcacl@btconnect.com; Tel.: +44-1764-684-664

Academic Editor: Harrie-Jan Hendricks Franssen

Received: 30 June 2016; Accepted: 14 December 2016; Published: 22 December 2016

Abstract: Irrigated land accounts for 70% of global water usage and 30% of global agricultural production. Forty percent of this water is derived from groundwater. Approximately 20%–30% of the groundwater sources are saline and 20%–50% of global irrigation water is salinized. Salinization reduces crop yields and the number of crop varieties which can be grown on an arable holding. Structured ZVI (zero valent iron, Fe^0 pellets desalinate water by storing the removed ions as halite (NaCl) within their porosity. This allows an “*Aquifer Treatment Zone*” to be created within an aquifer, (penetrated by a number of wells (containing ZVI pellets)). This zone is used to supply partially desalinated water directly from a saline aquifer. A modeled reconfigured aquifer producing a continuous flow (e.g., $20 \text{ m}^3/\text{day}$, $7300 \text{ m}^3/\text{a}$) of partially desalinated irrigation water is used to illustrate the impact of porosity, permeability, aquifer heterogeneity, abstraction rate, *Aquifer Treatment Zone* size, aquifer thickness, optional reinjection, leakage and flow by-pass on the product water salinity. This desalination approach has no operating costs (other than abstraction costs (and ZVI regeneration)) and may potentially be able to deliver a continuous flow of partially desalinated water (30%–80% NaCl reduction) for $\$0.05\text{--}0.5/\text{m}^3$.

Keywords: desalination; salinization; irrigation; zero valent iron (ZVI, Fe^0); aquifer

1. Introduction

Arable agriculture accounts for more than 70% of global water usage [1]. Total anthropogenic water usage is currently estimated at $10,688 \text{ km}^3 \cdot \text{a}^{-1}$ [2]. About $4000 \text{ km}^3 \cdot \text{a}^{-1}$ are abstracted from the riparian and groundwater environment [3]. Irrigation usage accounts for about 70% of this abstracted water [1,3]. Sixty-two percent of water withdrawals for irrigation [4] return to the groundwater and riparian system through a combination of evaporation (23%–30%), infiltration (7%–16%) and overland flow (26%–27%) [4,5]. Seventy-one percent of the global irrigated area is located in areas where the annual depletion of the watershed can exceed 75% [4].

About 24% of the total global harvested cropland is irrigated [6]. This irrigated cropland accounts for more than 40% of the global cereal yield [6] and more than 30% of global agricultural production [7]. Global cereal production would decrease by 20% without irrigation [3]. Global crop production will be required to more than double by 2050 in order to sustain the anticipated growth in global population [6]. The vast majority of this increase in agricultural production is expected to result from an increase in the amount of irrigated land [6] coupled with a more efficient use of irrigation [1–8].

The relative balance of irrigation water abstracted from the riparian system and irrigation water abstracted from groundwater varies regionally [8]. About 40% of global irrigation water is abstracted from shallow groundwater (aquifers) [8]. Locally, this can exceed 70% (e.g., India) [8]. Between 20% and 30% of global groundwater ($320\text{--}480 \text{ km}^3 \cdot \text{a}^{-1}$) abstracted for irrigation is saline [9].

In some countries (e.g., Uzbekistan) irrigated land may account for less than 15% of arable production, but more than 90% of the arable crop [10]. The groundwater used for irrigation (average $3.7 \text{ km}^3 \cdot \text{a}^{-1}$) has salinities within the range $2.25\text{--}3.75 \text{ g} \cdot \text{L}^{-1}$ [10].

At least 20% of the global irrigated crop land is adversely affected by salinization [11–17]. Some estimates indicate that the combination of irrigation and leaching may result in more than 50% of the global irrigated land being affected by salinization [18]. Globally, salinization is associated with between 560 and 1400 $\text{km}^3 \cdot \text{a}^{-1}$ of irrigation water [11–18]. About 405 km^2 of irrigated land is used for greenhouses [19]. The groundwater used to irrigate these greenhouses is saline in many coastal areas [19].

Salinized irrigation water reduces the associated potential crop yield by between 10% and 90% (relative to irrigation with freshwater) [16,18–25]. Salinization adversely affects the long term viability of the agricultural land. The associated saline irrigation runoff adversely affects: (i) the downstream riparian system; and (ii) the underlying aquifers receiving salinized infiltration water [1–25].

It is estimated that the value of lost agricultural production due to salinization exceeds \$27.3 billion/a [26]. The lost value associated with salinization of irrigation water also affects the broader local economy [27]. It is, therefore, reasonable to assume that any strategy, which can cost effectively help stabilize, or reverse, the adverse effects of salinization, will have a major economic impact on the local economy.

The amount of water required for irrigation, varies with crop and region [8]. It is also a function of the net amount of water received by precipitation and the associated evaporation [1–5]. Irrigated water requirements decrease as the irrigation type switches from flood, to drip, to sprinkler, and to more sophisticated irrigation technologies [8].

One possible solution, which can be used to combat salinization, is to use desalinated water for irrigation [28]. Desalinated irrigation water is currently used (on a small scale) in Spain, Israel, Kuwait, Saudi Arabia, UAE, Bahrain, Qatar, Chile, China, Australia [28,29]. The unsubsidized, full cycle cost of providing desalinated water from a modern large scale ($>100,000 \text{ m}^3 / \text{day}$) desalination plant varies with installation date and region. It is currently more than $\$3.5 / \text{m}^3$ for most ($>100,000 \text{ m}^3 / \text{day}$) plants installed within the last 5 years [16,17]. This is addressed further in Section 9.

In many areas, which use desalinated irrigation water, the delivered water price is heavily subsidized (for strategic and political reasons) and may fall within the range $\$0.2$ to $\$0.7 / \text{m}^3$ [28,29].

1.1. Impact of Irrigation Water Salinity on Crop Yield

Desalination (or partial desalination) of irrigation water, prior to use, is expected to increase the yield of a specific crop [16,18–25]. With any desalination technology used for irrigation, there are two important questions:

- (i) Is the technology likely to produce an adequate amount of water for a reasonable cost over a reasonable timeframe?
- (ii) Is the application, by irrigation, of the desalinated (or partially desalinated) water, likely to make a significant impact on the revenue and profitability of the agricultural holding?

These two questions can be considered with reference to a specific crop. In a freshwater irrigation environment, the estimated crop yield can be approximated as [30]:

$$\text{Yield (t/ha)}, Y = (a_1 b_1 c_1 / d_1)(abcde) \quad (1)$$

a_1 = plants per hectare ($10,000 \text{ m}^2$) (this is a function of the number of plants per meter length on a row and the row spacing, m); b_1 = seed pods (or grain heads or fruit) per plant; c_1 = fruit or seeds per pod/grain head; d_1 = seeds or fruit per ton; a = fractional yield change due to fertilizer application; b = fractional yield change due to fungicide application; c = fractional yield change due to pesticide application; d = fractional yield change due to herbicide application; e = fractional yield change due to

bactericide application. The fractional yield change is calculated as: (*Yield* with the application/*Yield* without the application).

Yield is strongly influenced by the planting strategy, variety, climatic variation, farming practice, fertilizers applied, local soil composition, irrigation water composition and irrigation strategy. The impact of salinity is to reduce the expected crop yield. An indicative relationship for crop yield decrement as a function of salinity is [16,20–22]:

$$\text{Salinity Adjusted Yield (t/ha), } Y_S = Y (1 - (c_{1s}(\text{Salinity, g/L}) - c_{2s})), \text{ where } 0 \leq Y_S \leq Y \quad (2)$$

c_{1s} and c_{2s} are regression defined constants (see references [16,20–22] for the value of these constants associated with more than 60 different crops). By definition, the expression ($c_{1a}(\text{Salinity, g/L}) - c_{2a}$) has the limit values of 0.0 and 1.0. Each of the variables in Equations (1) and (2) can be described by a distribution. The amount of irrigation water required, is location and crop specific, and may fall within the range 0 to 10,000 m³/ha/a [31,32].

1.2. Maximum Sustainable Desalination Cost for Saline Irrigation Water

Most irrigated crops have a low sales value (\$/ha, or \$/t) and are unable to economically sustain a high desalination cost (\$/m³) for irrigated water. The unsubsidized, delivered cost of potable quality desalinated water (from a conventional desalination plant) may fall within the range \$3 to \$100/m³ [16,17]. The incremental sales value (excluding operating, harvesting and storage costs) added by the use of desalinated water will be site specific. Historically, the high cost of providing desalinated water has prevented its widespread use for irrigation in areas, which currently use salinized irrigation water.

The maximum sustainable cost (M_c , \$/m³) of desalination for irrigation water for a specific crop, or agricultural holding, can be estimated as:

$$M_c, \$/\text{m}^3 = ((Y_{S2} - Y_{S1})R_1) - O_1 - F_1 - P_1 / W_1, \quad (3)$$

Y_{S1} = Crop yield using salinized water, t; Y_{S2} = Crop yield using partially desalinated water, t; R_1 = Sale price of crop, \$/t; O_1 = Incremental increase in operating costs and infra-structure costs associated with the increased yield, \$; F_1 = Incremental increase in financing costs associated with the increased yield, \$; P_1 = Profit required by the agricultural holding on the increased yield, \$; W_1 = amount of partially desalinated water which is required to achieve the increased yield, m³.

Irrigation using partially desalinated water is only economically viable if M_c is greater than the actual cost of supplying the partially desalinated irrigation water (A_c , \$/m³), i.e., $((M_c - A_c) > 0)$.

1.3. Zero Valent Iron

It has recently (2010) been discovered that Zero Valent Iron (Fe^0 , ZVI) could be used to partially desalinate water [16,17,33–38]. The potential, unsubsidized, delivery cost of this partially desalinated water may be less than \$0.1/m³ [16,17].

The two principal ZVI desalination approaches are:

- (a) placement of structured ZVI in pellets. The pellets are then placed in a water body and left for a period of time [16,17];
- (b) placement of structured ZVI in cartridges which are attached to a reactor incorporating fluid recycle [16,17,36].

This study investigates whether this trial technology could be transferred into the subsurface to produce an *Aquifer Treatment Zone* within a saline aquifer. The *Aquifer Treatment Zone* is created by the placement of removable ZVI desalination pellets (or cartridges), in infiltration devices (or wells) intersecting a saline aquifer. The abstracted water is used to provide partially desalinated irrigation water.

1.4. Definition and Construction of an Aquifer Treatment Zone

Trial data, from more than 300 ZVI desalination trials (0.0002 to 0.8 m³/batch) [16,17], are integrated with standard hydrological and chemical process engineering models. This integration is designed to identify the principal technical issues associated with a commercial scale-up (within an aquifer). The target proposed commercial scale *Aquifer Treatment Zone* will produce 1 to 100 m³/day of partially desalinated irrigation water.

The batch desalination trials used a diffusion process (with and without a water recycle) where structured ZVI catalysts (contained in pellets and cartridges) were placed in saline water. The associated methodology and desalination trial data have been placed in the Appendixs A–G.

This study has the following Appendices:

1. Appendix A: Trial Materials and Kinetic Methodology; Equations (A1)–(A4); Figures A1 and A2;
2. Appendix B: Kinetic Data associated ST series desalination pellets; Equation (B1); Figures B1–B3;
3. Appendix C: Equations and models which are required to provide a control data set for the aquifer and to provide effective monitoring of a proposed *Aquifer Treatment Zone* following installation; Equations (C1)–(C36b); Figures C1–C7;
4. Appendix D: Classifying the Potential Aquifer Resource;
5. Appendix E: Calculating and modeling the dimensions associated with a proposed *Aquifer Treatment Zone*. Equations (E1)–(E5); Table E1;
6. Appendix F: Concepts and Models Associated with a potential Recycle Strategy; Equations (F1)–(F3); Figures F1–F5; Table F1;
7. Appendix G: Modeling a potential Static Strategy when the Aquifer is heterogenous; Equations (G1)–(G4); Figure G1.

A list of abbreviations and symbols used in this study is placed after the Appendices.

Conversion of an aquifer to an *Aquifer Treatment Zone* requires sequential consideration of three issues: (i) the nature of the desalination product and its potential recovery from the aquifer; (ii) the front-end engineering requirements of a specific site; and (iii) an assessment of the costs associated with the installed *Aquifer Treatment Zone*.

2. Desalination Product

The different desalination catalysts used in this study (ST, MT, C to K) are described further in Section 7.3, and their performance is detailed in Appendixs B, E and F. ST, MT, D(i) are identifiers used for different Type A Catalysts. C, D(ii), E to K are identifiers used for Different Type B Catalysts. Notations such as ST3b refer to a trial using the ST catalyst, Trial Group Feed Water Salinity Grouping Identifier = 3 (e.g., 11.05 g NaCl/L), Statistical Trial identifier = b (e.g., Trial 2).

The desalination ZVI pellet trials [16] established that the NaCl was removed from the water (Figures B1–B3). The removed NaCl was held in ZVI pellets in some form. A number of pellets from the ST Trial Group [16] were allowed to dry in air (at a temperature of 0 to 20 °C) before being cut in half. The surfaces were then polished prior to examination using reflectance microscopy.

The petrography of the desalination pellets defines the desalination process. The petrography and its implications for the design of an *Aquifer Treatment Zone* are discussed in detail in Sections 3–5. Sections 4 and 5 define the adsorption-desorption mechanisms. These mechanisms are used in Appendixs A–G to demonstrate how desalination can be modeled and monitored within an aquifer.

The petrography is integrated with the front-end engineering associated with installing and operating an *Aquifer Treatment Zone* in Sections 6 and 7.

3. Desalination Product Petrography

3.1. Hygroscopic Nature of Cut Pellets

Freshly cut surfaces of the ZVI (ST Trial Group) can develop hygroscopic brine droplets on their surface (see Figure 1). Ion analyses established the presence of Na^+ and Cl^- ions in the hygroscopic and deliquescence brine droplets. NaCl is hygroscopic and has a well-defined deliquescence point (e.g., [39,40]).

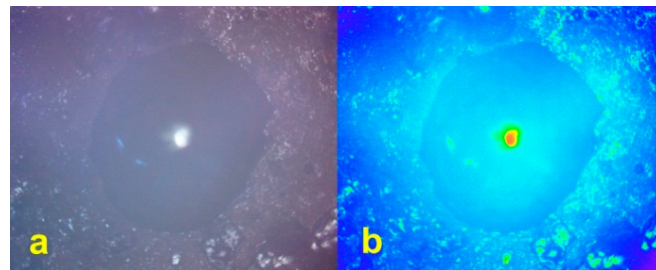


Figure 1. Trial ST3b pellet [16]. Zero valent iron, Fe^0 (ZVI) = 24.9 g/L; Feed Water: 6.52 g Cl^- /L + 4.53 g Na^+ /L; Product water = 2.06 g Cl^- /L + 1.29 g Na^+ /L; Removed: 4.46 g Cl^- /L + 3.24 g Na^+ /L; Feed Water pH = 6.32; Product Water pH = 8.26. (a) Reflected light, no filter, showing a central saline water droplet forming due to the presence of hygroscopic, deliquescent, sequestered NaCl. Photograph taken 4 days after the surface was dry cut and polished. White patches are sequestered solid NaCl infilling porosity; (b) Reflected light, no filter, converted to a grey scale before false color is applied. The false color analysis clearly shows both the water droplet and the distribution of solid sequestered NaCl (light green). Field of view = 4.5 mm.

3.2. Rough Surface of Cut Pellets Following Desalination

The freshly cut pellet surface (before polishing) is typically covered in white crystalline material (halite [41–48]), e.g., Figure 2.

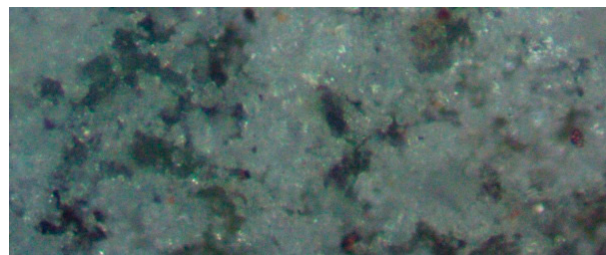


Figure 2. ST Trial Pellet (ST1a [16]) Following Desalination: Reflected Light; Halite on rough cut surface. Field of view = 0.378 mm; ZVI:water ratio = 18.31 g/L; Feed water salinity = 8.01 g/L; Product water salinity after 230 days = 2.52 g/L. NaCl removed = 5.49 g/L (0.30 g/g ZVI). Feed water pH = 6.27; Product water pH = 8.12.

3.3. Polished Surface of Cut Pellets Following Desalination

The polished ZVI surfaces established that the original porosity had been completely infilled with halite, in some pellets. e.g., Figure 3. Large open pores are infilled with halite, which has grown into the pore from the pore sides, e.g., Figure 4.

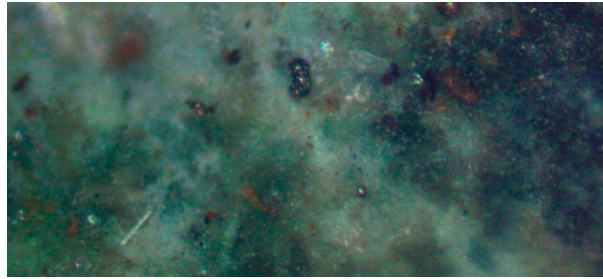


Figure 3. ST Trial Pellet (ST1b [16]) Following Desalination: Reflected Light; Halite infilling porosity on polished cut surface. Field of view = 0.49 mm; ZVI:water ratio = 23.10 g/L; Feed water salinity = 8.21 g/L; Product water salinity after 230 days = 1.99 g/L. NaCl removed = 6.22 g/L (0.27 g/g ZVI). Feed water pH = 6.25; Product water pH = 8.15.



Figure 4. ST Trial Pellet (ST1c [16]) Following Desalination: Reflected Light; Halite infilling circular pore on polished cut surface. The halite infilling the circular carrier pore shows a characteristic “*kristallbrocken*” texture [49] indicating that the pore was infilled by crystal masses growing out from the pore boundaries. The bulk of the matrix in the photomicrograph is constructed from goethite [41–48]. All the pores are infilled with halite. The blue lath shaped crystals are atacamite. Field of view = 0.52 mm; ZVI:water ratio = 25.34 g/L; Feed water salinity = 8.19 g/L; Product water salinity after 230 days = 2.28 g/L. NaCl removed = 5.91 g/L (0.23 g/g ZVI). Feed water pH = 6.21; Product water pH = 8.54.

3.4. Material Redistribution within the Pellets during Desalination

The porosity of the ZVI is physically expanded by the growth of the NaCl crystals (<1 micron) to form sheets of NaCl within the ZVI, e.g., Figure 5. The borders of the NaCl sheets show that the ZVI matrix may be replaced locally by NaCl to create $\text{FeO}_x(\text{OH})_y$ regoliths (e.g., Figures 5 and 6). The halite can contain regoliths of copper associated with the pellet shell, e.g., Figure 6. These regoliths indicate that the copper within the pellet can be affected by dissolution, during the desalination process.



Figure 5. ST Trial Pellet (ST1b [16]) Following Desalination: Reflected Light; Halite mass infilling and expanding porosity. Field of View = 0.937 mm.

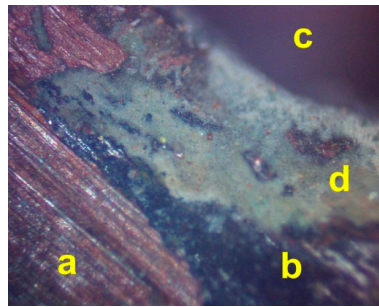


Figure 6. ST Trial Pellet (Trial ST2g [16]) Following Desalination showing halite accumulations on the side of a large pore: Reflected Light; (a) copper shell of pellet showing dissolution features; (b) authigenic ZVI product; (c) = porosity; (d) authigenic halite containing regoliths of copper and ZVI. Field of View = 0.945 mm; ZVI:water ratio = 26.72 g/L; Feed water salinity = 9.69 g/L; Product water salinity after 230 days = 2.47 g/L. NaCl removed = 7.22 g/L (0.27 g/g ZVI). Feed water pH = 6.31; Product water pH = 8.30.

3.5. Reprecipitation of Copper within the Pellets during Desalination

The copper contained within the pellet (Figure 7) can be dissolved and recrystallized as atacamite ($\text{Cu}_2(\text{OH})_3\text{Cl}$) [41] and tenorite (CuO) [41] during desalination. The Eh-pH regime (Figure 7) (and Cl^- ion regime) associated with these pellets is consistent [50–52] with both tenorite and atacamite precipitation (Figures 8 and 9).

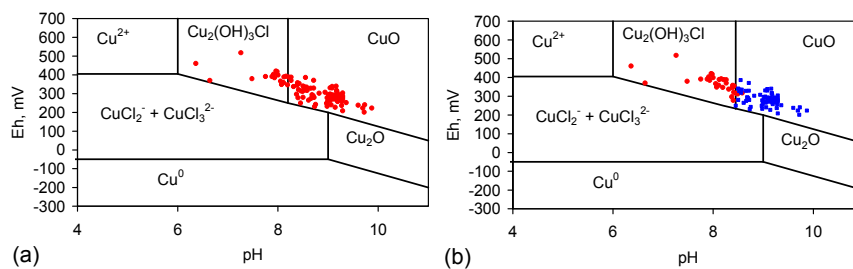


Figure 7. ST3f Trial Pellet [16]. (a) Standard Redox Stability fields for copper in the saline system Cu-O-H-Cl (at 25 °C) [51]. Data points are from Trial ST3f [16]; (b) Tenorite-Atacamite redox boundary adjusted for the inter-relationship between salinity and pH. Atacamite crystallizes when: $[\text{Log}(\text{H}^+)^2 + \text{Log}(\text{Cl}^-)]$ is greater than -18 (units are in moles; i.e., $\text{Log}([10^{-\text{pH}}]^2) + \text{Log}((0.6707(\text{Salinity, g/L})/35.45))$) [51]; ● = Atacamite precipitation favoured; ■ = tenorite precipitation favoured; ZVI:water ratio = 57.50 g/L; Feed water salinity = 9.98 g/L; Product water salinity after 165 days = 2.85 g/L. NaCl removed = 7.13 g/L (0.12 g/g ZVI). Feed water pH = 6.41; Product water pH = 9.47; Atacamite and polymorphs = ($\text{Cu}_2\text{Cl}(\text{OH})_3$); Tenorite = CuO .

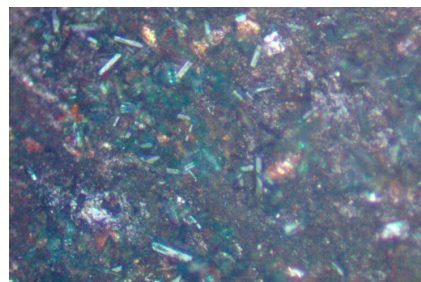


Figure 8. ST Trial Pellet (Trial ST3f [16]) Following Desalination showing atacamite and tenorite crystals: Reflected Light, with the characteristic blue-green internal reflections of atacamite ($\text{Cu}_2(\text{OH})_3\text{Cl}$) species; The golden reflectance is associated with tenorite (CuO). The bright white reflectance is associated with halite. The field of view = 0.43 mm.

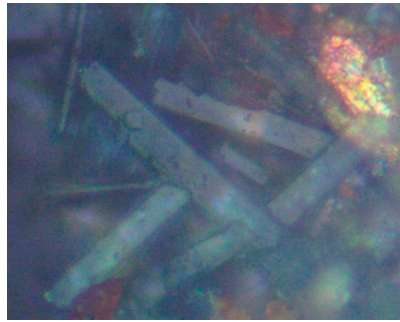


Figure 9. ST Trial Pellet (Trial ST3f [16]) Following Desalination showing a nest of atacamite crystals with the characteristic blue-green internal reflections of $\text{Cu}_2(\text{OH})_3\text{Cl}$ species. The strongly pleochroic golden grain is tenorite (CuO). Thickness = 2 microns; width = 14 microns; length = 25–110 microns. Reflected Light; Field of view = 0.133 mm.

3.6. Method of Halite Infill of Porosity within the Pellets during Desalination

The halite fills the pre-existing pores within the ZVI pellets using crystal masses which grow into the pore from the pore edge (Figures 10 and 11).

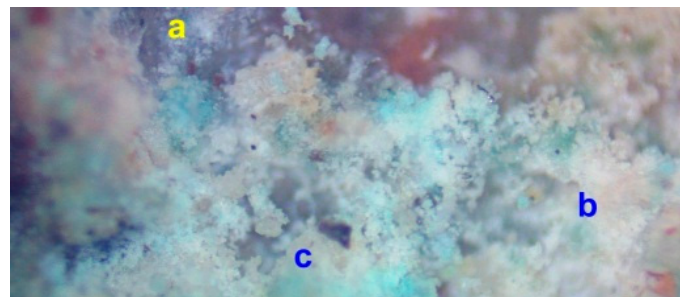


Figure 10. (ST3c Trial [16]) Pore within the ZVI product which is partially filled with NaCl (halite) crystals (blue-white). Reflected light. Field of view = 0.465 mm. a = ZVI (principally FeOOH species, i.e., goethite [43–47]). b = halite (NaCl) [41]; c = incompletely filled pore where the halite crystallites are growing into the pore from the pore edges. ZVI:water ratio = 30.12 g/L; Feed water salinity = 10.06 g/L; Product water salinity after 230 days = 2.82 g/L. NaCl removed = 7.24 g/L (0.234 g/g ZVI). Feed water pH = 6.31; Product water pH = 8.44.

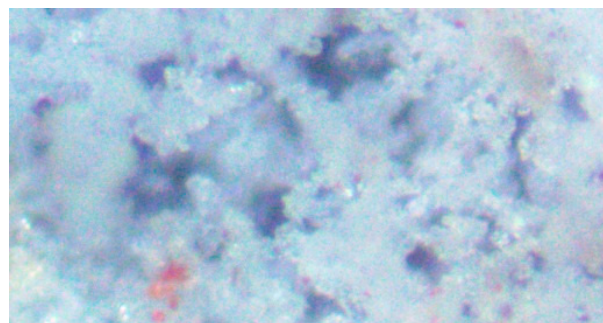


Figure 11. (ST2a Trial [16]) ZVI Product. Halite crystals partially infilling a pore and increasing pore tortuosity. The red-brown mineral is molysite (FeCl_3). Molysite occurs naturally in halite assemblages, e.g., [53]. Reflected light. Field of view = 0.099 mm; ZVI:water ratio = 28.53 g/L; Feed water salinity = 9.61 g/L; Product water salinity after 230 days = 2.62 g/L. NaCl removed = 6.99 g/L (0.25 g/g ZVI). Feed water pH = 6.31; Product water pH = 8.40.

3.7. Morphology of Halite Infill of Porosity within the Pellets during Desalination

The halite can be present as rounded nodules contained within purple ferrate (Na_2FeO_x , $\text{Na}_z\text{FeO}_x(\text{OH})_y$) nodules (and within goethite) (Figure 12). These ferrate nodules can form regoliths (or authigenic nodules) within the halite, or can form as authigenic nodules within the $\text{FeO}_x(\text{OH})_y$ matrix (Figure 12).

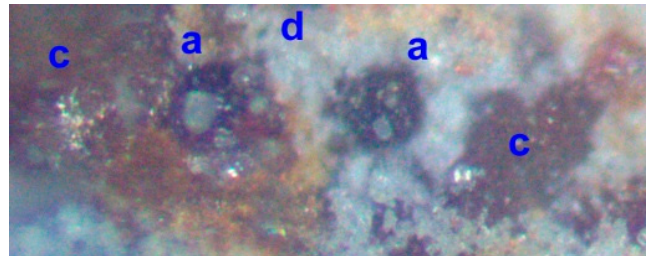


Figure 12. (ST2a Trial [16]) ZVI Product. (a) = ferrate ($\text{Na}_z\text{FeO}_x(\text{OH})_y$) nodule containing rounded halite nodules. (c) = goethite; (d) = halite crystals (white) infilling porosity. Field of view = 0.133 mm. Reflected light.

3.8. Morphology of Halite Infill of Porosity

The NaCl which is concentrated in the pore waters within the ZVI pellets during desalination will go through a number of phases [54]:



Where L = liquid phase, and α = solid (crystallized) phase. The pore water chemistry during desalination is complex and the relative ratio, or status, of these three potential phases may be influenced by temperature, pressure, ion concentrations, pH and Eh. A simple model of the form expressed by Equation (4) will result in halite formation from a mixture of L + α . Halite will form as either nodular halite (e.g., Figure 12) or by the crystalline infill of porosity by halite.

The iron (or copper) phase can be designated a β phase. In this instance, the following pore-water transitions are possible [54]:



$L_{(t=1)}$ = pore water composition at time, $t=1$; $L_{(t=2)}$ = pore water composition at time, $t=2$. The final product structure will therefore comprise: $\alpha + (\beta + \alpha)$. The α mineral will appear as grains of α mineral (e.g., authigenic halite). The β mineral will appear as grains of β mineral (e.g., authigenic $\text{FeO}_x(\text{OH})_y(\text{H}_2\text{O})_z$). This allows both phases to precipitate within the pellets as authigenic minerals during desalination.

Alternatively, when the original α mineral is a Fe species, the $(\beta + \alpha)$ phases can co-precipitate, or the β phase (halite) can precipitate after the α phase. This creates a characteristic “polygonal” mineral distribution of halite surrounding authigenic $\text{FeO}_x(\text{OH})_y(\text{H}_2\text{O})_z\text{Na}_d\text{Cl}_e$ species (Figure 13). In this instance the β phase forms a characteristic film around the α grains (Figure 13).

This brief analysis has established that the chemistry within the ZVI pellets during desalination is complex and involves dissolution and reprecipitation of Na^+ , Cl^- , and Fe^{n+} species.

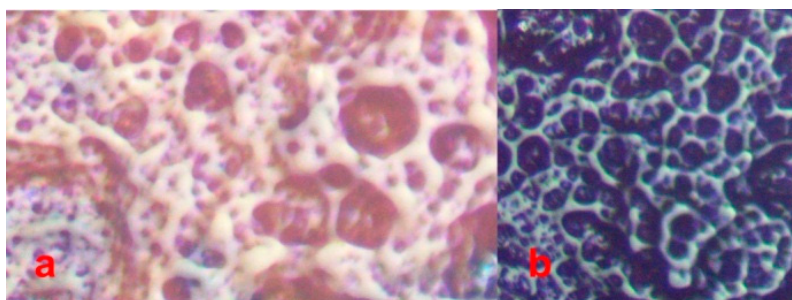


Figure 13. (ST3a Trial [16]) ZVI Product. Examples of halite crystals infilling a pore network around precipitated FeOOH grains. (a) Halite saturated (goethite + Fe(OH)₃) surrounded by halite infilling a network of pores. The Fe(OH)₃ may be derived from hydrolyzed molysite (FeCl₃) [41]. Field of view = 0.142 mm; (b) goethite/ferrate grains surrounded by halite, infilling a network of pores. Field of view = 0.090 mm. Reflected light.

3.9. Ironstone Precipitation

The ZVI pellets can develop localized “oolitic” ironstone concretions (Figure 14). These concretions are characterized by a wustite rim [41,44–47] and contain cuboid authigenic Fe⁰ crystals [41,44–47].

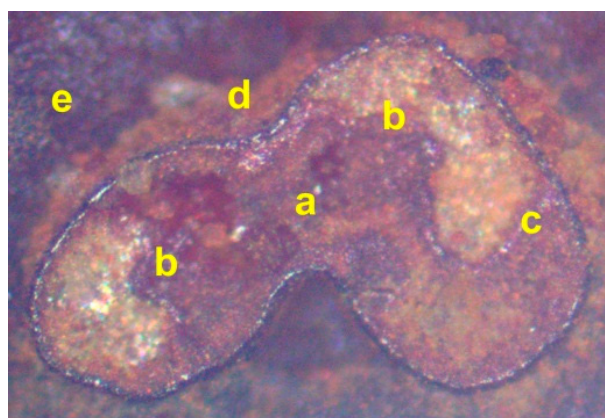


Figure 14. Trial ST1e [16] ZVI desalination pellet following desalination. (a) = authigenic oolitic goethite nodule; (b,c) = adsorbed oolitic goethite nodules containing authigenic cuboid Fe⁰ crystallites (1 to 5 microns in diameter) crystallizing within the goethite. The Fe⁰ crystallites vary in color from white to blue to yellow to pink (depending on orientation), are cuboid, isotropic, and have a reflectance of about 60%. Sub-nodule (c) includes a rim of (FeO (wustite) with exsolved Fe⁰ crystals) separating it from the main goethite (FeO(OH)) mass of the nodule; (d) = iron rich boundary of the nodule (FeO (wustite) with exsolved Fe⁰ crystals) and the associated active outer growth fringe (light brown) of the oolitic nodule. (e) = goethite matrix (dark). Reflected light. Field of view = 0.173 mm; ZVI:water ratio = 21.72 g/L; Feed water salinity = 8.22 g/L; Product water salinity after 230 days = 2.24 g/L. NaCl removed = 5.98 g/L (0.28 g/g ZVI). Feed water pH = 6.24; Product water pH = 8.42.

4. Chemical Implications of the Petrography for Aquifer Desalination

4.1. Dubinin-Astakhov Catalytic Model for ZVI Desalination

The intra-particle porosity of the FeO_x(OH)_y(H₂O)^{b+/-} particles within the ZVI pellets act as the catalytic site [17]. The particles adsorb Na⁺ and Cl⁻ ions from the water, and then desorb the ions as a [Na⁺Cl⁻] ion adduct (Figures 1–6 and 10–13) within the inter-particle porosity (Figure 15).

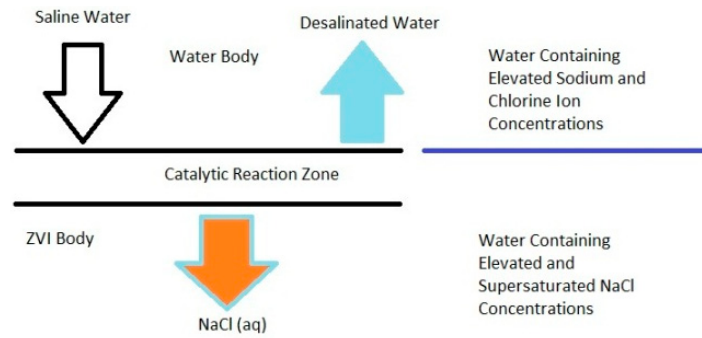


Figure 15. Catalytic NaCl sequestration model. Source: [17].

This type of adsorption-desorption cycle is adopted by the Dubinin-Radushkevich model [55]. This model assumes that the adsorbed species is desorbed to fill the associated nano/meso/macro-dead-end porosity. Under this model [55]:

$$\ln(q_e) = \ln(q_s) - k_{ad}\varepsilon^2, \quad (8)$$

$$q_e = (q_s) \exp(-k_{ad}\varepsilon^2), \quad (9)$$

q_e = ion removed at equilibrium/unit ZVI (g/g); q_s = theoretical isotherm saturation capacity, g/g; k_{ad} = Dubinin-Radushkevich isotherm constant ($M^2 \cdot kJ^{-2}$); ε = Dubinin-Radushkevich isotherm constant, g. While q_e is measured, the other variables are unknown.

Adsorption-desorption associated with goethite ($FeO_x(OH)_y(H_2O)_z$) [56,57], akaganeite ($FeO_x(OH)_y(H_2O)_zCl_n$) [58] and ferrate ($FeO_x(OH)_y(H_2O)_zNa_nK_m$) [59] have been explained elsewhere using a Dubinin-Radushkevich adsorption model or a multilayer film model [55–60].

4.2. Significance of Porosity within the ZVI

The volumetric Dubinin-Radushkevich adsorption model is [60,61]:

$$V_x = V_o \cdot \exp[-(RT/\beta_1 E_o \cdot \ln(P_s/P_a))^2], \quad (10)$$

V_x = volume (NaCl) adsorbed by the ZVI and desorbed into the dead-end porosity (V_o) at time $t = n$, and at a relative pressure of (P_a/P_s) and temperature, T ; P_s = initial pressure; P_a = adsorption pressure; V_o = the initial inter-particle nano-meso-macro dead-end pore volume; E_o = characteristic energy of adsorption of a standard adsorbate [61]; β_1 = the affinity coefficient of the adsorbate; $E_1 = \beta_1 E_o$ [61]; E_1 = characteristic energy for a specific fluid-solid system; R = the gas constant.

This model is rewritten as the Dubinin-Astakhov equation where [60]:

$$V_x = V_o \cdot \exp[-(RT/\beta_1 E_o \cdot \ln(P_s/P_a))^m], \quad (11)$$

m = a factor which is related to pore size distribution and morphology. It follows that [60,61]:

$$V_x/V_o = \exp[-(RT \cdot \ln(P_a/P_s)/E)^{2(\text{or } m)}], \quad (12)$$

Desalination ceases when $V_x/V_o = 1$. The porosity destruction rate constant associated with (V_x/V_o) is different to the desalination rate constant, k_r (Appendix A, Equations (A1)–(A4)), associated with ($C_{t=n}/C_{t=0}$), though both are related.

Equation (12) demonstrates that:

- the desorption of Na^+ and Cl^- ions into dead-end porosity will result in their sequestration (Figures 1–6); $V_o > 0\%$ at $t = 0$;

- (b) Placement of desorbed Na^+ and Cl^- ions into pores (V_{op}) which are in direct communication with the main water body will result in the desorbed Na^+ and Cl^- ions returning to the main water body. $V_{op} > 0\%$ at $t = 0$;
- (c) The inter-particle porosity $= \varphi = V_o + V_{op}$, and $V_o = a \cdot \varphi$; $V_{op} = b \cdot \varphi$, where $a + b = 1$. Once $V_x/V_o = 1$, $\{a\} = 0$, the residual porosity is V_{op} , i.e., $\{b\} = 1$. An irreducible water salinity level, B_S , occurs when $\{a\}$ reduces to 0.

4.3. Significance of Fluid Pore Pressure within the ZVI Pellet

The fluid pore pressure within the pore, P_p , is different to the bulk (aquifer) pressure, P_s , and can be estimated as [61]:

$$P_p(d_p) = P_s \cdot (\exp(-E_p(d_p)/RT)), \quad (13)$$

E_p = average potential energy for the molecules being adsorbed (KJ/mole) [61] = $23.761d_p^{-0.8782}$; d_p = pore width, nm, i.e., the pressure drop between the bulk pressure and the pore pressure (within the ZVI pellet) controls the desalination rate.

It follows that [60,61]:

$$V_x/V_o = \exp[-(RT \cdot \ln(P_s/P_p)/E)^2], \quad (14)$$

These Equations (8)–(14) imply:

1. Na^+ and Cl^- ion removal rates will increase with increased pressure differentials between the pressures in the pores and the wider aquifer;
2. Na^+ and Cl^- removal can have different rate constants [17];
3. Smaller pores will be filled preferentially relative to larger pores.

5. Catalytic Implications of the Petrography

Desalination Model

The detailed catalytic desalination mechanism is unknown. It is believed [17] to involve a cycle of oxidation from Fe^{0-II} to Fe^{III} (and possibly Fe^{IV} to VIII) followed by reduction to Fe^{0-II} (Figure 16).

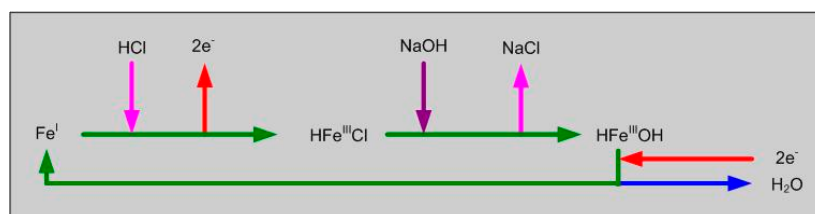


Figure 16. Catalytic ZVI desalination model [17]. The number of electrons transferred is a function of the oxidation number of the reduced state and the oxidized state. The potential range is from Fe^0 to Fe^{VIII} . $\text{CO}_2 + \text{H}_2\text{O} + \text{Cl}^- = \text{HCO}_3^- + \text{HCl}$ [16,17]; $0.5\text{O}_2 + 2\text{Na}^+ + \text{H}_2\text{O} + 2e^- = 2\text{NaOH}$ [16,17]. $\text{NaOH} = \text{NaO}^- + \text{H}^+$ [16,17]. Fe^{III} can reduce to Fe^0 . Fe^{III} can reduce to Fe^{II} . Fe can oxidize to Fe^{IV} to VIII . HCl can be replaced with $\text{H}_x\text{Cl}_y\text{O}_z$ [16]. Fe^0 and Fe^{I} formation is demonstrated in Figure 14. $\text{HFe}^{\text{II}}\text{Cl}$ and $\text{HFe}^{\text{III}}\text{Cl}$ formation is demonstrated in Figures 11 and 13; Fe^{IV} to VIII formation is demonstrated in Figures 12 and 13; $\text{HFe}^{\text{III}}\text{OH}$ formation (and associated species) is demonstrated in Figures 1, 3–6, 8, 10, 12 and 14. NaCl formation is demonstrated in Figures 1–6, 8 and 10–13.

6. Commercial Implications of the Petrography for Aquifer Desalination

The petrographic analyses demonstrate that the removed Na^+ and Cl^- ions are extracted from the water and are stored as NaCl(s) within the ZVI pellets. These observations indicate that pellets with a large internal structural porosity are able to remove more Na^+ and Cl^- ions. They will have a higher rate constant, k_r , than similar pellets with a lower structural porosity. This is demonstrated in Figure B1.

Commercial scale up of the trial data, combined with a transfer of the reaction environment from a surface based reactor to a sub-surface aquifer, requires a conceptual and front end hydrological engineering and design analysis (FEHED) for each proposed location. This analysis is undertaken prior to the investment decision being made. The commercial investment decision will be controlled by the parameters defined in Equations (1)–(3). The purpose of the FEHED is to establish that the partially desalinated water product can be delivered for a cost ($\$/\text{m}^3$) of less than M_c Equation (3).

7. Hydrological and Chemical Engineering Requirements for Commercialization

7.1. Conceptual and Front-End Hydrological Engineering and Design (FEHED)

The primary data requirements for the FEHED process are provided in Table 1. This process requires the kinetic parameters for desalination to be both known and modeled (Appendix A and B).

Table 1. Example set of primary data required to reconstruct an *Aquifer Treatment Zone*.

Item	Data Category	Data Subcategory	Example
1	Agricultural Holding Data		
	1a	Holding Dimensions and Area	25 ha
	1b	Legal rights to modify water composition in an aquifer	
	1c	Irrigation Requirement	$20 \text{ m}^3 \cdot \text{day}^{-1}$
	1d	Aquifer Thickness	1 m
2	Target Irrigation Water Salinity		
	2a	Aquifer Salinity	$4 \text{ g} \cdot \text{L}^{-1}$
	2b	Required Irrigation Water Salinity	$2 \text{ g} \cdot \text{L}^{-1}$
	2c	Crop yield with irrigation using saline aquifer water	$1 \text{ t} \cdot \text{ha}^{-1}$
	2d	Crop yield with irrigation with partially desalinated water	$5 \text{ t} \cdot \text{ha}^{-1}$
3	Agricultural Economics Data		
	3a	Crop yield decrement as a function of salinity	[16,18–25]
	3b	Crop market value	$\$300/\text{t}$
4	Experimental Desalination Data		
	4a	Rate constants	Equations (A1)–(A4) and (B1); Figures B1–B3; Table E1
	4b	Relationship between residence time, t_d , in the reaction environment and desalination	Equations (A1)–(A4) and (B1); Figure B3
	4c	Rate of Salinity Decline as a function of t_d	Catalyst ST: (Figure B3)
	4d	Statistical variation of desalination around the mean at the 99% confidence limits	Catalyst ST: 59.1% to 65.8% Catalyst K: 31.7% to 47.0%
	4e	Statistical desalination at the 1st and 3rd quartiles, e.g., Catalyst ST: 54.4% to 70.8%; Catalyst D: 24.8% to 65.8%; Catalyst E: 58.9% to 92.1%; Catalyst K: 33.2% to 45.5%	
	4f	Statistical variation of Na^+ Removal around the mean at the 99% confidence limits	Catalyst ST: 59.1% to 65.8% Catalyst K: 39.1% to 62.8%

The first stage in the process is an assessment of the available catalyst data in order to establish the amount of catalyst required and the *Aquifer Treatment Zone* size required by each catalyst. This stage is addressed in Section 7.2.

The second stage in the FEHED process is the selection of the preferred catalyst. This stage is addressed in Section 7.3.

The third stage in the FEHED process is the creation of a control desalination data set (e.g., Figures B1–B3; Tables E1 and F1), a kinetic model (e.g., Equations (A1)–(A4)) and a control hydrological model. Section 7.4 and Appendix C detail the equations and models that can be used to create the control hydrological model.

The fourth stage in the FEHED process is analysis of the different development strategies which could be used to create the *Aquifer Treatment Zone*. In this study two catalyst dependent strategies are considered (in Sections 7.5 and 7.6): (i) a Static Strategy; (ii) a Recycle Strategy. Each strategy integrates the hydrological and chemical models (Appendix A–C) to define the design and operating parameters for the proposed *Aquifer Treatment Zone*. These models are summarized in Appendix E–G.

The base data set, which is used to illustrate the various hydrological and chemical models in Appendix A–G, is derived from the desalination trials using the ST catalyst (e.g., Figures 1–6 and 8–14; Figure A1; Figures B1–B3).

These trials have demonstrated that if ZVI catalyst pellets are placed in a body of water, they will desalinate the water (Figures B1–B3). The two sided statistical 99% confidence limits for the mean desalination after 200 days are:

- (a) 15 mm diameter Cu⁰ cased pellets (without operational optimization) = 59.1% to 65.8%, $n = 50$;
- (b) 75 mm diameter MDPI cased pellets (without operational optimization) = 58.2% to 83.4%, $n = 15$. i.e., 99% confidence limits (BS2846) are: mean \pm (Standard Deviation) ($t_{0.995}/(n)^{0.5}$), where n = number of samples; $t_{0.995}$ is the value (for n) of the students t test distribution (at the 99% confidence limits).

Similar data sets can be obtained for alternative catalysts (e.g., Tables 1, E1 and F1; Figure B1). This study assumes that the pellets (or cartridges) are placed in removable containers at a number of loci within the aquifer (e.g., in infiltration devices, wells, or boreholes [62–65]). Removal of the pellets from the aquifer, will allow the NaCl to be periodically removed from the water body.

Once the agricultural land owner has decided that the desalination project may be economically viable (e.g., Equations (1)–(3)), the FEHED process sequentially steps the project through three phases (Appendix D):

1. prospective resource;
2. contingent resource;
3. developed resource.

7.2. Scale Up of Trial Desalination Kinetic Data to Provide an Assessment of the Amount of ZVI Required and the Size of the Aquifer Treatment Zone

The trial data associated with a specific catalyst (Item 4, Table 1) forms the primary database for the conversion of a saline aquifer to a proposed *Aquifer Treatment Zone*. The initial stages in this process are [66–74]:

1. Conversion of the salinities (C) at $t = 0$ and $t = n$ for batch trials to:
 - a. Rate constants, k_r (Equations (A1) to (A4); Figures B1–B3);
 - b. Required residence times, t_d , for the water within the reaction environment (Equations (A1) to (A4); Figures B1–B3).
2. Up scaling the ZVI quantities used in the trials:
 - a. The petrography demonstrates (Figures 1–6 and 8–13) that increasing the amount of ZVI will effectively increase the available ZVI voidage (porosity) available for the sequestered NaCl;
 - b. The trial data demonstrates that the amount of NaCl removed per unit time is independent of the concentration of ZVI, g/L, P_w (Figure 17a,b);
 - c. These trial observations indicate that:
 - i. Each 1 g of ZVI will be expected to remove at least 0.35 g NaCl before it needs to be removed from the reaction environment and is replaced (Figure 17a–c).
 - ii. Scale up by the placement of 10 t ZVI in a saline aquifer would result in the removal of up to 3.5 t NaCl from the aquifer, before the replacement of the ZVI is required (Figure 17a–c). This experimental scale up allows:
 1. the anticipated volume of water which can be desalinated by a single ZVI charge to be defined (Figure 17d)
 2. the anticipated replacement frequency of the ZVI to be defined (Figure 17e).

3. Assessing from the trial data set, the size of the *Aquifer Treatment Zone* which is required to deliver the target volume of irrigation water:
- In a commercial development the ZVI will be placed in a number of loci (wells) which intersect the aquifer. The number of loci required is defined by the ZVI concentration data used in the trials (e.g., Figure 17a,b).
 - The required residence time, t_d , to achieve the required irrigation water salinity is defined by the trials kinetic data (e.g., Equations (A1) to (A4); Figures B1–B3). The residence time is combined with the irrigation water volume required (Table 1) to define the minimum volume of water, and the minimum gross rock volume, contained within a proposed *Aquifer Treatment Zone*, V_{aq} (Equations (E1)–(E3) and (E5)).
 - This minimum water volume is then integrated with the known aquifer properties in order to identify an aerial extent for the proposed *Aquifer Treatment Zone* Equation (E4).

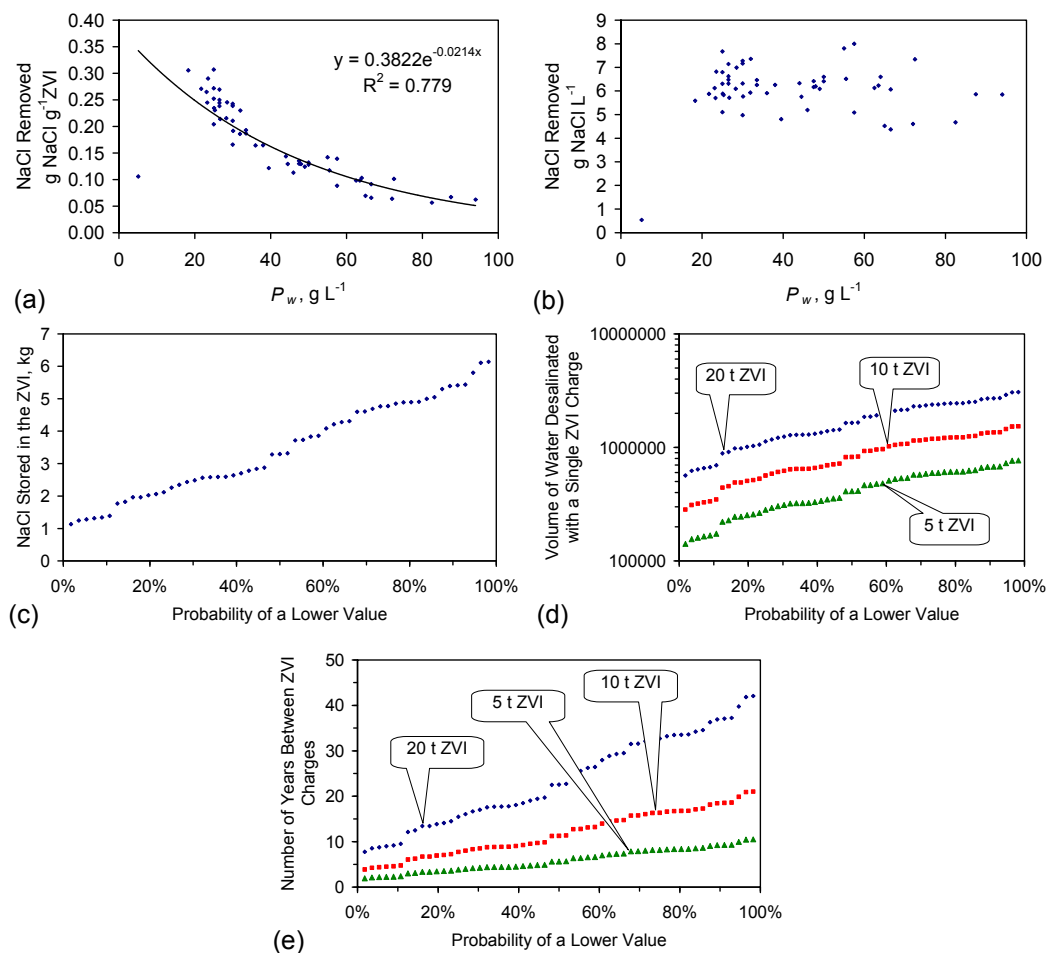


Figure 17. ST Desalination Pellets. Data Trial Duration: 230 days; $n = 55$; Data Source: [16]. (a) Relationship between NaCl removed (g·g⁻¹ ZVI) and P_w , g NaCl·g⁻¹ ZVI: Data [16]; (b) Relationship between the total amount of NaCl removed, g·L⁻¹, and P_w , g NaCl·g⁻¹ ZVI: Data [16]; (c) Implied relationship between probability and the amount of NaCl (kg) that can be sequestered in 20 kg of pellets. Mean = 3.45 kg; Standard Deviation = 1.44 kg; 1st Quartile = 2.30 kg; Median = 3.29 kg; 3rd Quartile = 4.77 kg; (d) Volume of water than can be treated by a single ZVI charge before the ZVI needs to be recharged as a function of the amount of ZVI placed in a 4000 m³ treatment zone where the aquifer salinity is 4 g/L and the irrigation water product salinity is 2 g/L; (e) Number of years between ZVI charges (or ZVI regeneration interval) vs. probability.

7.3. Selection of Catalyst for the Proposed Aquifer Treatment Zone

The trials [16,17] have established that Fe^0 (Figure A1) can be used to create two types of structured ZVI desalination catalyst. They are:

1. *A Type A Catalyst:* This catalyst type (catalysts ST and MT) has a rigid porosity (Figure A2) and will, when placed in saline water, gradually remove NaCl from the water over a period of time (e.g., 100–1500 days). It has a low k_r (Figures B1–B3) and a low B_S . The irreducible (or equilibrium) salinity, B_S , increases with decreasing catalyst porosity (Equations (8)–(14)). Fe^0 powders, with no effective porosity, do not desalinate water (Figure B1) [36]. The statistical 1st and 3rd desalination quartiles for $t_d = 200$ days, for the three Type A catalysts considered in this study are: (i) ST catalyst (Figure A2; Figures B1–B3), 15 mm diameter pellet: 54.4% to 70.8%; $n = 50$; (ii) ST catalyst (Figure B3b), 75 mm diameter pellet: 63.2% to 76.8%; $n = 13$; (iii) MT catalyst (Figure B1), 20–25 mm diameter pellet: 6.1% to 13.7%; $n = 24$. The amount of NaCl that can be removed is controlled by the porosity (Equations (8)–(14)) and the amount of catalyst placed in the reaction environment (Figure 17). The Type A catalyst will require a residence time in the aquifer of 100–500 days before the maximum (design) equilibrium desalination is achieved (e.g., Figures F1–F3).
2. *A Type B Catalyst:* This catalyst type (catalysts C to K) has an expandable, or poro-elastic, porosity (e.g., Tables E1 and F1). The catalyst will, when placed in saline water, in a reaction environment incorporating water recycle, result in a relatively rapid removal of NaCl from water (e.g., 3 to 50 h). It has a high k_r (Tables E1 and F1) and a relatively high B_S (e.g., 20%–80% (e.g., Table 1, item 4e)). It can preferentially remove Na^+ or Cl^- ions. Once an initial B_S is achieved, or the water recycle ceases, desalination continues to progress at a substantially slower rate (e.g., Figures B1–B3). The Type B catalyst will require a residence time in the aquifer of 1–30 days before the maximum (design) equilibrium desalination (e.g., F4, F5).

Two subsurface ZVI desalination strategies have been identified. They are:

1. *A Static Strategy:* where the ZVI catalyst is placed in the aquifer and no water is recycled to the aquifer;
2. *A Recycle Strategy:* where some of the product water is recycled back to the aquifer.

A Type A catalyst is designed for use in the “Static Strategy”. *A Type B catalyst* is designed for use in the “Recycle Strategy”. The choice of catalyst controls the development strategy and costs associated with a proposed *Aquifer Treatment Zone*.

The desalination strategy used in a proposed *Aquifer Treatment Zone* can be switched from one approach to the other, during its operating life.

7.4. Control Hydrological Data and Models Required for the Proposed Aquifer Treatment Zone

Conversion of an aquifer to an *Aquifer Treatment Zone* requires the installation of one or more abstraction wells [75], and the installation of a number of loci (wells) containing the ZVI catalyst. Observation loci (wells) may be placed outside the proposed *Aquifer Treatment Zone* and a number of reinjection/infiltration loci (wells) may be placed within the proposed *Aquifer Treatment Zone*.

Each of these loci provides a spatial data point which provides information about: (i) the aquifer geology (thickness, porosity, permeability, mineralogy); (ii) aquifer hydrology and chemistry (piezometric level, water chemistry (pH, Eh, EC, ion concentrations, salinity)).

Three sets of hydrological control data are required prior to placement of the ZVI in the aquifer. They are: (i) aquifer prior to abstraction; (ii) aquifer during a prolonged abstraction test; (iii) aquifer following a prolonged abstraction test.

This information is used during the FEHED to build a hydrological, hydrochemical and geological model of the aquifer and its expected performance during operation.

Periodic monitoring of these loci following installation of a proposed *Aquifer Treatment Zone* will allow: (i) the performance of the aquifer to be monitored; (ii) any changes in performance to be identified. This will allow an appropriate remedial program to be instigated to mitigate against adverse changes in the aquifer.

The primary hydrological aquifer parameters, which are used to provide the control database, build the hydrological aquifer model, and monitor operation are documented in Table 2.

Table 2. Hydrological measurements and modeling required in order to: (i) convert an aquifer into a proposed *Aquifer Treatment Zone (ATZ)*; and (ii) monitor the performance of an installed *Aquifer Treatment Zone*. Further details are provided in Appendix C and G.

Item	Hydrological Parameter	Measured or Modelled Item	Equations and Figures
1	Control Data Set (Aquifer)		
	1a	Permeability	Equations (G1)–(G4), Figure G1
	1b	Porosity	Equations (G1)–(G4), Figure G1
	1c	Thickness	Equations (G1)–(G4), Figure G1
	1d	Piezometric Surface	Equations (C1) to (C4)
2	Control Models		
	2a	Isopache (thickness) Model	Equations (G1)–(G4), Figure G1
	2b	Iso-permeability Model	Equations (G1)–(G4), Figure G1
	2c	Iso-potential Model	Equations (C2) and (C3)
	2d	Flow Rate Model	Equations (C1)–(C4)
3	Control Abstraction Test		
	3a	Piezometric Surface	Equations (C1)–(C4)
	3b	Iso-potential Model	Equations (C2) and (C3)
	3c	Flow Rate Model	Equations (C1)–(C4)
	3d	Drawdown Model	Equation C5
	3e	Drawdown Permeability Model	Equations (C6) and (C10)–(C12)
	3f	Radius of Influence of the Abstraction Well	Equation (C7)
	3g	ATZ volume as a function of the abstraction rate	Equation (C8)
	3h	Flow rate and flow direction at each loci	Equation (C9)
	3i	Design Parameters for the <i>Aquifer Treatment Zone</i>	Equations (C1)–(C9), Figure C3
4	Operational Monitoring		
	4a	Iso-potential, flow rate, and drawdown measurements and modelling	Equations (C1)–(C12)
	4b	Permeability Reductions associated with ZVI	Equation (C13), Figure C4
	4c	Halocline monitoring	Figure C5
5	Diffusion Modelling		
	5a	Impact of fluid velocity changes	Equations (C14)–(C21), Figure C6
6	Space Velocity Modelling		
	6a	Impact on the desalination rate	Equations (C22)–(C26)
	6b	Impact of water residence time in the ATZ	Equation C27
7	Modifications to Aquifer Properties during Prolonged Abstraction		
	7a	Redox parameters	Figure C7
	7b	Permeability reduction due to gas occlusion or mineralization	Equations (C28)–(C30)
	7c	Permeability reductions and redox modifications associated with biofilms	Equations (C31)–(C36)

7.5. Construction of the Proposed *Aquifer Treatment Zone* Using the *Static Strategy*

A proposed *Aquifer Treatment Zone* constructed using the *Static Strategy* will have the following characteristics:

- a radial pattern of ZVI loci;
- a single abstraction well located within the “*Aquifer Treatment Zone*” ;
- an excess of ZVI is placed in each ZVI loci to increase the life expectancy of each ZVI charge. The life expectancy of a ZVI charge could be designed to exceed 20 years (Figure 17);
- a simple process flow diagram (Figure 18);
- a simple construction (Figure 19).

This type of approach:

- (a) is suitable for most agricultural holdings;
- (b) can be installed using basic, simple, low cost, and widely available equipment and tools. Many of these tools may already be available on the agricultural holding, as the required augers are commonly used to install fence posts; and
- (c) requires no operating energy during its life (apart from power for the abstraction pump).

A side effect of this approach is that any water flowing through the *Aquifer Treatment Zone* (Figure 19) will be treated by the ZVI. ZVI treatment will remove a variety of cations and anions (e.g., nitrates and organic pollutants) from the water [16,66,68].

Costs Associated with the Static Strategy

The principal costs are the installation of the ZVI loci, ZVI, observation loci, abstraction loci, abstraction well/pump, distribution tank or impoundment, and associated pipe work.

This strategy will require the ZVI pellet charge to be installed with a view to removal and replacement every x years (e.g., Figure C3h).

The ZVI catalyst life expectancy and *Aquifer Treatment Zone* life expectancy has not been demonstrated in a commercial environment. The unsubsidized amortized cost (capex + opex) of the partially desalinated irrigation water, when this technology is eventually commercialized, may fall within the range $\$0.05/\text{m}^3$ – $\$0.5/\text{m}^3$.

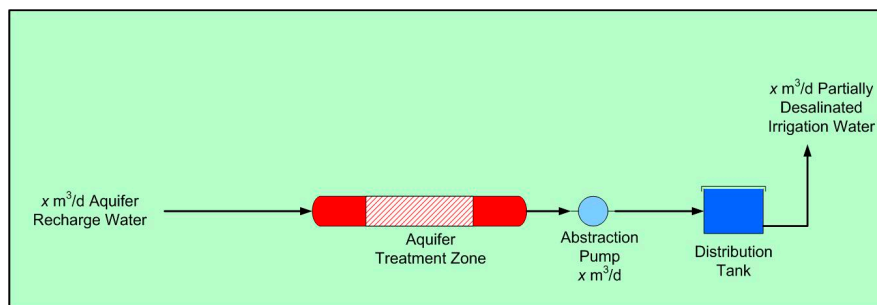


Figure 18. Process flow diagram for a schematic aquifer, which has been reconstructed as a *Static Aquifer Treatment Zone*.

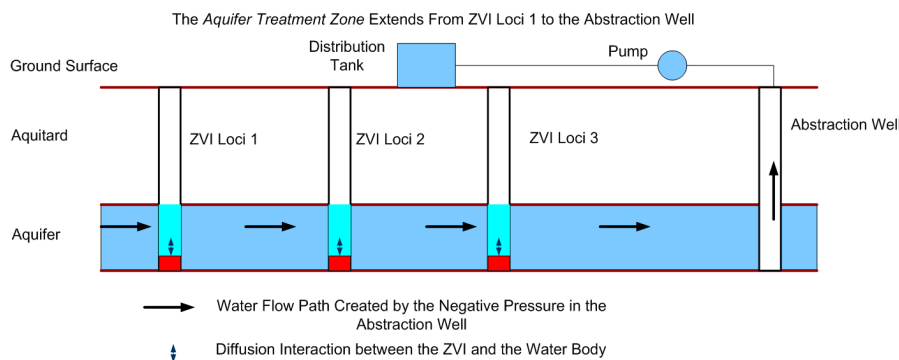


Figure 19. Cross section through a schematic *Aquifer Treatment Zone*. The zone containing the ZVI pellets/cartridges is colored red.

7.6. Construction of the Proposed *Aquifer Treatment Zone* Using the *Recycle Strategy*

The operation of a Type A desalination catalyst (e.g., ST catalyst) can be described and modeled using Equations (8)–(14), (A1)–(A4). The primary control on k_r and B_S (for a specific t_d , P_w , P_i and

a_s) is V_o . Modeling demonstrates (Appendix F) that the introduction of a recycle loop in the process flow (Figure 20), can, depending on the location of the reinjection loci, result in the equilibrium B_S increasing or decreasing (Figures F1–F3; Equations (F1)–(F3)).

The Type B desalination catalyst removes V_o as a constraint, by allowing V_o to expand with time.

7.6.1. Poro-Elastic vs. Rigid V_o

A specific catalyst formulation (catalyst D) was used to construct both a Type A catalyst (Catalyst D(i) with a rigid V_o and a Type B catalyst (Catalyst D(ii) with a poro-elastic V_o .

The two catalysts were trialed in a 240 L recycle reactor (Figure 20) with a P_w of 0.5 g/L with a t_d of 10 to 24 h (at a temperature of between 5 and 20 °C). The 99% confidence limits on the mean desalination were:

- (i) catalyst D(i) = 8.4% to 13.7%, $n = 31$;
- (ii) catalyst D(ii) = 9.9% to 65.0%, $n = 18$.

Both catalysts continued to desalinate over the next 100–700 days using the rate constants demonstrated in Figure B1 (when $(y + n) = 0$ (Figure 20)). This trial established that a higher k_r and lower B_S is achieved (over a 24 h period) by constructing the catalyst with a poro-elastic V_o .

7.6.2. Recycle Strategy

In a recycle environment, in the presence of a Type B catalyst, a higher k_r occurs when $(y + n) \geq 0$ (Figure 20; Tables E1 and F1), i.e., k_r has a partial dependency with V (Figure F4). Further desalination ceases when a new equilibrium for $(V - D)$ is achieved (Equations (C14)–(C21)). This equilibrium controls B_S and the salinity of the product water. The trial results in Tables E1 and F1 demonstrate that the equilibrium position for $(V - D)$ can be associated with a rapid desalination of 40%–75%.

These trial observations demonstrate (Tables E1 and F1) that it may be possible to construct an *Aquifer Treatment Zone* by incorporating a recycle loop in the process flow (Figure 20). The trial results (Tables E1 and F1) indicate that this will allow, by comparison with the Static Strategy, the amount of partially desalinated irrigation water produced from a specific *Aquifer Treatment Zone* volume, to be substantially increased (Table F1).

The *Recycle Strategy* construction (Figure 20) requires that the volume of water abstracted from the *Aquifer Treatment Zone* is greater than the amount of water required for irrigation (Figure 20). The excess water is then reinjected into the *Aquifer Treatment Zone*.

The *Recycle Strategy* has infiltration loci (for water recycle) and a network of distribution pipes to the infiltration loci (Figure 21). The trial results (Tables E1 and F1) indicate that P_i for a *Recycle Strategy* is lower than P_i for a *Static Strategy* (Figure 17). This reduces the number of ZVI loci required, and the amount of ZVI required, to achieve a specific irrigation water abstraction rate.

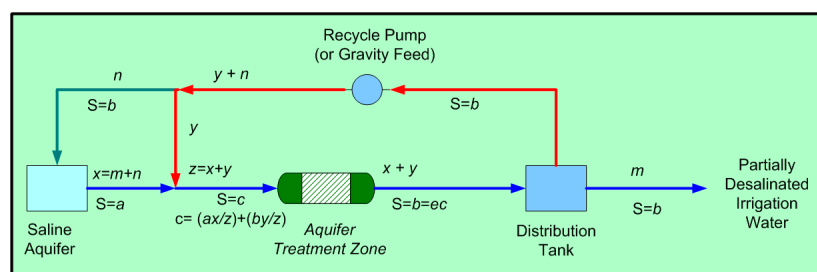


Figure 20. Process flow diagram for a schematic aquifer, which has been reconfigured as an *Aquifer Treatment Zone* with recycle (*Recycle Strategy*). S = salinity.

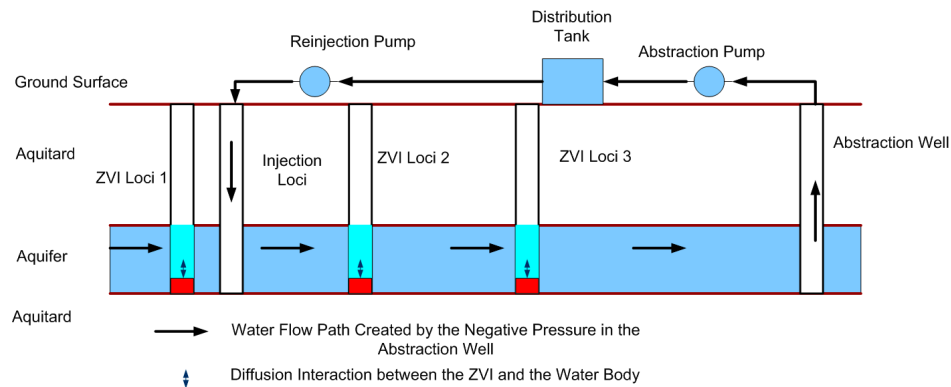


Figure 21. Cross section through a schematic *Aquifer Treatment Zone* incorporating recycle. The zone containing the ZVI pellets/cartridges is colored red.

The principal additional operating cost of the *Recycle Strategy* (relative to the *Static Strategy*) is the increased operating cost of the abstraction well (Figure 20). For a specific target irrigation water abstraction rate, the *Recycle Strategy*, will have a smaller *Aquifer Treatment Zone*, and will require less ZVI (Table F1).

The amount of water abstracted for recycle is a function of the catalyst selected. The examples in Tables E1 and F1 demonstrate that $(y + n)/m$ (Figure 20) is between 0.45:1 and 7.45:1. i.e., the recycle water volume is between 9 and 149 m³/day for an *Aquifer Treatment Zone* producing 20 m³/day of partially desalinated irrigation water.

In most locations, the air-water contact in the distribution tank will be above the air-water contact in the aquifer (Figure 22). In these circumstances, a recycle pump is unlikely to be required. The recycle water distribution can be effected using buried pipe work, gravity drainage and infiltration (Figure 22). This strategy removes a requirement for a recycle pump and external power source.

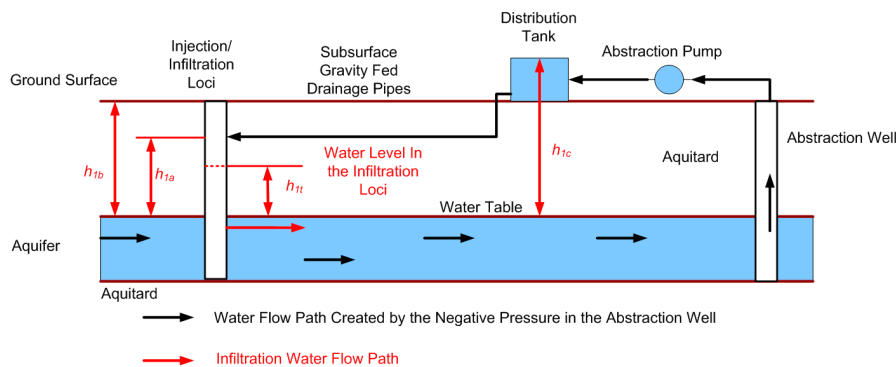


Figure 22. Cross section of a schematic *Aquifer Treatment Zone* showing gravity feed water recycle. The maximum head is controlled by the water level in the distribution tank, h_{1c} . The subsurface pipe enters the infiltration device at a height, h_{1a} , above the water table. The water level can rise in the infiltration device to the ground surface (height h_{1b}). If the water level rises above height h_{1b} , the infiltration device will act as a point source for overland flow. The infiltration rate is controlled by the surface area of the infiltration device within the aquifer, the permeability of the surface of the infiltration device, the head, h_{1t} , created by the presence of recycle water in the infiltration device, and the negative pressure (or iso-potential gradient) created by the abstraction well.

8. Commercial Scale-Up Risk

Scaling-up the ZVI desalination trials, using a *recycle strategy*, to a 20 m³/day commercial *Aquifer Treatment Zone* involves a throughput scale-up of between 6 and 3000 (Figure C5, Tables E1 and F1). A larger scale-up factor is required for the *static strategy* (Figure B1). The commercial

risks associated with the scale-up of trial data relate to cost and performance. These commercial risks can increase as the magnitude of the scale-up increases. A commercial scale-up from trial data of between 6 and 3000 is at the lower end of conventional practice [76–80].

Standard chemical process engineering industrial practice is to use the results from small scale trials as a basis for an investment decision, e.g., [76–80]. It is not unusual for the direct commercial, throughput, scale-up (from bench/pilot trials to commercial plants) associated with petrochemical (and chemical) processes to be in the order of 500,000 to 100,000,000.

The scale-up associated with the commercialization of post-1980s ZVI water treatment processes includes:

1. Permeable Reactive Barriers (PRB's) inserted in aquifers, e.g., [81,82]: Small scale (batch and continuous flow) trials containing 0.001 to 5 kg Fe⁰ were scaled-up to >300 PRB's containing 2 to 1000 t Fe⁰ each;
2. Industrial Waste Water Treatment Plant, Shanghai: processing 60,000 m³/day [83,84]. A number of 2 h duration pre-development batch flow trials (containing 0.5 kg Fe⁰) were undertaken [83]. They were succeeded by a single continuous flow pre-development trial (containing 40 kg Fe⁰) at a rate of 120 L/d [83]. This pilot trial was operated for 6 months prior to commercialization [83]. The throughput scale-up factor was 500,000. The scale-up factor in the amount of Fe⁰ used was 22,950.

9. Comparative Desalination Cost Structure

Large (>100,000 m³·day⁻¹) plants (Multi-stage flash distillation (MSFD), reverse osmosis (RO)), which are integrated with a thermal fuel power station have the lowest current desalination water costs (\$/m³). The cost of the desalination process is subsidized by the electricity sales associated with the power station. The cost structures associated with large (>90,000 m³·day⁻¹) integrated conventional desalination systems are summarized in Table 3.

An *Aquifer Treatment Zone* producing 90,000 m³/day will require access to a large aquifer. The normalized trial data (associated with different catalysts (Table F1)) indicates that the required target volume of water within the *Aquifer Treatment Zone* may be: (i) between 12,000 m³ and 170,000 m³ (RC1–RC3, RC5–RC9, Table F1; mean = 73,309 m³; 99% upper confidence limit = 169,108 m³), or (ii) <2,000,000 m³ (RC4, Table F1).

The standard chemical engineering cost scale up equation is [85,86]:

$$C_e = C_k \cdot (P_{lc}/P_{pc})^a, \quad (15)$$

C_e = Expected cost, \$ (excluding site costs); C_k = Known cost of the constructed unit; P_{lc} = Larger Plant throughput, m³ day⁻¹; P_{pc} = Constructed unit throughput, m³ day⁻¹; a = an exponent scale up factor (range = 0.3–1.2 [86]). It is commonly taken as 0.6, range 0.4–0.8 [85,86]. The constructed unit has a known cost and throughput capacity.

Table 3 includes an example target set of costs for a large 90,000 m³·day⁻¹ ZVI in situ desalination aquifer complex. This provides an indication of how economies of scale Equation (15) may impact on the delivered cost of the partially desalinated irrigation water.

Conventional desalination delivers a water product with >97% of the Na⁺ ions removed. By way of contrast, ZVI desalination is only expected to remove between 20% and 70% of the Na⁺ ions (commercial target zone is 35%–60% Na⁺ removal).

Table 3. Comparison of integrated power station-desalination unit complexes. MSFD = Multi-stage flash distillation + power station; RO = Reverse Osmosis + power station; ZVID = ZVI desalination + power station; ZVI = ZVI desalination without the power station; Assumed Target Capital Investment for the schematic ZVI desalination *Aquifer Treatment Zone* is \$300 MM, (calculated using Equation (15)), when {a} = 1.0. MM = million; \$ = US dollars. MSFD, RO, and Power Station Costs and Structures are from Reference [87]. Power Station characteristics [87]: 24.2 MPa Steam Pressure; 6 KPa Condenser Pressure; 25.2 MJ·kg⁻¹ Coal HLV; 92% boiler efficiency; 96.5%–98% turbine efficiency; 10,000 m³·h⁻¹ water supply to the power station. Fuel Costs based on 2014 fossil fuel commodity prices. The power station costs used in the Target ZVID cases are also taken from Reference [87]. Different cost components may have different values of the scale-up constant {a}. The scaled target ZVI examples indicate the water delivery cost range which may be achievable. Power requirements associated with water abstraction and recycle are site and catalyst specific. They are therefore not shown for the ZVID and Scaled Target ZVI cases.

	Actual MSFD	Actual RO	Target ZVID	Scaled Target ZVI				
Power Plant Capacity, MWh	291.0	291.0	291.0					
Power Usage, MWh	9.8	31.1	0.0					
Net Power Available for Sale, MWh	281.2	259.9	291.0					
Net Power Sales Value, \$ MM/a, at \$70/MWh	172.4	159.4	178.4					
Pressure, MPa		7.0	0.0					
ZVI Desalination scale up constant {a}			1.0	1.0	0.95	0.9	0.8	0.7
Sea Water Feed, m ³ /day	390,921.6	296,712.0	90,196.8	90,196.8	90,196.8	90,196.8	90,196.8	90,196.8
Product Water, m ³ /day	149,803.2	90,196.8	90,196.8	90,196.8	90,196.8	90,196.8	90,196.8	90,196.8
Reject Brine, m ³ /day	241,118.4	206,515.2	0.0	0.0	0.0	0.0	0.0	0.0
Capital Investment, \$ MM/a	35.2	44.7	29.6	6.8	3.8	2.4	0.8	0.2
Pre-Treatment and Pressurisation Cost, \$ MM/a		17.0						
Labour Cost, \$ MM/a	8.8	6.7	2.0	2.0	1.1	0.7	0.2	0.1
Membrane Replacement Cost, \$ MM/a		11.8						
Chemical Treatment Cost, \$ MM/a	5.3							
ZVI Replacement Cost, \$ MM/a			10.0	10.0	5.7	3.5	1.1	0.4
Spares Cost, \$ MM/a	7.2							
Power Station Fuel Cost, \$ MM/a	203.2	143.3	120.0	0.0	0.0	0.0	0.0	0.0
Operations and Maintenance Cost, \$ MM/a	18.8	24.9	21.0	2.0	1.1	0.7	0.2	0.1
Net Cost, \$ MM/a	106.1	89.0	4.1	20.8	11.7	7.3	2.3	0.7
Net Cost, \$/m ³	1.94	2.70	0.13	0.63	0.36	0.22	0.07	0.02

10. Conclusions

This study has investigated whether ZVI desalination pellets and cartridges could potentially be used to desalinate a body of water within an aquifer. Two different aquifer reconstruction strategies have been identified and modeled, a *static strategy* and a *recycle strategy*.

10.1. The Static Strategy

This requires a relatively long residence time within the aquifer (e.g., 100–300 days). The expected pre-tax cost of this strategy is in the order of \$0.05–\$0.5/m³, where the bulk of the cost (excluding the costs associated with abstraction) is a capital cost. The principal operating cost is the abstraction pump.

10.2. The Recycle Strategy

This requires a relatively short residence time within the aquifer (e.g., 0.3–3 days). The delivered water cost may be less than \$0.1/m³. This strategy will have a requirement for reinjection/infiltration. It has a higher pumped abstraction rate from the aquifer than the *static strategy*. The recycle strategy allows active management of the aquifer to be undertaken to control the salinity of the abstracted irrigation water.

10.3. Dual Use Strategy

An aquifer, which is initially developed using a *Static Strategy*, can be subsequently converted to allow operation using a *Recycle Strategy*, and vice-versa.

ZVI regeneration and replacement intervals are a function of catalyst and design. The replacement interval could potentially be once every 1 to 20 years.

10.4. Next Stage

The next stage will be controlled field testing in an aquifer stepping up through a range of volumes and throughput (e.g., 1 to 100 m³·day⁻¹) sizes. This testing program will be designed to establish, and mitigate, the issues associated with scale-up, prior to commercialization.

A successful commercial scale test program will allow commercial saline aquifer reconstructions (targeting 1–1000 m³·day⁻¹ of partially desalinated product water) to be undertaken.

Acknowledgments: This study was funded by DCA Consultants Ltd.

Author Contributions: The author undertook the research in this paper and wrote the paper.

Conflicts of Interest: The author declares no conflict of interest. The author undertook the design of the study; the data collection, analyses, and interpretation of data; and wrote the manuscript, and took the decision to publish the results.

Appendix A. Trial Materials and Kinetic Methodology

A1. ZVI

An earlier study [16] documented desalination associated copper sheathed structured ZVI pellets. This study uses the rate constant data from these trials [16] as a database.

The Fe powders have a natural loose packing density which results in the formation of tortuous macropores with narrow pore throats (Figure A1). This natural porosity is expanded during the pellet manufacturing process [16,17] into a rigid framework (Figure A2).

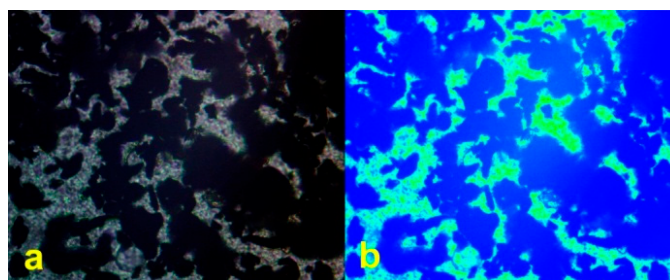


Figure A1. Typical clumped packing structure of Fe^0 grains and associated porosity in a Fe^0 column. Transmitted light. Macro pores occupy 22% of the visible porosity. Field of view = 0.93 mm. (a) Transmitted light. Fe^0 = black, porosity = grey; (b) Pseudo-color analysis. Fe^0 = Blue. Porosity = green.

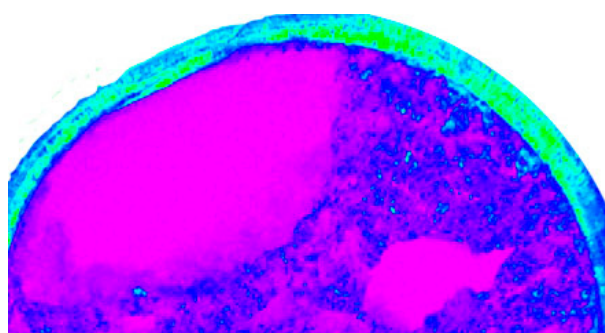


Figure A2. Pseudo-color analysis of a 15 mm diameter copper sheathed ZVI desalination pellet (Used in Trial ST1c [16]). Porosity = purple; Residual Fe^0 = green; $\text{Fe}_x\text{O}_y\text{H}_z$ = blue; Cu^0 sheath = cyan; Structural Porosity = 76%. ZVI: water ratio = 25.38 g/L; Feed water salinity = 8.19 g/L; Product water salinity after 230 days = 1.48 g/L. NaCl removed = 6.71 g/L (0.26 g/g ZVI). Feed Water pH = 6.21; Product water pH = 8.54. Pore classification: Macropores (>50 nm), the pore size distribution is multimodal with a mixture of largely interconnected, high surface area, sinusoidal, bulbous pores characterized by one or more narrow pore throats. The characteristics of fluid flow in this type of pore network are described in references [62–65,88,89].

A2. Microscopy

A ME580TWP-PZ-2L-14MP dual light (reflected and transmitted light), trinocular, polarizing, metallurgical microscope (($\times 40$ to $\times 2000$) incorporating a 14 MP digital camera (14 MP Aptina color CMOS model MU1400-204)) was used in this study to examine the pellets, before and after usage. The microscope and camera were branded by Amscope Inc., Irvine, CA, USA and supplied by United Scope (Ning Bo) Co Ltd. Zhejiang, China. The microscope is a BH200M Series unit manufactured by Ningbo Sunny Instruments Co. Ltd., Zhejiang, China. The camera was linked to an Amscope x64, 3.7.6701 (version date: 31/12/2015) digital microscope software package (branded by Amscope, Irvine, CA, USA). This software package was used to analyze the microscope slides and resin blocks. Calibration slides were used to scale the digital microscope image:

- (i) divisions at 0.15 mm, 0.1 mm, 0.07 and 0.01 mm supplied by No. 1 Microscope Wholesale Store, Henan, China, and
- (ii) divisions at 0.01 mm supplied by United Scope (Ning Bo) Co Ltd. Zhejiang, China.

The microscope provided natural light, plane polarized light and circular polarized light. It had a plane polarizing analyzer. The microscope was able to operate in a polarized light mode under both transmitted light and reflected light to aid mineral identification.

A3. Saline Water Construction

The saline water was constructed by dissolving either NaCl (Trials using Catalysts ST, MT, C and E (Figures B1–B3, Tables E1 and F1)) or Zechstein halite (Trials using Catalysts D, F–K (Tables E1 and F1) in natural spring water. The natural spring water was extracted from a private water supply in Dunning, Ochil Hills, Perthshire, Scotland [16,17,36–38,67]. The water was reservoided in a fractured Devonian, Old Red Sandstone volcanic series aquifer (fractured andesites, fractured dacites, fractured pyroclastics) [16,17].

A typical ion composition of the natural spring water is [16,17]: Anions: Cl = 11.67 mg·L⁻¹; N(NO₃) = 11.28 mg·L⁻¹; S(SO₄) = 4.16 mg·L⁻¹; P(PO₄) ≤ 0.10 mg·L⁻¹; F = 0.024 mg/L; N(NO₂) = 0.04 mg·L⁻¹; HCO₃⁻/CO₃²⁻ ≤ 10 mg·L⁻¹; Cations: K = 1.69 mg·L⁻¹; Ca = 32.91 mg·L⁻¹; Na = 6.32 mg·L⁻¹; Al ≤ 150.0 µg·L⁻¹; Fe ≤ 30.0 µg·L⁻¹; Mn = 1.70 µg·L⁻¹; P ≤ 0.005 mg·L⁻¹; S = 4.31 mg·L⁻¹; B = 29.40 µg·L⁻¹; Ba = 135.60 µg·L⁻¹; Cd = <0.2 µg·L⁻¹; Co ≤ 0.2 µg·L⁻¹; Cr ≤ 0.2 µg·L⁻¹; Cu = 77.7 µg·L⁻¹; Ni = <3 µg·L⁻¹; Pb ≤ 10 µg·L⁻¹; Si = 5.21 mg·L⁻¹; Sr = 144.9 µg·L⁻¹; Zn = 37.4 µg·L⁻¹; As ≤ 5 µg·L⁻¹; Mo = <20 µg·L⁻¹; Se ≤ 20 µg·L⁻¹; Sn ≤ 20 µg·L⁻¹; Sb ≤ 10 µg·L⁻¹. This water analysis is reproduced from References [16,17].

A4. Water Analyses

Four parameters were routinely monitored for each sample. They were:

- (i) ORP (oxidation reduction potential);
- (ii) pH;
- (iii) electrical conductivity (EC);
- (iv) temperature.

A4.1. pH

The pH meter used was manufactured, or branded, by Hanna Instruments Ltd., Leighton Buzzard, Bedfordshire, UK. It was calibrated at pH = 4, 7, 10 using calibration fluids manufactured or branded by Hanna Instruments Ltd., Leighton Buzzard, Bedfordshire, UK, and Milwaukee Instruments Inc., Rocky Mount, NC, USA.

A4.2. Eh

The ORP (oxidation reduction potential) meter used was manufactured, or branded, by Hanna Instruments Ltd., Leighton Buzzard, Bedfordshire, UK. The ORP measurements were converted to Eh values using a quinhydrone calibration [16,17,90]. The quinhydrone calibration (to the standard hydrogen electrode), was undertaken at pH = 4, and 7 (i.e., Eh, mV = -65.667 pH + 744.67 + ORP (mV) [17]).

A4.3. EC (Electrical Conductivity)

The EC meters used were manufactured, or branded, by Hanna Instruments Ltd., Leighton Buzzard, Bedfordshire, UK. The meters were calibrated at 0.7, 1.4, 2.0, 12.88 mS·cm⁻¹. In the feed water the EC increases with increasing water salinity. The measured regression correlation between EC and water salinity (constructed from NaCl) is: Salinity (g/L) = 0.5401EC (mS·cm⁻¹) - 0.1 (at 4–6 °C) [16]. The correlation between EC and water salinity (constructed from Zechsten halite) varies with the halite composition. An example correlation (R² = 0.8581, n = 25) is: Salinity (g/L) = 0.7328EC (mS·cm⁻¹) - 0.1287 (at 4–6 °C).

A4.4. Na⁺ and Cl⁻ Ion Concentrations

Bante 931 precision ion meters (manufactured by Bante Instrument Ltd., Shanghai, China), with Na⁺ and Cl⁻ ion selective electrodes, were used to analyze the Na⁺ and Cl⁻ ion concentrations. The ion meters were calibrated using 0.001, 0.01, 0.1 and 1.0 molar Na⁺ and Cl⁻ solutions.

A4.5. Temperature

Temperature was measured using meters manufactured, or branded, by Hanna Instruments Ltd., Leighton Buzzard, Bedfordshire, UK.

A5. Reactor

Two diffusion reactor types (0.3–840 L capacity) have been used (Static Diffusion and Diffusion reactors incorporating recycle) to obtain the desalination data [16,17].

A6. Pellets and Cartridges

This study defines a pellet as a cylinder with one or more impermeable side(s) and two or more permeable ends. A cartridge is defined as a cylinder with one or more impermeable sides, one or more impermeable ends and one permeable end. A cylinder is defined as an object (of any shape) which can be placed in the reaction environment. The examples (Appendix A–F) used pellets and cartridges with a circular cross section.

A7. Conversion of Batch Flow Kinetic Data to Continuous Flow Kinetic Data

The measured salinity concentrations (C) in the product water, as a function of time, t , for $t = 0$ to $t = n$, are routinely measured in trials for each catalyst (e.g., Figure B1, Table E1). This information is used to derive a statistical kinetic data set which can be used to model desalination. The reaction order associated with desalination can be modeled, as a first approximation, using pseudo-first order kinetics [69–74]. Desalination using Type A catalysts appears to approximate to a pseudo-first order reaction where B_S can be $<0.1C_{t=0}$. Desalination using Type B catalysts appears to approximate to a pseudo-first order reaction until equilibrium is achieved, B_S can be $>0.5C_{t=0}$.

Standard chemical engineering practice converts rate constants, k_r , calculated from batch flow trial data (e.g., Figures B1–B3), into continuous flow reactor data [69–74]. In a batch flow reactor, for a specific residence time (reaction time) duration, t_d [69–74]:

$$k_r = k_{actual} P_w a_s, \quad (A1)$$

k_{actual} = normalized actual rate constant; P_w = amount of ZVI catalyst, e.g., $\text{g}\cdot\text{L}^{-1}$; $\text{t}\cdot\text{m}^{-3}$; a_s = normalized surface area of ZVI particle, $\text{m}^2\cdot\text{g}^{-1}$; $k_{10} = \text{Log}_{10}(k_r)$.

The continuous flow reactor can be operated to create a residence time for the water in the reaction environment of t_d , where t_d = Flow rate, or abstraction rate ($\text{m}^3/\text{unit time}$)/Volume of the reaction environment, m^3 [38,67,69–74]. In this instance [69–74]:

$$k_r = k_{actual} P_i a_s = k_{actual} P_w a_s, \quad (A2)$$

P_i = the amount of ZVI catalyst in the *Aquifer Treatment Zone*. k_r is [69–74]:

$$k_r = (\ln(C_{t=0}/C_{t=n}))/t_d, \quad (A3)$$

If k_r is known (e.g., Figures B1–B3, Table E1), and $C_{t=0}$ (aquifer salinity) is known, then $C_{t=n}$ (irrigation water salinity) is known for any value of t_d , i.e.,

$$C_{t=n} = (1/\exp(k_r t_d))C_{t=0}, \quad (A4)$$

t_d is a function of the size of the *Aquifer Treatment Zone* and the irrigation water abstraction rate. It follows that if the required, $C_{t=n}$, is known (or is defined by the irrigation water user), that the required t_d is also known.

Appendix B. Kinetic Data Associated with ST Series Desalination Pellets

Detailed desalination profiles for more than 70 ZVI desalination trials using ZVI desalination pellets have been published [16]. These trials fell into two groups:

1. trials using ZVI pellets with a high structural inter-particle porosity (e.g., ST Trial group [16]) and;
2. trials using ZVI pellets with a low structural inter-particle porosity (MT Trial group [16]).

Desalination, D_r , is assessed as:

$$D_r = 1 - (C_{t=n}/C_{t=0}) = ((C_{t=0} - C_{t=n})/C_{t=0}), \quad (\text{B1})$$

where $C_{t=0}$ = feed water salinity at time $t = 0$; $C_{t=n}$ product water salinity at time $t = n$.

B1. Desalination Rate Constant

The rate of desalination is defined by k_r , [16,17], Equation (A3). The relationship between D_r and trial duration, t_d , is provided in Figure B1. The rate of desalination (and amount of desalination achieved after a specific time period) is a function of the pellets inter-particle porosity (Figure B1), where:

- (a) k_r is independent of the salinity of the feed water [16,17,35], or can increase with water salinity [33,34], Figure B2;
- (b) D_r increases, as P_w (Equation (A1)) increases, until a critical concentration of ZVI is present [16]. This critical concentration is within the range 10–30 g/L (Figure 17a,b);
- (c) Salinity ($C_{t=n}$) measured as a function of time t , follows the general decline pattern of a first order reaction (Figure B3).

The observations demonstrate that placement of the ZVI pellets in a body of water will result in desalination occurring.

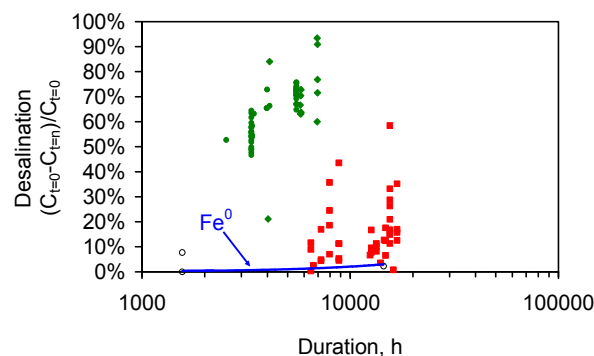


Figure B1. Desalination associated with ZVI pellet desalination. Type A catalysts (ST and MT). ST Series trials = Green markers; MT Series Trials = Red Markers. Blue regression line is for control trials of Fe^0 placed in saline water. $n = 104$; operating temperature, non-isothermal varying with atmospheric temperature over the range $-15\text{ }^\circ\text{C}$ to $20\text{ }^\circ\text{C}$; reactor size, variable, 0.2 to 10 L, ZVI concentration = 5 to $>100\text{ g/L}$ [16]. Details of the ST and MT series trials are provided in Reference [16]. $C_{t=0}$ = initial concentration; $C_{t=n}$ = concentration at time $t = n$. Throughput scale up required to achieve $20\text{ m}^3/\text{day}$, for $t = 200$ days (4800 h) is between 400,000 and 20,000,000.

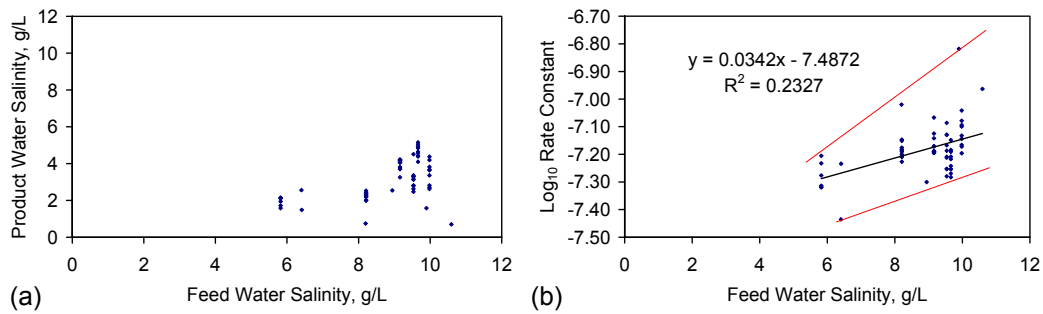


Figure B2. Desalination associated with ZVI catalyst pellet desalination. Type A catalyst (ST) [16]. $n = 59$; (a) Feed Water Salinity vs. Product Water Salinity; (b) Feed water salinity vs. Log₁₀ Rate Constant, k_{10} . Red lines indicate the upper and lower bounds of the data set. The black line is the regression trend. Data: [16].

B2. Desalination Pellet Dimensions

Trials have been undertaken using 15 mm diameter Cu⁰ cased pellets, and 20 mm, 25 mm, 40 mm and 75 mm diameter MDPE (medium density polyethylene) cased pellets and cartridges [16,17]. These trials established (Figure B3):

1. the composition of the impermeable pellet sheathing material does not affect the rate of desalination, or the amount of desalination that can occur. The ability to use MPDE (or an alternative) as a sheathing material (instead of copper) substantially reduces the pellet cost. Suitable alternatives include: (i) ABS: acrylonitrile-butadiene-styrene; (ii) Buna-N: Copolymer of butadiene and acrylonitrile; (iii) CPVC: chlorinated polyvinyl chloride; (iv) EPDM: Ethylene-propylene-diene monomer; (v) FPM: Fluoro-carbon elastomer; (vi) GRP: Glass reinforced plastics; (vii) HDPE: high density polyethylene; (viii) PA 11: polyamide 11; (ix) PB: polybutylene; (x) PE: polyethylene; (xi) PEX: cross-linked polyethylene; (xii) PIR: polyisocyanurate; (xiii) PK: polyketone; (xiv) PP: polypropylene; (xv) PTFE: polytetrafluoroethylene; (xvi) PVC: polyvinyl chloride; (xvii) PVDF: poly vinylidene fluoride; (xviii) PVP: polyvinylpyrrolidone; (xix) SBR: styrene-butadiene;
2. pellets with diameters of 15 mm, 20 mm, 25 mm, 40 mm and 75 mm are effective;
3. the pellets can have one, or two, open ends, which are in contact with the water body;
4. individual pellets can be structured with lengths of more than 0.5 m;
5. desalination continues to occur when air and water temperatures drop below 0 °C [16].

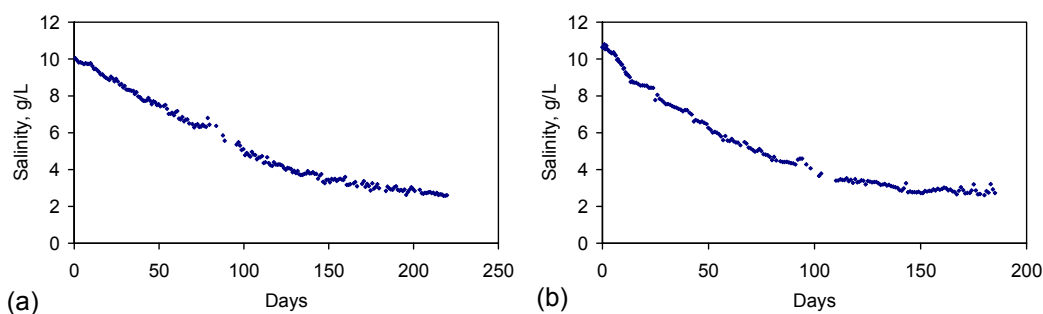


Figure B3. Desalination associated with ZVI catalyst pellet desalination. Type A catalyst (ST). (a) ST Trial ST3a [16]; (b) ST Trial PE3. Trial Details: (i) ST3a. Pellet Details: ZVI:water ratio = 31.94 g/L; Feed water salinity = 10.04 g/L; Product water salinity after 219 days = 2.60 g/L. NaCl removed = 7.44 g/L (0.23 g/g ZVI). Feed Water pH = 6.35; Product water pH = 8.4. Temperature Range = -15 to 14 °C. (ii) PE3. Pellet Details: Outer diameter = 75 mm (MDPE shell). ZVI:water ratio = 55 g/L; Feed water salinity = 10.64 g/L; Product water salinity after 185 days = 2.72 g/L. NaCl removed = 7.92 g/L (0.14 g/g ZVI). Feed water pH = 6.48; Product water pH = 8.62.

Appendix C. Equations and Models Which Are Required to Provide a Control Data Set for the Aquifer and to Provide Effective Monitoring of a Proposed Aquifer Treatment Zone Following Installation

This Appendix provides the principal equations and models which can be used to (i) provide a control (or reference) data set and (ii) monitor the hydrological performance of an *Aquifer Treatment Zone* following installation.

C1. Flow Rate and Iso-Potential Modelling

Prior to reconstruction as an *Aquifer Treatment Zone*, an aquifer has a permeability (k_{aquifer}). The hydraulic head (h) and the underlying aquifer flow rate (Q_{aquifer}) is controlled by the potential gradient ($\nabla\Phi$). The vectorial direction of flow is spatially controlled by the iso-potential contours (iso- Φ) [91]. From Darcy's Law (e.g., [75,92–98]):

$$u = K(h_1 - h_2)/l_1 = K(h)/l_1 = K \cdot \Phi/l_1 \quad (\text{C1})$$

$$Q_{\text{aquifer}} = k_{\text{aquifer}} \cdot \Phi, \quad (\text{C2})$$

$$\nabla Q_{\text{aquifer}} = \nabla k_{\text{aquifer}} \cdot \nabla \Phi, \quad (\text{C3})$$

K = a permeability constant [75] = uI_1/h ; $K = 1$ Darcy when $u = 1 \text{ cm} \cdot \text{s}^{-1}$; I_1 = total length of flow path in the aquifer, m, [75,97]; u = flow velocity ($\text{cm} \cdot \text{s}^{-1}$) = measured Q ($\text{cm}^3 \cdot \text{s}^{-1}$)/ A [75]; Φ = Fluid potential (Pa), e.g., $\Phi = P_A/d_w + gz$ [75]; $z = (h_1 - h_2)$ [75]; h = head, e.g., $\text{m}^3 = h_1$ (upstream water source elevation) – h_2 (downstream water discharge elevation) [75,92]; d_w = density of water; g = gravitational constant. ∇ = gradient operator.

The iso-potential contours effectively solve [91,92] the Richards equation [99]:

$$Q_{\text{aquifer}} = \delta/\delta x(k_{\text{aquifer}} \cdot (\delta\Phi/\delta x)) + \delta/\delta y(k_{\text{aquifer}} \cdot (\delta\Phi/\delta y)) + \delta/\delta z(k_{\text{aquifer}} \cdot (\delta\Phi/\delta z)), \quad (\text{C4})$$

C1.1. Simple Reconstruction of an Aquifer

The simplest reconstruction of an aquifer (Figure C1) requires:

1. a single abstraction well to be used to provide water for irrigation;
2. The abstraction pump creates a point source with a negative head (sink) [75];
3. The pump reconfigures the potential, Φ , to create a radial series of iso-potential contours surrounding the abstraction well [75]. Their values range from Φ_{Initial} to $\Phi_{\text{abstraction well}}$, where Φ_{Initial} is located a radial distance, r_e , from the well [75].
4. the abstraction well is surrounded by a number of point loci (e.g., infiltration devices, wells, boreholes) containing ZVI pellets or cartridges.

The measured elevation of the water table, at each loci allows the iso-potential contours to be defined [91,100].

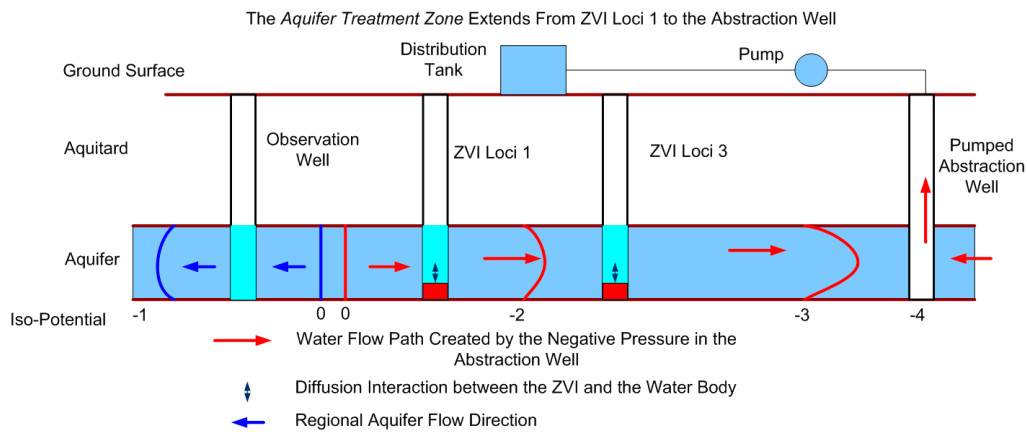


Figure C1. Cross-Section through a schematic Aquifer which has been reconfigured to produce partially desalinated water. ZVI pellets and cartridges are shown in red.

C1.2. Identification of Heterogeneity in the Proposed “Aquifer Treatment Zone”

The initial assumption (for any aquifer) is that it is homogenous. Aquifers are locally heterogeneous (Appendix G). They can be associated with two, or more, no flow boundaries, or may be compartmentalized [75,91,92].

A review of the issues associated with transmissivity, storage coefficients, compartmentalization, channelized flow and boundaries is outwith the scope of this study.

Observation loci (Figure C2) can be used to confirm the boundaries of the installed Aquifer Treatment Zone.

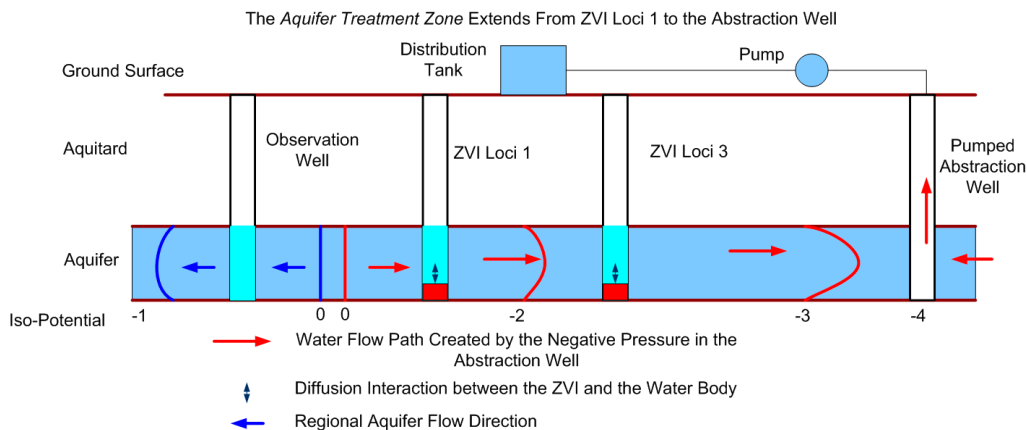


Figure C2. Cross section through a schematic aquifer which has been reconfigured to produce partially desalinated water. ZVI pellets and cartridges are shown in red.

C2. Assessment of the Size of a Proposed Aquifer Treatment Zone

C2.1. Hydrological Parameters Associated with a Proposed Aquifer Treatment Zone

For a constant abstraction rate, A_R , the flow velocity, V , at a distance x_1 from the well will be greater than the flow velocity at a distance x_{1+n} from the well; the distance $x_{1+n} < r_e$ [75]. At the abstraction well, $V = A_R$. If the abstraction well has perforated the entire aquifer height, and the aquifer, is homogenous with an even thickness, then as a first approximation, at a radial distance, r_1 :

$$V (\text{m}^3 \cdot \text{m}^{-1} \cdot \text{t}^{-1}) = A_R / 2\pi r_1, \tag{C5}$$

Drawdown [75] can result in part of an aquifer becoming under-saturated with time. The under-saturation results in the contents of the aquifer porosity changing:

- at $t = 0$, the porosity contains mobile water + irreducible (bound) water;
- at $t = n$, following drawdown, the porosity can contain mobile water + irreducible water + mobile air + irreducible air.

The two phases (air + water) can be accounted for by using a simple permeability modifier, e.g., the Brusaert [100] model:

$$k = k_0 \cdot S_w^{n1}, \quad (C6)$$

k = intrinsic permeability [92,96]; $k = Q/P_r$ [92,96,101,102]; k_0 = intrinsic permeability at saturation; S_w = mobile water saturation, $0 < S_w < (1 - S_{wi})$; S_{wi} = irreducible water saturation, $0 < S_{wi} < 1$; $n1$ = a saturation constant [100]; Calculated as $S_{wi} = g + (j + d)/b$ where $g + j + b + d$ are constants; and $n1$ is in the range 0.1 to 25; P_r = pressure difference, Pa, represented by h ; Q = normalized flow rate, (volume) (unit time)⁻¹ or flow rate, (volume) (unit time)⁻¹(unit weight, area, or volume of ZVI (or aquifer))⁻¹ = $kP_r = k \cdot \Phi$.

C2.1.1. Radial Area of Influence of the Abstraction Well

A simple homogenous aquifer is bounded by two aquitards, separated by a thickness, T_h . A single abstraction well is used to create a circular *Aquifer Treatment Zone*, with a radius, r_a . Under steady state conditions [75]:

$$A_R \text{ (e.g., } 20 \text{ m}^3 \cdot \text{d}^{-1}) = ((2\pi \cdot r_a k_{\text{aquifer}} T_h) / \mu) (\delta P / \delta r_a), \quad (C7)$$

A_R = required abstraction rate; P = constant driving force, Pa (or head, m); k_{aquifer} = permeability of the aquifer; μ = viscosity of water. In this study $P = P_r = \Phi$.

C2.1.2. Volume Influenced by the Abstraction Well during a Control Pump Trial

At time $t = n3$ at a radial distance r_e [75]:

$$A_V (P = P_{\text{Aquifer}}) = (A_R)(n3) / (\varphi \cdot S_{wi} N_G), \quad (C8)$$

A_V = Aquifer volume defined by the abstraction pump; $P_{\text{aquifer}} = P = \Phi$, at a radial distance, r_e , from the abstraction well bore. A_V increases as A_R increases.

C2.1.3. Flow Rate at Each Loci

At any instant in time, the flow rate (or velocity, V_1) at each ZVI loci, is a function of its distance from the abstraction loci (A_l).

$$V_1, \text{ m/s} = A_R / (2\pi \cdot A_l), \quad (C9)$$

Equations (C7)–(C9) allow: (i) the aquifer Treatment Zone Volume, created by a specific abstraction pump to be evaluated (Figure 3a); (ii) the relationship between A_R , φ and t_d to be defined (Figure C3b). Integration of Equations (A1)–(A4) with Equations (C7)–(C9) and the data in Figure 17) allows the basic construction parameters associated with the installation of a proposed *Aquifer Treatment Zone* to be calculated (Figure C3c–f).

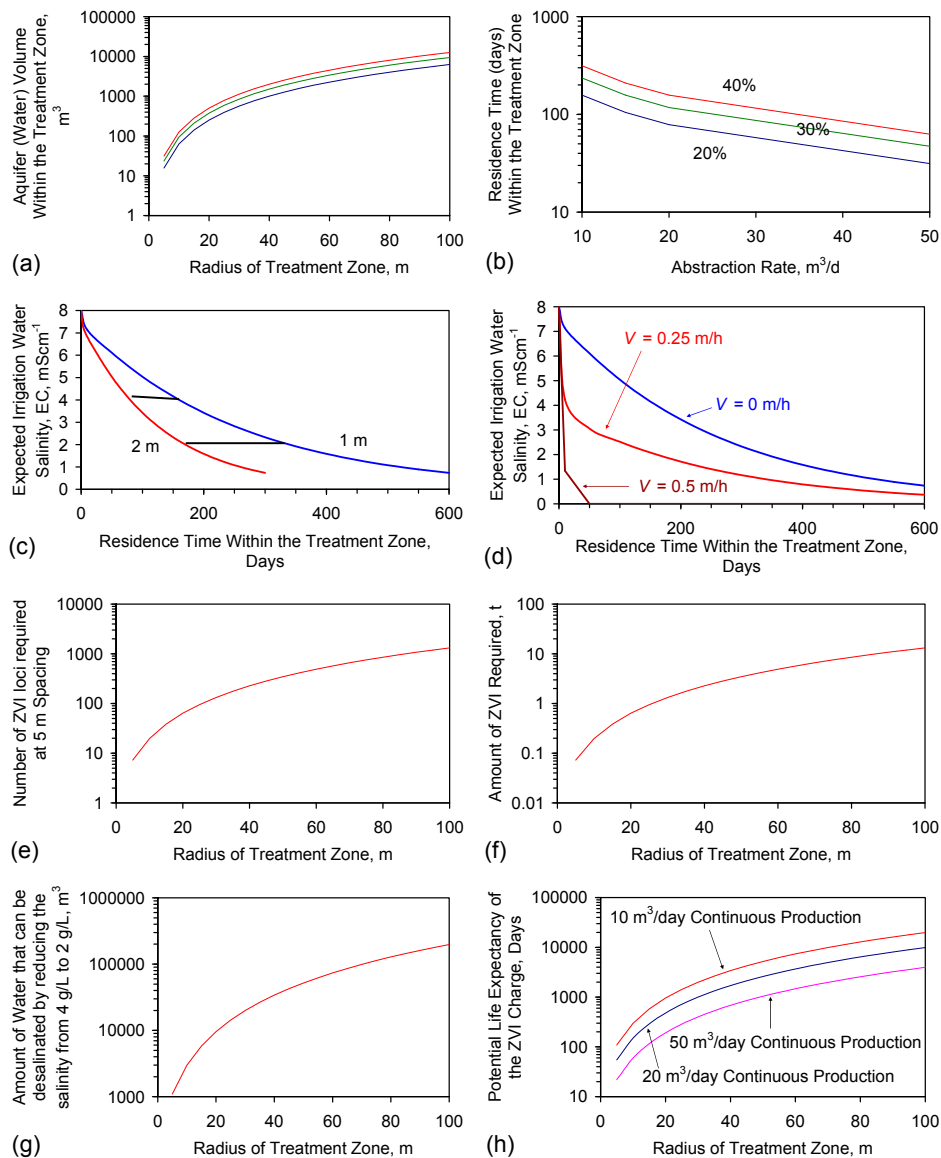


Figure C3. Example Modeled *Aquifer Treatment Zone* parameters. (a) Stored water volume in the aquifer within a radial distance of the abstraction well for porosities of 20%, 30% and 40%; (b) Residence time for the water within the a 100 m diameter) treatment zone as a function of aquifer porosity (20%, 30%, 40%) associated with continuous abstraction rates for irrigation in the range 10 to 50 m³/day. Aquifer thickness = 1 m; (c) Relationship between water residence time within the treatment zone, abstracted water salinity and aquifer thickness. The reference relationship is shown by the 1 m thickness case. The residence time required is independent of thickness but is dependent on the rate constant. The illustrated 2 m thickness case indicates that the effective aerial extent of the *Aquifer Treatment Zone* can be reduced by 50% to accommodate the increased aquifer volume. The actual residence time required by water in the 2 m case is provided in this graph by the 1 m example. Assumption $V = 0$ m/h, Rate Constant based on the regression relationship for the ST Trial Group ZVI Pellets (Figure B2b); Water salinity outside the treatment zone = 4 g/L (EC = 8 mS·cm⁻¹); (d) Expected salinity as a function of effective V and residence time in the treatment zone; (e) Radius of treatment zone vs. number ZVI loci required at a 5 m radial spacing; (f) Radius of treatment zone vs. amount of ZVI required, based on 10 kg at each ZVI loci and a 5 m ZVI loci radial spacing; (g) The amount of water that can potentially be desalinated by a single ZVI charge as a function of the radius of the treatment zone (based on removal of 30 t NaCl/t Fe⁰ [17]); (h) The potential life expectancy of the ZVI charge (days) vs. radius of the treatment zone and the abstraction rate for irrigation (based on removal of 30 t NaCl/t Fe⁰ [17]). The reference aquifer thickness = 1 m in Figure C3d–h.

C2.2. Complex Treatment of Under-Saturated Flow

The simple permeability model (Equation (C6)) can be replaced by a more complex permeability model. The more complex model will treat each immiscible fluid (water and air) separately. This creates separate iso-potential relationships, permeability relationships, and flows for each fluid [75,92,103]. The two fluids can flow in different directions and at different rates (e.g., [92,104]).

When $S_w < 1$, Gas (air) slippage, Klinkenberg effects and Knudsen diffusion impact on k_{gas} [104,105]. Their impact on permeability can be addressed by combining a Knudsen diffusion model with a forced viscous Hagen-Poiseuille flow model [104], when $S_w < 1$ i.e.,

$$k_{\text{air}} = k_{t=0(\text{gas})} \cdot (1 + aK_n) \quad (\text{C10})$$

$$k_{\text{water}} = k_{t=0(\text{water})} \cdot S_w^{n1}, \quad (\text{C11})$$

a = a constant; K_n = Knudsen Number [105,106]. As an initial simplification, $k_0 = k_{t=0}$, and $S_w = 1$ (i.e., flow is saturated). The Hagen-Poiseuille model (e.g., [62,88,94–97,106]) defines the relationship between k , and ϕ as:

$$k = \phi \cdot r^2 / \eta, \tau\sigma, \quad (\text{C12})$$

ϕ = Inter-particle or inter-aggregate porosity; η = fluid viscosity, $\text{N} \cdot \text{s}^{-1} \cdot \text{m}^{-2}$; τ = pore tortuosity, e.g., $(L_c/L)^2$ [92,94,107,108]; σ = complexity of pore geometry; r = pore throat radius, m; L = Apparent flow path length; L_c = Actual flow path length. $L_c = L$ when the pores are represented by perfect cylinders. In most pores, $L_c > L$.

The principal versions and derivatives of Equation (C4) are provided elsewhere [109–124].

C3. Hydrological Issues Associated with the Placement of ZVI in an Aquifer

C3.1. ZVI Permeability

ZVI corrodes and re-crystallizes when placed in water (e.g., [125–132]). The corrosion products are hydrated (oxy) hydroxides ($\text{Fe}(\text{OH})_x$, FeOOH) [16,17]. The associated volume change results in the porosity, and permeability, k_{ZVI} , declining with time (e.g., [133–141]).

A constant head, continuous flow test through ZVI confirms (Figure C4) that the permeability of Fe^0 reduces, (and the Eh and pH of the product water change), with time, t . The permeability is calculated as [36,62,75,92,94,104]:

$$k = Q/P \quad (\text{C13})$$

where k = permeability, $\text{m}^3 \cdot \text{m}^{-2} \cdot \text{L}^{-1} \cdot \text{t}^{-1} \cdot \text{Pa}^{-1}$; Q = flow rate $\text{m}^3 \cdot \text{m}^{-2} \cdot \text{L}^{-1} \cdot \text{t}^{-1}$; P = Measured potential or head, Pa; l = reference column length, m; t = unit time, seconds; m^{-2} = normalized cross sectional area of flow = 1 m^2 .

The re-crystallization of the ZVI increases the probability that open pores (within the ZVI) will be converted to dead-end pores over time.

The reduction in k with t (Figure C4) is associated with the bulk (>99%) of the through flow being confined to high permeability, low tortuosity, macropores [66]. This structural change results in the actual residence time of the through flow, t_d , (within the ZVI) reducing with time, t [66]. This observation may explain why NaCl removal is rarely reported in the product water from Fe^0 permeable reactive barriers (PRB), e.g., [37,142]. Decreases in the inter-particle porosity are associated with the formation of intra-particle porosity [17].

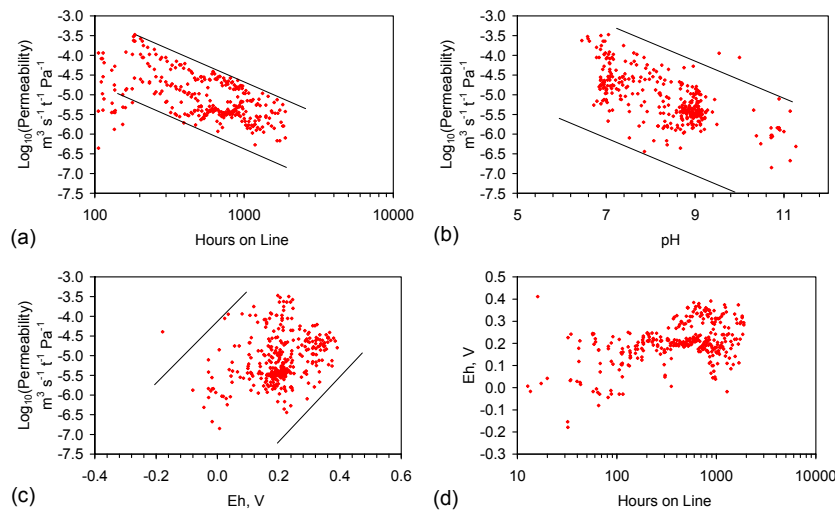


Figure C4. ZVI permeability decline as a function of: (a) time; (b) pH of the water leaving the ZVI column; (c) Eh of the water leaving the ZVI column; (d) Eh vs. time. Further details of the ZVI, flow apparatus and testing procedures are provided in References [16,17,38]. Data Source: [17].

C3.2. Haloclines: Interaction between the ZVI Loci and the Surrounding Aquifer

Haloclines are a natural feature of the marine environment (e.g., [143]) and develop within the ZVI desalination environment [16,17].

Three salinity zones may be associated with the ZVI pellets in a partially closed environment (Figure C4). They are:

- zone of super saturation of NaCl within the ZVI pellets;
- zone of elevated Na^+ and Cl^- concentrations in the water immediately adjacent to the ZVI pellets. This can represent less than 2.5% of the water volume which is influenced by the ZVI [16,17];
- zone of reduced Na^+ and Cl^- concentrations in the bulk of the water surrounding the ZVI pellets [16,17];

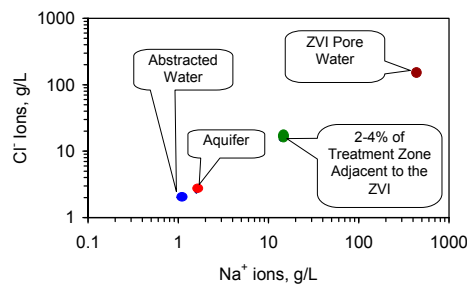


Figure C5. Salinity distributions in a synthetic “Aquifer Treatment Zone” following 69.65 h operation. Type B Catalyst. Saline water enters the treatment zone at an average rate of $15.8\% \text{ h}^{-1}$ of the water volume in the treatment zone; *Aquifer Treatment Zone* Volume = 5.8 L; Water Volume Treated = 63.8 L; Temperature = 5–12 °C; $P_w = 23 \text{ g Fe/L}$ [16]; Pellet casing: MDPE (0.02 m × 0.5 m); Water Recycle Rate: 50% to 67% h^{-1} of the water volume contained in the *Aquifer Treatment Zone*; Average time spent in the treatment zone = 5.3 h; Average Na^+ concentration in the feed water = $1.65 \text{ g}\cdot\text{L}^{-1}$; Average Cl^- concentration in the feed water = $2.56 \text{ g}\cdot\text{L}^{-1}$; Average Na^+ concentration in the product water = $1.01 \text{ g}\cdot\text{L}^{-1}$; Average Cl^- concentration in the product water = $2.02 \text{ g}\cdot\text{L}^{-1}$; Average salinity reduction = 28.1%; Removed ions retained in the ZVI = 40.98 g Na^+ ions (38.9%) + 34.46 g Cl^- ions (21.1%). Average pH of feed and product water = 5.99; Eh of feed water = 545 mV. Eh of product water = 587 mV. ZVI Type: E143 [16], see References [16,17] for batch operation details associated with this ZVI Type. Scale-up factor required to achieve a throughput to $20 \text{ m}^3/\text{d} = 833.3$.

C4. Modeling Diffusion Fluid Flows Which Affect the Water Salinity

C4.1. Diffusion Flow Analysis

In stagnant water, the change in aquifer salinity is a function of the mass flux (J) between the ZVI and the water, where [144]:

$$J = J_{adv} + J_{dif} + J_{dis}, \quad (C14)$$

J_{adv} = advective mass flux; J_{dif} = mass flux due to molecular diffusion across the saturated pore space; J_{dis} = dispersive mass flux. From Ficks Second Law [144]:

$$\delta(c_2)/\delta t = -\nabla(J_{adv} + J_{dif} + J_{dis}), \quad (C15)$$

$$\delta(c_2)/\delta t = -\nabla v(c_2) + \nabla[(D_m I + D_d)\nabla(c)] \quad (C16)$$

c_2 = concentration of [A] where $([A]/[A_0])$ increases with increasing distance from x ; [A] = NaCl concentration at time t ; t = unit time, e.g., seconds (s), hours (h), days (d), years (a); $[A_0]$ = NaCl concentration at time $t = 0$; v = fluid velocity within the pore space; D_m = effective molecular diffusion coefficient; D_d = dispersion tensor; I = identity tensor.

A high k_r is associated with a high value of $\{v\}$ and J . A low k_r and J occurs when $\{v\} = 0$, and J .

C4.2. Non-Fickian Diffusion Flow

The diffusion transport through heterogeneous porous material is generally non-Fickian [144]. Non-Fickian flow results from variations in porosity, thickness, net to gross, permeability, fluid flux, and potential. If we allow for a source, $g_1 = x/t$, {where x is a point within a continuum and g_1 is a ZVI Loci within a treatment (desalination) zone bounded by r_a }, then the concentration (c_2) at each point x,y,z within the desalination field is governed by the advection-dispersion equation [144], e.g.:

$$\delta(c_2)/\delta t = -\nabla v(c_2) + \nabla D_d \nabla(c_2) + g_1, \quad (C17)$$

A 1-Dimensional non-Fickian model (applies at each ZVI loci) where:

- (i) the fluid velocity (V) is constant, and
- (ii) the only direction of flow is towards the abstraction well, e.g., [144]:

$$\delta(c_2)/\delta t = -V \cdot \delta(c_2)/\delta x + D \cdot \delta^\alpha(c_2)/\delta x^\alpha \quad (C18)$$

D = constant dispersion coefficient. α = order of fractional differentiation; $1 < \alpha \leq 2$. In a treatment field, (c) , t , and V are known or can be predicted. Rearranging Equation (C18) results in:

$$\delta(c_2)/\delta t + V = (D \cdot \delta^\alpha(c_2)/\delta x^\alpha)/\delta(c_2)/\delta x = DB, \quad (C19)$$

$$B = (\delta^\alpha(c_2)/\delta x^\alpha)/\delta(c_2)/\delta x, \quad (C20)$$

If as a simplification, B is set as 1.0, then:

$$\delta(c_2)/\delta t = D - V, \quad (C21)$$

i.e., increasing V reduces $C_{t=n}$ and increases k_r (Figure C6).

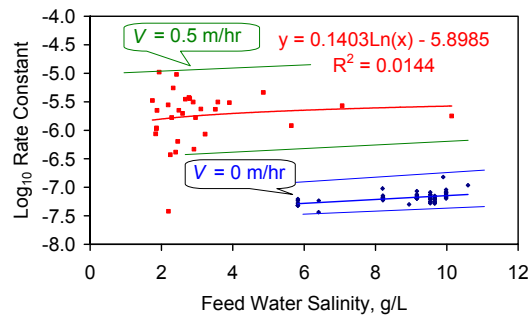


Figure C6. Rate constant vs. feed water salinity at fluid velocities of 0 m/h (Type A Catalyst. ST Trial Group Series) and 0.5 m/h (Type B Catalyst. E146/7 Trial series). The E146/7 Trial series (operated at 5–25 °C; Reactor Size = 240 L) established removal of 9.89 t Na⁺/t Fe + 23.65 t Cl⁻/t Fe over 50 batch treatment cycles [16,17]. ♦ = ST Trial Series Data [16]; ■ = E146/7 Trial Series Data [16,17].

C5. Space Velocity

The salinity $\delta(c_2)/\delta t$ at a point x,y is a function of SV [17,38,69–72,94]:

$$SV = \text{Aquifer Flow Rate (Q)} / \text{ZVI Amount (t)}, \tag{C22}$$

$$SV = \text{Aquifer Treatment Zone water volume} / \text{ZVI Amount (t)} / C_t, \tag{C23}$$

$$Q (\text{m}^3 \cdot \text{t}^{-1} \cdot \text{t}^{-1}) = k\Phi = SV, \tag{C24}$$

$$\text{Ln}([A_o]/[A]) = k_r t = k_r / SV = k_r / k\phi, \tag{C25}$$

$$\text{Log}([A]/[A_o]) = -k_r t / 2.303 = -k_r / SV / 2.303 = -k_r / k\phi / 2.303, \tag{C26}$$

k_{observed} = observed rate constant = k_r ; C_t = Irrigation water residence time in the Aquifer Treatment Zone; $[A_o]$ = salinity entering the Aquifer Treatment Zone $[A_o]$; $[A]$ = water salinity leaving the Aquifer Treatment Zone; $[A_o] > [A]$.

The residence time associated with a specific space velocity is defined as [72].

$$W_{RT} = 1 / SV = 1 / k\Phi, \tag{C27}$$

C6. Mineral Precipitation, Gas Occlusion, and Biofilms within the Aquifer

C6.1. Impact of Mineral Precipitation and Gas Discharge from the ZVI on Aquifer Permeability

The ZVI changes the pH and Eh of the aquifer water (Figure C7) [16,17,36,38,67,68]. This change results in the dissolution of cations present in the ZVI and the precipitation of hydroxides, oxyhydroxides and associated chlorides [68,145,146]. Their precipitation, either as colloids within the water body, or as precipitates adhering to pore walls, will alter the inter-particle porosity (ϕ), and permeability, of the aquifer (and ZVI) [16,145,146].

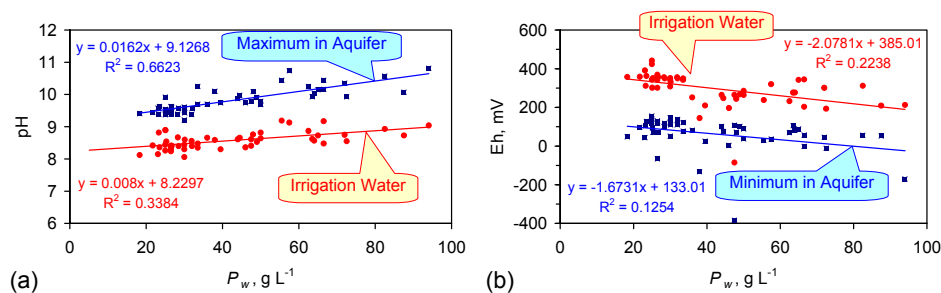


Figure C7. Cont.

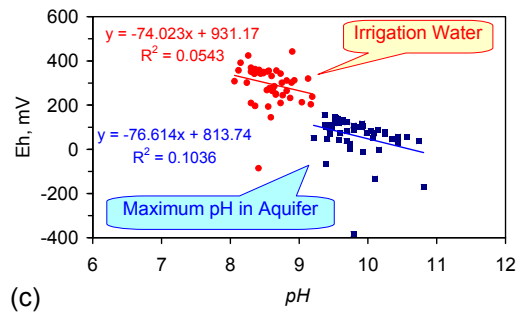


Figure C7. ST ZVI desalination pellets [16]; Type A Catalyst: Indicative Eh and pH of the irrigation water, maximum pH/minimum Eh in the aquifer as a function of P_w . (a) pH vs. P_w ; (b) Eh vs. P_w ; (c) Eh vs. pH. Data Source: Desalination Pellet Trials ST1a to ST5j [16]. Feed water pH = 5.8–6.6.

C6.2. Estimating Permeability Changes Due to Mineral Precipitation and Gas Occlusion

Extending Equation (C6), to address decreases in porosity due to mineral precipitation results in:

$$k_{(t=n)} = k_0 \cdot S_p^{n2}, \quad (C28)$$

$$k_{(t=n)} = k_0 \cdot S_w^{n1}, \quad (C29)$$

$n1$ = a saturation constant (Brusaert [92] model); Calculated as $g + (j + d)/b$ where $g + j + b + d$ are constants; and $n1$ is in the range 0.1 to 25; $n2$ = a reaction order constant, e.g., 1. S_p = water saturation after exclusion of porosity for precipitates, $0 < S_p < (1 - S_{wi})$; estimated as $([\varphi_{(t=0)} - \varphi_{(t=n)}]^3 / [(1 - (\varphi_{(t=0)} + \varphi_{(t=n)})) / (1 - (\varphi_{(t=0)}))]^2)$, when $n2 = 1$ by [139]; S_w = mobile water saturation, $0 < S_w < (1 - S_{wi})$. Porosity changes due to precipitation and gas (or air) occlusion, k can be defined as:

$$k_{(t=n)} = k_0 \cdot S_p^{n2} \cdot S_w^{n1}, \quad (C30)$$

These changes interact on the iso-potentials through Equation (C4).

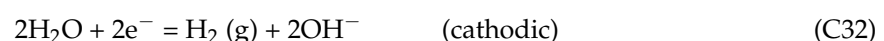
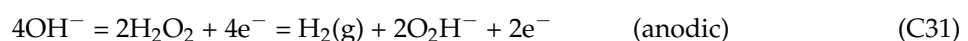
C6.3. ZVI Gas Generation

Gas production (H_2 , O_2) associated with ZVI [66] can be abiotic [38,68,139,145–151] or biotic. These gases can occlude porosity and reduce permeability before they are either adsorbed by the matrix or dissolved in the water (e.g., [68]).

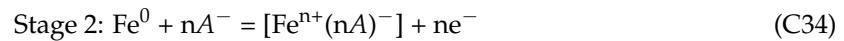
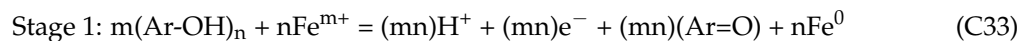
C6.4. Biofouling, Biofilms

All natural aquifer water contains bacteria and other micro-organisms. Permeability losses associated with biofouling occur at the upstream ZVI-water contact. ZVI creates a toxic habitat for some species, while for other species it is a preferred habitat [66,68,152,153]. Many of the iron bacteria species associated with mineralized ZVI biofilms, are aerobic species.

The standard abiotic, cathodic and anodic reactions in ZVI (during corrosion), which produce hydrogen include [32,66,68,139,145–151]:

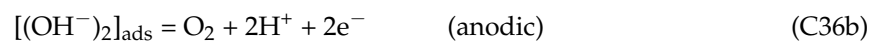
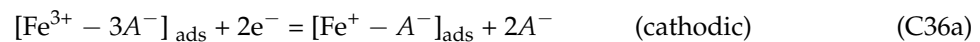
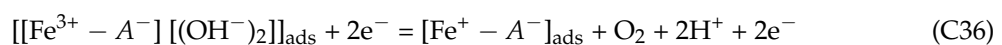


The mineralized ZVI biofilms associated with iron bacteria form as a result of the following reactions, e.g., [66,154]:



A = anions; $[\text{Fe}^{n+}(\text{nA})^-]$ = Mineralized Bacteria; Ar-OH = aromatic, or another chemical, with OH bonds; Ar=O = aromatic, or another chemical, containing an oxygen double bond. The micro-environment (inhabited by the iron bacteria) is converted from an anoxic environment (Equations (C31) and (C32)) to an aerobic environment by the following cyclic reactions, e.g., [154]:

Stage 3: Oxygen formation: Freshwater and Saline Environment



Biofouling is a major problem, with some groundwater recharge schemes, where water is reinjected, or infiltrated, into an aquifer [155].

Appendix D. : Classifying the Potential Aquifer Resource

The initial site screening will place the aquifer resource into one of three categories [156,157]:

1. Prospective resource;
2. Contingent resource;
3. Developed resource.

This categorization will then define what additional works are required in order to develop the resource. This study adopts the SPE 2001 resource classification scheme [156]. A review of the alternative resource schemes which have been approved by regulatory authorities globally is provided in Reference [158].

D1. Prospective Resource

A prospective resource falls into one of three categories [156]:

1. *Play*: Shallow aquifer which is believed to extend under the proposed *Aquifer Treatment Zone* ground surface but has not been demonstrated to be present by drilling or by the insertion of wells.
2. *Lead*: Shallow aquifer whose presence has been identified by one or more wells or infiltration devices, but requires more data acquisition before it can be deemed to be suitable for conversion to an *Aquifer Treatment Zone*.
3. *Prospect*: Shallow aquifer which has been identified and has been partially defined, but is insufficiently defined to represent a viable *Aquifer Treatment Zone* target.

D2. Contingent Resource

A contingent resource falls into one of three categories [156]:

1. *Development Pending*: Requires further data acquisition (aquifer, hydro/geochemical, regulatory, crop economics) and/or evaluation (financing, insurance, regulatory, crop analysis) in order to confirm commerciality;

2. *Development on Hold*: Awaiting changes in market conditions (e.g., crop prices) or removal of other constraints to development (e.g., political, regulatory, financing, insurance, customers, seed availability, etc.);
3. *Development not Viable*: No current plans exist to develop the defined resource or acquire additional data at this time due to aquifer constraints, legal, regulatory, chemical, commercial, insurance, crop, political, environmental issues, or one or more other constraints. A development site which is not viable at a specific time may become viable if one or more of the underlying constraints changes.

D3. Developed Resource

A developed resource falls into one of three categories [156]:

1. *On Production*: The *Aquifer Treatment Zone* has been installed and is in operation producing partially desalinated water;
2. *Under Development*: All necessary approvals and consents have been obtained, and construction of the *Aquifer Treatment Zone* is underway;
3. *Planned for Development*: The project satisfies all technical constraints, and there is a firm intent from the land owner to progress with the installation of an *Aquifer Treatment Zone*. Installation is being held up by one or more of detailed development planning, regulatory, financing and insurance approvals, and contracts finalization.

Appendix E. Calculating and modeling the Dimensions Associated with a Proposed *Aquifer Treatment Zone*

This appendix provides the primary equations and data which are required to: (i) define the size and aerial extent of a proposed *Aquifer Treatment Zone*; (ii) define the amount of ZVI required and the number of ZVI loci required; (iii) and the data required to define (for the Recycle Strategy (Figure 20)) the required abstraction pump capacity, and the required volume of water that requires to be reinjected or infiltrated.

The energy required for the abstraction pump is a function of pump type and manufacturer. A regression analysis of water pumps with a capacity of between 88 and 230,000 m³/day indicates that the power required, kWh = 0.0039 pump capacity, m³/d (R² = 0.91; n = 24).

The recycle strategy requires that part of the abstracted water is recycled (Figure 20). The recycled water can either be pumped to an infiltration/injection loci, or it can flow (using gravity) to the infiltration loci. The latter strategy does not require a recycle pump.

The capacity of a gravity fed infiltration loci (for recycle water (Figure 20)) is controlled by its permeability, surface area, and the head of water in the infiltration loci (or between the loci and the distribution tank).

The data in Table E1 can be used to design the soakaway/infiltration device requirements for a proposed *Aquifer Treatment Zone* [62–65].

E1. Area of Influence of Each ZVI loci Placed within an Aquifer

The ZVI, placed within loci (located in the aquifer), will exert an influence on the chemistry of x m³ of the water (I_c) in the surrounding aquifer [16,66–68]:

$$I_c, \text{ m}^3 = 1000/P_w Z_1, \quad (\text{E1})$$

P_w = Unit weight of ZVI/Unit water volume treated, e.g., 20 g/L = 20 kg/m³; Z_1 = weight of ZVI, e.g., kg.

E2. Sizing the Aquifer Treatment Zone

The required residence time (days) of the water in the proposed *Aquifer Treatment Zone* (prior to abstraction), will depend on the magnitude of the salinity reduction required (Figures B1–B3).

The volume of water required within the *Aquifer Treatment Zone* (V_{aq} , m^3) is:

$$V_{aq}, m^3 = I_w R_2 = I_w t_d, \quad (E2)$$

I_w = Irrigation water volume required, $m^3 \cdot day^{-1}$; R_2 = Number of days the water is required to reside in the proposed *Aquifer Treatment Zone* (e.g., Figures B1–B3). The minimum volume of water (m^3) located within the treatment zone (W_{TZ}) is:

$$W_{TZ} = A_R W_{RT}, \quad (E3)$$

W_{RT} = required water residence time (e.g., 200 days) in the reaction environment.

The required abstraction rate (A_R) for partially desalinated water is $n m^3 \cdot day^{-1}$. For illustration purposes, $\log_{10}(k_r) = -7.35$ (determined from the regression equation in Figure B2); $[C_o] = 4 g \cdot L^{-1}$; After 200 days, $[A] = 1.84 g \cdot L^{-1}$; After 400 days, $[A] = 0.85 g \cdot L^{-1}$; After 600 days, $[A] = 0.395 g \cdot L^{-1}$.

E3. Sizing Identifying the Ground Surface Area Which Overlies the Aquifer Treatment Zone

The minimum ground surface area (L_T , m^2) overlying the proposed *Aquifer Treatment Zone* can be calculated as:

$$L_T, m^2 = (V_{aq} / A_T) / \phi, \quad (E4)$$

ϕ = Inter-particle porosity of the aquifer; A_T = Net water column thickness in the aquifer, m.

E4. The Required Aquifer Gross Rock Volume

The required gross rock aquifer volume (A_V), m^3 , enclosed within the *Aquifer Treatment Zone* becomes (e.g., [75,159]):

$$A_V = W_{TZ} / (\phi S_{wi} N_G), \quad (E5)$$

N_G = Aquifer net to gross ratio (i.e., net aquifer volume/total aquifer volume). S_{wi} = mobile water saturation within the aquifer which is recoverable by the abstraction well.

E5. Assessment of the Significance of Catalyst Selection on the Number of ZVI Loci Required

The area of influence of each ZVI loci is a function of V and P_w (Equations (C21), (E1) to (E5)). The range for P_w is:

- Type A Catalyst Group: between 5 g/L and 300 g/L (Figure 17);
- Type B Catalyst Group: between 0.072 and 28 g/L (Table E1).

Each ZVI loci is a perforated well (or infiltration device), which intersects the aquifer and contains ZVI pellets or cartridges. The ZVI can be removed, monitored and periodically replaced.

The ZVI is placed in a series of discrete loci to allow the water within the aquifer to flow between (and around) the loci (e.g., [160–165]). This avoids the flow by-pass situations which are associated with ZVI permeable reactive barriers (e.g., [166–168]).

Table E1. Trial results associated with the operation of *semi-closed Aquifer Treatment Zone with Recycle* (Figure 20). The recycle ratio, $R_{rc} = y \text{ (m}^3/\text{day)}/m \text{ (m}^3/\text{day)}$. R_{rt} = average residence time (t_d) of the water in the reaction environment. Cartridge casing = MDPE. Each trial example used a different Type B catalysts (Table F1). A single catalyst charge was used in each trial group. Optimised operation assumes that t_d is matched to the onset of B_5 . This reduces R_{rt} (associated with each catalyst) into the range 3 to 12 h.

Trial Group	Reactor Size, L	P_{wr} g Fe ⁰ /L	Sub-Optimised R_{rc}	Optimised R_{rc}	A_0 , g/L	$A_{t=n}$ g/L	R_{rt} , h	Log ₁₀ ($k_{observed}$)	Log ₁₀ (k_{actual})	Water Volume Treated, L	Scale-Up Required to Achieve 20 m ³ /day	Scale-Up Required to Achieve 20 m ³ /day with Optimised Operation
RC1	5.8	23.28	3.60	2.48	4.21	3.03	5.80	-4.80	-6.17	63.8	833.3	574.7
RC2	240.0	0.50	11.08	3.00	2.97	2.14	22.15	-5.39	-5.09	12000.0	76.9	20.8
RC3	8.0	28.00	20.25	1.35	2.65	0.79	45.00	-5.13	-6.57	32.0	4687.5	312.5
RC4	5.8	8.79	302.28	7.45	4.25	2.81	487.00	-6.63	-7.57	34.8	69,971.3	1724.1
RC5	5.8	4.80	11.75	3.10	36.17	25.71	18.93	-5.30	-5.98	92.8	2719.8	718.4
RC6	5.8	0.86	12.22	3.72	15.66	8.67	19.68	-5.08	-5.01	75.4	2827.6	862.1
RC7	5.8	4.66	9.62	3.10	8.84	7.04	15.50	-5.39	-6.06	29.0	2227.0	718.4
RC8	5.8	0.86	2.84	1.86	6.46	5.30	4.58	-4.92	-4.86	17.4	658.0	431.0
RC9	800.0	0.07	3.21	0.45	2.10	1.28	42.74	-5.49	-4.34	9600.0	44.5	6.3

Appendix F. Concepts and Models Associated with a Recycle Strategy

The trial results have established (Table E1) that the highest values of k_r are associated with low values of t_d in a reaction environment incorporating recycle, where $(y + n) > 0$ (Figure 20). In the trials (Table E1) (y/m) is between (i) 2.8 and 302 for sub-optimized operation; and (ii) 0.45 and 7.5 for optimized operation. This implies that optimized operation of a proposed *Aquifer Treatment Zone* producing $20 \text{ m}^3/\text{day}$, will also abstract and recycle an additional 9 to $150 \text{ m}^3/\text{day}$.

This Appendix highlights the principal issues which require to be addressed during a FEHED analysis for a proposed *Aquifer Treatment Zone*.

F1. Engineering Concepts Associated with Catalytic Recycle

The process flow diagram for the *Recycle Strategy* (Figure 20) defines the recycle rate ratio as $(y + n)/(x + y)$ [169,170]. In the *Static Strategy*, $(y + n) = 0$. In the *Recycle Strategy*, $(y + n) \geq 0$.

F1.1. Modelling the Recycle Water Flow Rate (V)

Increasing V (the recycle water flow rate within the aquifer) can increase k_r (Figure C6). In the *Static Strategy*, $V = 0$. In the *Recycle Strategy*, $V \geq 0$. Increases in V require the *Aquifer Treatment Zone* to be restructured to allow part of the abstracted water to be either:

- (a) reinjected into the aquifer within the proposed *Aquifer Treatment Zone*, or
- (b) recirculated within the proposed *Aquifer Treatment Zone*.

V is directly proportional to the recycle ratio [169,170], where:

- (i) The volume of water entering the *Aquifer Treatment Zone* is denoted as $x + y, \text{ m}^3/\text{d}$ (Figure 20).
- (ii) The volume of abstracted water, which is radially reinjected into the *Aquifer Treatment Zone* at a distance r_{inj} from the abstraction well is denoted as $y \text{ m}^3/\text{d}$ (Figure 20).
- (iii) The volume of water, which is used for irrigation = m (Figure 20).
- (iv) The volume of water present in a confined (or closed) proposed *Aquifer Treatment Zone* during recycle is W_{TZ1} .

F1.2. Closed Environment

In a closed environment, the amount of water entering the system exactly equals the amount of water leaving the system. The recycle ratio has the effect of increasing t_d within the reaction environment.

The iso-potentials will require any water $(x + y)$ in the treatment zone to flow to the abstraction well [75,91,92,171].

F1.3. Recycle Loop

Introducing a recycle loop (Figure 20) with reinjection, (or infiltration), at the periphery of the *Aquifer Treatment Zone*, within a totally closed reactor system, increases the effective residence time (R_{et}). The effective residence time (R_{et}) of the water within the treatment zone is: $(W_{TZ1}/m)(R_{rc} + 1)$ [169,170,172,173]. The effective t_d in an environment incorporating recycle is R_{et} . It follows from (i) Equations (A1) to (A4), that increasing R_{rc} will increase k_r ; (ii) Equations (C14) to (C21), that the equilibrium establishment of $(V - D)$ can result in B_S increasing, as R_{rc} increases.

F2. Primary Engineering and Hydrological Concepts Associated with Catalytic Recycle

F2.1. Semi-Closed Aquifer Treatment Zone With Aggressive Recycle

A semi-closed *Aquifer Treatment Zone* is created when the water volume retained within the iso-potential contours remains constant with time. The hydrology of this type of system is complex, but relies on:

- (i) a strong negative potential being created by the abstraction well, and
- (ii) a dispersed, low positive potential being associated with reinjection, (or infiltration), of the recycle water on the periphery of the *Aquifer Treatment Zone*.

Volumetric balance is maintained within the bounding iso-potential contour:

- (i) by matching the net fluid outflow from the system for irrigation water, with
- (ii) a dispersed inflow around the treatment zone periphery by fresh saline water from the aquifer.

The permeability of the aquifer and the recycle ratio will control the number of reinjection sites and the shape of the iso-potential contours. Increasing the potential associated with a reinjection or infiltration loci beyond a critical level can, in some circumstances, result in leakage from the *Aquifer Treatment Zone* into the wider aquifer (Figure 20).

Trials (Figure C5, Tables E1 and F1) of a “*semi-closed Aquifer Treatment Zone with Recycle*” established that increasing the recycle ratio increased the rate of desalination (where $n = 0$, and $m \geq 0$, $x = m$).

The cost of installing and operating a proposed *Aquifer Treatment Zone* with recycle is reduced if:

- (i) the recycle ratio can be reduced;
- (ii) the number of ZVI loci and infiltration loci can be reduced;
- (iii) the volume of water contained within the aquifer treatment zone can be reduced.

Each of these parameters is controlled by the ZVI catalyst used. The ZVI catalyst controls (Table F1):

- (i) the ZVI requirement;
- (ii) the number of ZVI loci;
- (iii) the amount of desalination;
- (iv) the reinjection/reinfiltration requirement;
- (v) the size of the *Aquifer Treatment Zone*;
- (vi) the amount of irrigation water which can be abstracted from a specific *Aquifer Treatment Zone* Volume.

Reinjection is widely used in the petroleum industry to reconfigure an aquifer as an enhanced oil recovery zone (e.g., [174,175]). Reinjection creates additional aquifer issues relating to aerial, vertical and volumetric sweep efficiency, irregular water encroachment, water breakthrough, differential water mobility, integrity of the upper and lower bounding aquitards, etc. [174,175]. All of these problems may apply to an *Aquifer Treatment Zone* which incorporates recycle.

Table F1. Expected Performance of a semi-confined schematic *Aquifer Treatment Zone* containing 4000 m³ of water. The data values (and scaled volumes) are based on trial observations (Figures B2 and C5, Table E1). The aquifer volumes and feed water salinities have been normalized to demonstrate the operational differences between the catalysts. The duration of all the sub-optimized trials was extended beyond the initial appearance of B_5 . Optimized irrigation water production rates assume that t_d approximates to the start of B_5 . Catalyst ST* is a *Type A Catalyst*. Catalysts C to K are *Type B Catalysts*. ZVI required is based on trial data and has not been optimized.

Trial Group	Aquifer Volume, m ³	Irrigation Water (without Optimisation), m ³ ·day ⁻¹	Recycle Water, m ³ ·day ⁻¹	Optimised Irrigation Water, m ³ ·day ⁻¹	Feed Water Salinity, g·L ⁻¹	Product Water Salinity, g·L ⁻¹	Mean Desalination	Mean Na ⁺ Removal	ZVI Required, t	Catalyst
ST	4000	20	0	20	4.00	1.84	54.0%	54.0%	120	ST
RC1	4000	16,552	59,586	24,000	4.00	2.88	28.0%		93.12	C
RC1a	4000	18,113	65,208		4.00	2.88	28.1%	38.9%	93.12	
RC2	4000	4334	48,000	16,000	4.00	2.88	27.9%		2.00	D
RC3	4000	2133	43,200	32,000	4.00	1.19	70.2%		112.00	E
RC4	4000	197	59,586	8,000	4.00	2.64	33.9%		35.16	F
RC5	4000	5071	59,586	19,200	4.00	2.84	28.9%		19.20	G
RC6	4000	4878	59,586	16,000	4.00	2.21	44.6%		3.44	H
RC7	4000	6194	59,586	19,200	4.00	3.19	20.4%		18.64	I
RC8	4000	20,961	59,586	32,000	4.00	3.28	18.0%		3.44	J
RC9	4000	2246	7,200	16,000	4.00	2.43	39.3%		0.28	K
RC9a	4000	9600	7,200		4.00	2.41	39.6%	50.6%	0.28	

F3. Modeling of Catalytic Recycle

F3.1. Desalination Without Recycle: Type A Catalyst

The passage of saline (4 g/L) aquifer water through a 4000 m³ *Aquifer Treatment Zone* (using the ST* series catalyst, A2, B1–B3) which has:

- (i) a 60 m radius around the abstraction well,
- (ii) 20 m³·day⁻¹ abstraction (without recycle, i.e., $y = 0$ m³·day⁻¹; $m = x = 20$ m³·day⁻¹),
- (iii) $t_d = 200$ days,

is expected (Figure B2) to result in the salinity of the abstracted irrigation water, reducing from 4 g/L to about 1.84 g/L (Table F1). This is equivalent to a 54% reduction in salinity (R_6), calculated as:

$$R_6 = (100(1 - ((\text{Input salinity}(A_0) - \text{Output salinity}(A))/\text{Input salinity}(A_0))))), \quad (\text{F1})$$

F3.2. Desalination With Recycle: Type A Catalyst

In a closed system ($n = 0$ m³·day⁻¹), the additional feed water, W_4 , (e.g., $m = 20$ m³·day⁻¹) is mixed with the recycle water, W_5 , (e.g., $y = 480$ m³·day⁻¹) prior to entering the *Aquifer Treatment Zone* (Figures F2 and F3). The salinity of the water (C_6) entering the *Aquifer Treatment Zone* can be calculated as:

$$C_6 = (C_0 (W_4/(W_4 + W_5))) + (C_R (W_5/(W_4 + W_5))), \quad (\text{F2})$$

C_0 = aquifer water salinity; C_R = recycle water salinity. This model is expected to increase t_d from 200 days (using the ST catalyst) to $R_{es} = 5000$ days. This strategy is expected (Figure B2) to reduce the salinity by >98%.

F4. Hydrological Issues Associated with the Reinjection Loci

F4.1. Gravity Fed Reinjection Sites

The low recycle water volumes received by each reinjection loci (Tables E1 and F1) will allow gravity fed soakaways, or infiltration devices, to be used for reinjection. Infiltration devices can either be constructed to:

- (a) allow the infiltrating (reinjecting) water to enter the groundwater (aquifer) by percolation from above (e.g., [62–65,176–181]). This situation occurs when the base of the infiltration device is always above the groundwater piezometric surface;
- (b) allow the infiltrating (reinjecting) water to directly enter the groundwater (aquifer) by (e.g., [62–65]) when the base of the infiltration device is always below the groundwater piezometric surface [62–65].

F5. Desalination Issues Associated with Recycle

F5.1. Impact of Increasing the Aquifer Abstraction Rate without Recycle

The effective reduction in salinity = R_6 . Increasing the abstraction rate from 20 m³·day⁻¹ to 500 m³·day⁻¹ (when $y + n = 0$) decreases the average length of time taken for water to travel from the periphery of the proposed *Aquifer Treatment Zone* to the abstraction well (t_1) from 200 days to 8 days. R_6 associated with 200 days = 54% (Table F1, Figure B2). R_6 associated with 8 days = 3% (based on k_r for Catalyst ST*, Figures B1–B3).

The resultant salinity of the product water at time intervals of t_1 is:

$$C_R = C_6 (1 - R_6), \quad (\text{F3})$$

F5.2. Impact of Different Recycle Strategies

The salinity of the irrigation water recovered from the proposed *Aquifer Treatment Zone* will gradually decline with increased residence time. Figure F1 illustrates four scenarios associated with the Type A Catalyst ST* (Table F1).

Recycle is to a peripheral location, where $n = 0$ (Figure 20). This approach decreases the expected amount of desalination by reducing the average effective residence time of the water in the treatment zone on each cycle.

A conventional surface based reactor overcomes this problem by effectively expanding the volume of the reactor by the recycle ratio [169,170,172,173], i.e., from 4000 m³ to 96,000 m³. This increase in effective volume increases the average residence time of the water in the reaction environment from 200 days to 4800 days. This change would allow the expected irrigation water salinity in Figure F1 to reduce to less than 0.1 g/L.

A proposed *Aquifer Treatment Zone* is unable to expand the size of the aquifer to accommodate re-injection. Therefore the impact of reinjection (at a peripheral location) combined with recycle is to increase the salinity of the irrigation water, relative to the position with no reinjection and recycle (Figure F1).

In this instance, the salinity of the irrigation water (y_1) is less than the salinity of the aquifer (x_1) and greater than the salinity of the irrigation water with no recycle (z_1), i.e., $x_1 > y_1 > z_1$ (Figure F1).

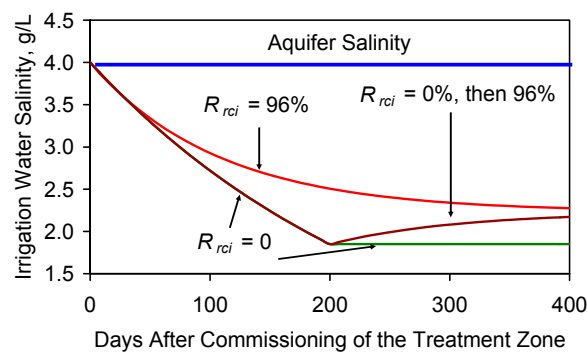


Figure F1. Change in salinity of the irrigation water abstracted from the modeled *Aquifer Treatment Zone* with time. Aquifer salinity = 4 g/L. Process Flow Diagram = Figure 20. R_{rci} = Reinjection ratio = $y/(y + m)$. Water reinjected at the aquifers periphery. (i) = aquifer salinity = irrigation water salinity without the *Aquifer Treatment Zone*; (ii) irrigation water salinity if $R_{rci} = 0$; (iii) irrigation water salinity if $R_{rci} = 0$ for 200 days, followed by $R_{rci} = 0.96$ (96% of the abstracted water is reinjected); (iv) irrigation water salinity if $R_{rci} = 0.96$. Aquifer Thickness = 1 m; Rate Constant = Figure B2b. Recycle ratio = $480/20 = 24$; $R_{rci} = y/(y + m)$, $m = 20 \text{ m}^3 \cdot \text{day}^{-1}$, $x = 20 \text{ m}^3 \cdot \text{day}^{-1}$, $y = 480 \text{ m}^3 \cdot \text{day}^{-1}$, $n = 0 \text{ m}^3 \cdot \text{day}^{-1}$ (Figure 20).

F5.3. Impact of Leakage of Reinjecting Water to the Principal Aquifer

Injection of the recycle water at loci on the periphery of the treatment zone may result in leakage of recycle water to the wider aquifer ($n \geq 0$ (Figure 20)). This will result in the inflow of fresh saline water from the aquifer into the *Aquifer Treatment Zone* (x , (Figure 20)) exceeding the amount of water abstracted for irrigation (m , (Figure 20)). In this instance:

- (i) the salinity of the irrigation water will increase (Figure F2) as the value of n increases;
- (ii) increasing n will result in the irrigation water salinity approaching the salinity of the saline aquifer (Figure F2).

The modeled examples in Figures F1 and F2, indicate that there is no advantage in reinjecting abstracted water on the periphery of the *Aquifer Treatment Zone*, as this is likely to create the situation where $x_1 > y_1 > z_1$, and in an extreme situation $x_1 = y_1$.

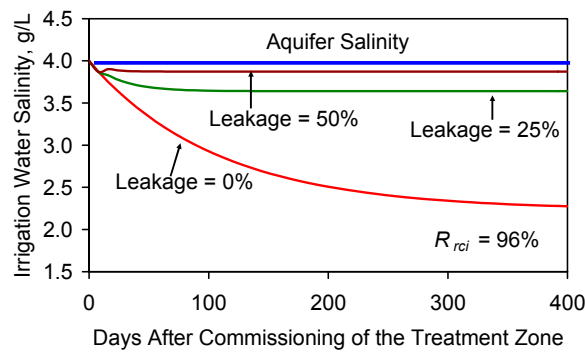


Figure F2. Change in salinity of the irrigation water abstracted from the modeled *Aquifer Treatment Zone* with time. Aquifer salinity = 4 g/L. Process Flow Diagram = Figure 20. R_{rci} = Reinjection ratio = 480/500. z_g (leakage) = $(n/(y + n))$. Assumptions: (i) $n = 0 \text{ m}^3 \cdot \text{day}^{-1}$. Leakage = 0%; (ii) $n = 120 \text{ m}^3 \cdot \text{day}^{-1}$; Leakage = 25%; (iii) $n = 240 \text{ m}^3 \cdot \text{day}^{-1}$. Leakage = 50%; Aquifer Thickness = 1 m; Rate Constant = Figure B2b.

F6. Impact of Changing Reinjection Location on Desalination

F6.1. Placement of the Injection Loci within the Aquifer Treatment Zone

The position of the injection loci can be moved from the periphery, to a point within the proposed *Aquifer Treatment Zone*. This may result in the amount of leakage (n) reducing to $0 \text{ m}^3 \cdot \text{day}^{-1}$. The benefit of this approach can be demonstrated by considering an example where the proposed *Aquifer Treatment Zone* periphery is:

- 50–60 m from the abstraction well (4524 m^3 water volume), and
- the injection loci are 30 m from the abstraction well (1131 m^3 water volume),

The expected water salinity within the aquifer at the point 30 m from the abstraction well is $2.24 \text{ g} \cdot \text{L}^{-1}$. The impact of re-injection at this location is to gradually reduce the salinity of the irrigation water (Figure F3) into the range $1.3\text{--}1.4 \text{ g} \cdot \text{L}^{-1}$.

This reinjection strategy may create the situation where $x_1 > z_1 > y_1$.

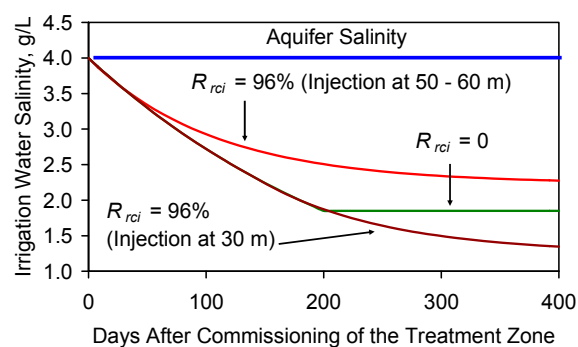


Figure F3. Change in salinity of the irrigation water abstracted from the modeled *Aquifer Treatment Zone* with time. Aquifer salinity = 4 g/L. Process Flow Diagram = Figure 20. R_{rci} = Reinjection ratio = 480/500. $z_g = (n/(n + y))$; $n = 0 \text{ m}^3 \cdot \text{day}^{-1}$; Assumptions: (i) No Injection; $n = 0 \text{ m}^3 \cdot \text{day}^{-1}$. Leakage = 0%; (ii) Injection at 50–60 m from the abstraction well; $n = 0 \text{ m}^3 \cdot \text{day}^{-1}$; Leakage = 0%; (iii) Injection at 30 m from the abstraction well; $n = 0 \text{ m}^3 \cdot \text{day}^{-1}$. Leakage = 0%; Aquifer Thickness = 1 m; Rate Constant = Figure B2b.

F7. Impact of Catalyst on Desalination

F7.1. Impact of Changing the Rate Constant

The modeled results in Figures F1–F3 assume that k_r is constant. The salinity of the product irrigation water (c_2) is a function of V :

Increasing aquifer fluid velocity, V (by increasing the recycle ratio) must

- (1) decrease c_2 (and increase k_r), unless
- (2) the increase in V is matched by a corresponding increase in the dispersion coefficient D (Equation (C21)).

In Figures F1–F3, the expression $(D - V)$ remains constant as V increases, or decreases. The trial data in Figure C6, Tables E1 and F1 demonstrate that $(D - V)$ decreases (and k_r increases) as V increases.

The implications of this observation are:

- (i) reinjection at the periphery of the *Aquifer Treatment Zone* without leakage, (with the desalination rate constants (for $V = 0.5$ m/h) will result in $(D - V)$ decreasing as V increases;
- (ii) suitable catalyst design (combined with reinjection) may allow the residence time required to reduce the water salinity to the required level to be substantially reduced, relative to a base case with no reinjection (Figure F4).

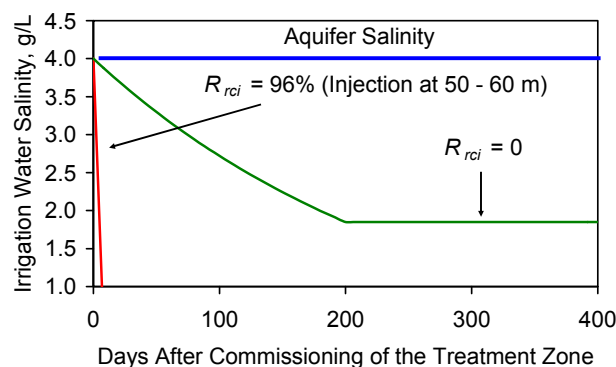


Figure F4. Change in salinity of the irrigation water abstracted from the modeled *Aquifer Treatment Zone* with time. Aquifer salinity = 4 g/L. R_{rci} = Reinjection ratio = 480/500. Assumptions: (i) No Injection; $n = 0$ m³·day⁻¹. Leakage = 0%; (ii) Injection at 50–60 m from the abstraction well; $n = 0$ m³·day⁻¹; Leakage = 0%; Aquifer thickness = 1 m.

F7.2. Equilibrium or Base Salinity Level

If V is set at a constant value, then (for most *Type B catalysts*) the value for $(D - V)$ reaches an equilibrium value after 3 to 60 h [16,17]. The associated equilibrium salinity level, B_S [17,36,37] is between 30% and 85% of the initial water salinity ($A_0, C_{t=0}$), i.e., between $0.3 C_{t=0}$ and $0.85 C_{t=0}$. Active management of the reinjection process may allow B_S (Figure F5) to be controlled and actively manipulated.

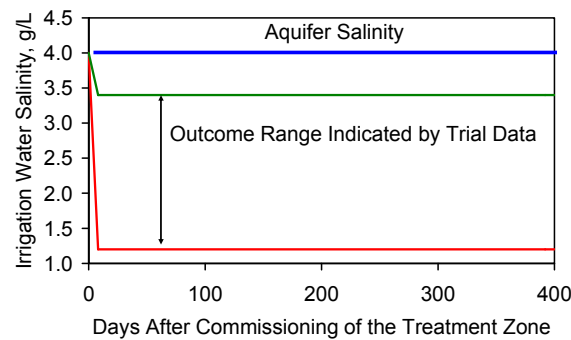


Figure F5. Change in salinity of the irrigation water abstracted from the modeled *Aquifer Treatment Zone* with time. Aquifer salinity = 4 g/L. R_{rci} = Reinjection ratio = 480/500. Injection at 50–60 m from the abstraction well; $n = 0 \text{ m}^3 \cdot \text{day}^{-1}$; Leakage = 0%; B_S range taken from Tables E1 and F1. Aquifer thickness = 1 m.

Appendix G. Modeling Aquifer Heterogeneity, Static Strategy

G1. Impact of Geology on Desalination

Heterogeneous aquifers contain permeability variations, thickness variations, facies changes, and flow compartments. The net impact of increasing permeability variation within the aquifer is to:

- (i) increase differential flow from the aquifer to the abstraction well through the *Aquifer Treatment Zone*;
- (ii) decrease the effective residence time of the aquifer water as it passes through a fixed volume *Aquifer Treatment Zone* to the abstraction well. Figures B1 and C3 demonstrate that any decrease in residence time, must for a specific k_r , decrease the amount of desalination.

G2. Impact of Permeability Variation within the Aquifer

Permeability variations within the aquifer will result in differential flows within the *Aquifer Treatment Zone*. In a simple example, the abstraction well may intersect a higher permeability zone within the aquifer (e.g., Figure G1). In this instance, the abstraction well will receive water (J) from two sources: (i) a higher permeability zone; and (ii) a lower permeability zone.

$$J = [Q_{\text{higher permeability aquifer}} + Q_{\text{lower permeability aquifer}}], \quad (\text{G1})$$

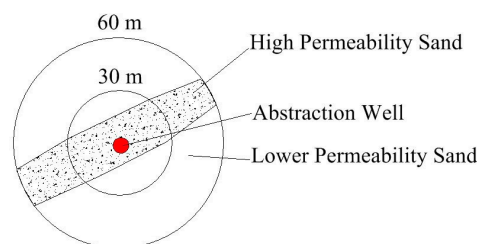


Figure G1. Schematic plan view of a schematic aquifer showing the 60 m radius of the treatment zone, abstraction well, and the distribution of the lower and higher permeability sand (aquifer).

In the simple example illustrated in Figure G1, the higher permeability facies occupies 26% of the area (and rock volume). The permeability (or hydraulic conductivity) of the higher permeability facies, may be 10 times that of the lower permeability facies:

- (i) The initial design of the aquifer (based on the lower permeability aquifer) will assume that the average residence time is 200 days (based on a $20 \text{ m}^3 \cdot \text{day}^{-1}$ abstraction rate).

- (ii) The presence of the higher permeability sand will result in an average residence time within this higher permeability sand of 20 days. This will result in about 80% of the abstracted water being derived from this sand. The remaining 20% will be derived from the lower permeability sand.

This differential permeability will result in (Figure G2a):

- (i) water arriving at the abstraction well from both the lower permeability aquifer and the higher permeability sand;
- (ii) the water contribution to abstraction well from the higher permeability sand will be $16 \text{ m}^3 \cdot \text{day}^{-1}$; salinity (c_h) = $3.7 \text{ g} \cdot \text{L}^{-1}$;
- (iii) the average equilibrium residence time of the water within the lower permeability sand increasing to 814 days (based on 3256 m^3 water volume in the lower permeability sand and a $4 \text{ m}^3 \cdot \text{day}^{-1}$ abstraction rate); salinity (c_l) = $0.17 \text{ g} \cdot \text{L}^{-1}$;

G3. Assessing the Relative Contribution of Different Water Sources

There are a number of different approaches which could be used to account for the relative contribution of the two different sandstone facies to the abstracted water (e.g., [182–184]). In this study, the assumption made (e.g., [182]) is:

$$J = (a/a + b)[k_{\text{higher permeability aquifer}} \Phi] + (b/a + b)[k_{\text{lower permeability aquifer}} \Phi], \quad (\text{G2})$$

a = water volume in the higher permeability aquifer; b = water volume in the lower permeability aquifer. This simple assessment approach allows the expected salinity (c) of the abstracted irrigation water to be assessed, for illustration purpose, as:

$$c = (a/a + b)c_h + (b/a + b)c_l, \quad (\text{G3})$$

$$\delta c / \delta t = (a/a + b)\delta c_h / \delta t + (b/a + b)\delta c_l / \delta t, \quad (\text{G4})$$

The net impact of the higher permeability zone is to increase the salinity of the irrigation water, when compared with expected salinity associated with the homogenous design case (Figure G2). The net impact of increasing the ratio of $[Q_{\text{higher permeability aquifer}} / Q_{\text{lower permeability aquifer}}]$ is to increase the equilibrium salinity of the abstracted irrigation water (Figure G2a).

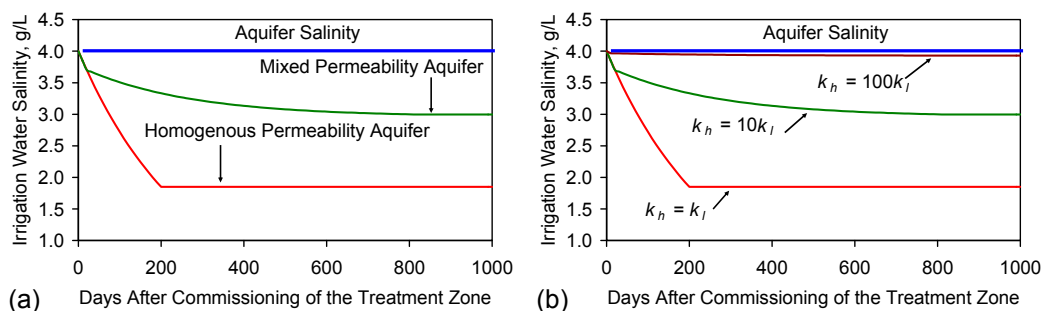


Figure G2. Expected (modeled) salinity of the irrigation water as a function of time. (a) The mixed permeability aquifer case illustrated in Figure G1; (b) Mixed permeability aquifer demonstrating the impact of changing the ratio of permeabilities between the higher permeability aquifer (k_h) and the lower permeability aquifer (k_l). Assumption: Average water residence time in the Aquifer Treatment Zone = 200 days when $(k_h) = (k_l)$; 20 days when $(k_h) = 10(k_l)$; 2 days when $(k_h) = 100(k_l)$; Aquifer Thickness = 1 m; Rate Constant = Figure B2b. $(y + n) = 0$.

G4. Impact of Differential Permeability Variation (and Flow by-Pass) within the Aquifer

In most aquifers, permeability changes are associated with discrete facies within the aquifer [185]. These may form:

- (i) channels (e.g., Figure G1; Figure G2a), or;
- (ii) a series of higher permeability discrete lenses [185] within the treatment zone. This results in the effective by-pass of some of the surrounding lower permeability aquifer [185]. The net result of this change is to increase the equilibrium abstracted water salinity (when compared with a homogenous aquifer). The exact changes will be location specific, but the general trend expected is demonstrated in Figure G2b.

Abbreviations and Symbols

A	cross-sectional area of the flow pathway;
A	anion in chemical equations;
A_c	actual cost of supplying the partially desalinated irrigation water, $\$/\text{m}^3$;
A_r	aromatic chemical with an OH group;
A_R	required abstraction rate, $\text{m}^3 \cdot \text{day}^{-1}$;
A_T	Net water column thickness in the aquifer, m;
A_V	required aquifer volume, m^3 ;
A_{inf}	area of the base of the infiltration device, m^2 ;
A_{sinf}	area of the sides of the infiltration device, m^2 ;
$[A]$	NaCl, or Cl^- , or Na^+ concentration at time $t = n$;
$[A_0]$	NaCl concentration at time $t = 0$;
a	fractional yield change due to fertilizer application;
a	a constant (Equation (26));
a_1	plants per hectare;
a_s	normalized surface area of ZVI particle, $\text{m}^2 \cdot \text{g}^{-1}$.
a_{si}	particle size, e.g., nm, mm;
B_S	irreducible salinity;
b	fractional yield change due to fungicide application;
b_1	seed pods, or grain heads, or fruit per plant;
$C_{t=0}$	feed water salinity at time $t = 0$;
$C_{t=n}$	product water salinity at time $t = n$;
C_0	aquifer water salinity;
C_R	recycle water salinity.
C_S	water salinity entering the <i>Aquifer Treatment Zone</i> ;
c	fractional yield change due to pesticide application;
c_2	concentration of [A] where $([A]/[A_0])$ increases with increasing distance from x ;
c_1	number of fruit or seeds per pod/head/plant;
c_{1s}, c_{2s}	linear regression defined constants linking salinity to crop yield decrement;
D	constant dispersion coefficient
D_d	dispersion tensor;
D_m	effective molecular diffusion coefficient;
D_r	fractional amount of desalination that has occurred;
d	fractional yield change due to herbicide application;
d_1	seeds or fruit per unit weight, t;
d_p	pore throat width (diameter), nm;
d_w	density of water;
e	fractional yield change due to bactericide application;
E	$\beta_1 E_0$;
E_0	characteristic energy of adsorption of a standard adsorbate;
E_p	average potential energy for the molecules being adsorbed (KJ/mole);
E_1	characteristic energy for a specific fluid-solid system;
F	Faraday Constant;
F_d	The driving force for the discharge between the distribution tank and the invert point in the infiltration loci;
F_1	Incremental increase in financing costs associated with the increased yield, \$;
g	gravitational constant;
g_1	a ZVI Loci within a treatment (desalination) zone at a point x, y, z ;

h	hydraulic head, e.g., $m^3 = h_1$ (upstream water source elevation) $- h_2$ (downstream water discharge elevation);
h_{1a}	vertical distance between the invert point (intersect point) of the drainage pipe with the infiltration loci and the aquifer water table;
h_{1b}	vertical distance between the ground level and the aquifer water table;
h_{1c}	vertical distance between the water level in the distribution tank and the aquifer water table;
h_{1t}	depth of water in the infiltration loci measured from the base of the loci, if the base is located above the aquifer water table, or the surface of the water table if the base of the loci is located below the base of the aquifer water table;
I	identity tensor;
I_1	total length of flow path in the aquifer, m;
I_c	aquifer water volume (m^3) where the chemistry of the aquifer water has been altered by the ZVI;
I_{c1}	Installation cost, \$;
I_w	Irrigation water volume required, $m^3 \cdot \text{day}^{-1}$;
J	mass flux;
J	the infiltration rate or flux, $m^3 \cdot s^{-1}$, at time, t , at an infiltration loci;
J_{adv}	advective mass flux;
J_{dif}	mass flux due to molecular diffusion across the saturated pore space;
J_{dis}	dispersive mass flux;
K	a permeability constant;
k	intrinsic permeability, $m^3 \cdot m^{-2} \cdot s^{-1} \cdot Pa^{-1}$; $k = Q/P$;
k_{hinf}	intrinsic horizontal permeability of the sides of the infiltration device, $m^3 \cdot m^{-2} \cdot s^{-1} \cdot Pa^{-1}$;
k_{vinf}	intrinsic vertical permeability of the base of the infiltration device, $m^3 \cdot m^{-2} \cdot s^{-1} \cdot Pa^{-1}$;
$k_{aquifer}$	Intrinsic permeability of the aquifer;
k_0	intrinsic permeability at saturation;
k_{actual}	normalized actual rate constant = $k_{observed} / (a_s P_w)$
k_{ad}	Dubinin-Radushkevich isotherm constant ($M^2 \cdot kJ^{-2}$);
$k_{observed}$	observed rate constant = k_r ;
kp	rate of particle growth;
k_r	the rate constant (unit (e.g., moles) per unit time (e.g., seconds) per unit ZVI);
k_{10}	$\text{Log}_{10} k_r$;
K	a permeability constant = uI_1/h ; $K = 1$ Darcy when $u = 1 \text{ cm} \cdot s^{-1}$;
K_n	Knudsen Number;
L	liquid phase;
L	Apparent flow path length;
L_c	Actual flow path length. $L_c = L$ when the pores are represented by perfect cylinders. In most pores, $L_c > L$;
L_T	required land take size, m^2 ;
l	reference column length, m;
M_c	maximum sustainable cost (M_c , $\$/m^3$) of desalination for irrigation water for a specific crop, or agricultural holding;
M_n	Manning number for the recycle pipe;
m	a factor which is related to pore size distribution;
N_G	Aquifer net to gross ratio (i.e., net aquifer volume/total (aquifer + aquitard) volume within the aquifer unit);
n_t	number of electrons transferred;
$n1$	a saturation constant; Calculated as $g + (j + d)/b$ where $g + j + b + d$ are constants; and $n1$ is in the range 0.1 to 25;
$n2$	a reaction order constant, e.g., 1;
$n3$	number of hours on line;
O.D.	outer diameter;
O_1	Incremental increase in operating costs and infra-structure costs associated with the increased yield, \$;
O_c	Operating Cost, \$;

P	bulk pressure exerted by the water, constant driving force, Pa (or head, m); In this study $P = P_r = \Phi$;
P_a	adsorption pressure;
P_i	the amount of ZVI in the <i>Aquifer Treatment Zone</i> e.g., $\text{g}\cdot\text{m}^{-3}$;
P_p	the fluid pore pressure within the pore;
P_r	pressure difference, Pa, represented by h;
P_s	initial pressure;
P_A	aquifer pressure;
P_1	Profit required by the agricultural holding on the increased yield, \$;
P_w	amount of ZVI in a batch flow reactor; e.g., $\text{g}\cdot\text{L}^{-1}$, or $\text{g}\cdot\text{m}^{-3}$;
Q	normalized flow rate, (volume) (unit time) $^{-1}$ or flow rate, (volume) (unit time) $^{-1}$ (unit weight, area, or volume of ZVI (or aquifer)) $^{-1} = kP_r = k\Phi$.
Q_{aquifer}	aquifer flow rate prior to reconstruction as an <i>Aquifer Treatment Zone</i> ;
q_e	ion removed at equilibrium/unit ZVI (g/g);
q_s	theoretical isotherm saturation capacity, g/g;
q	mass flux;
r	pore throat radius, m;
r_a	radius of circular desalination treatment field;
r_e	represents the radial distance from the abstraction well bore where $\Phi_{\text{Initial (aquifer)}} = \Phi_{\text{abstraction well}}$;
r_1	radial distance from the abstraction well;
r_{inj}	radial distance of an injection loci from the abstraction well;
R	the gas constant;
R^2	coefficient of determination;
R_{ef}	Removal Efficiency (%);
R_{rc}	Reinjection or Recycle Ratio = y/x ;
R_{rci}	Reinjection or Recycle Fraction of Abstracted Water = $y/(x + y)$;
R_{rt}	Average residence time of the water in the reaction environment;
R_6	Reduction in salinity (%);
R_{wp}	wetted perimeter of the recycle pipe, m, ft;
R_1	Sale price of crop, \$/t;
R_2	Number of days the water is required to reside in the <i>Aquifer Treatment Zone</i> in order for its salinity to reduce to the required level;
S	slope of recycle pipes;
S_m	minimum slope of recycle pipes required to meet local regulations;
SV	space velocity, m^3 (water) $t^{-1}\cdot\text{W}^{-1}$;
S_p	water saturation after exclusion of porosity for precipitates, $0 < S_p < (1 - S_{wi})$; = $[\varphi(t=0) - \varphi(t=n)]^3 / [(1 - (\varphi(t=0) + \varphi(t=n)))/(1 - (\varphi(t=0)))^2]$, when $n_2 = 1$ [119];
S_w	mobile water saturation, $0 < S_w < (1 - S_{wi})$;
S_{wi}	irreducible water saturation, $0 < S_{wi} < 1$;
T	temperature, K;
T_F	dispersed treatment field;
T_h	aquifer thickness, m;
t	unit time, e.g., seconds (s), hours (h), days, years (a);
t_d	Residence time in the reaction environment = Flow rate, or abstraction rate (m^3 /unit time)/Volume of the reaction environment;
u	flow velocity ($\text{cm}\cdot\text{s}^{-1}$);
V	a constant fluid velocity at a point x , created by an abstraction well at time t ;
V_0	the initial inter-particle nano-meso-macro pore volume which is not in direct communication with the main water body (dead-end porosity);
V_{op}	the initial inter-particle nano-meso-macro pore volume, which is in direct communication with the main water body;
V_{fb}	minimum full bore velocity (or 75% full bore velocity) required in the recycle pipes to meet regulatory requirements, $\text{m}\cdot\text{s}^{-1}$, $\text{m}^3\cdot\text{m}^{-2}\cdot\text{s}^{-1}$;
V_x	volume (NaCl) adsorbed at a relative pressure of (P_a/P_s) and temperature, T ;
V_{aq}	volume of water required within the <i>Aquifer Treatment Zone</i> , m^3 ;

v	fluid velocity within the pore space;
W	Normalized ZVI (or aquifer) unit, e.g., weight (t), volume (m^3), cross sectional area (m^2);
W_{RT}	required water residence time in the reaction environment;
W_{TZ}	minimum amount of water (m^3) located within the <i>Aquifer Treatment Zone</i> ;
W_{TZ1}	amount of water (m^3) located within the <i>Aquifer Treatment Zone</i> ;
W_1	amount of partially desalinated water which is required to achieve the increased yield, m^3 ;
W_4	additional feed water from the wider aquifer which is mixed with the recycle water in the <i>Aquifer Treatment Zone</i> . This water replaces water which is lost due to leakage of recycle water to the wider aquifer;
W_5	residual recycle water (after losses due to leakage into the wider aquifer);
x and x,y,z	a point within a continuum, e.g., a spatial location where x, y, z are referenced to specific locations and datum. For example, z refers to elevation; x refers to north-south position; y refers to east-west position;
x	water flow rate abstracted from the <i>Aquifer Treatment Zone</i> for irrigation; Saline water entering the <i>Aquifer Treatment Zone</i> from the aquifer;
x_1	salinity of the aquifer;
y	water flow rate abstracted from the <i>Aquifer Treatment Zone</i> for reinjection/recycle;
y_1	Salinity of the irrigation water abstracted from the <i>Aquifer Treatment Zone</i> with recycle—“ <i>Recycle Strategy</i> ”;
Y	crop yield, t/ha, when irrigated with non-saline (fresh) water;
Y_{S1}	Crop yield using salinized water, t;
Y_{S2}	Crop yield using partially desalinated water, t;
Y_S	Salinity Adjusted Yield (t/ha);
Z_1	weight of ZVI.
z	$(h_1 - h_2)$; This application is used to define potential;
z	water flow rate associated with losses from the <i>Aquifer Treatment Zone</i> to the wider aquifer associated with reinjection/recycle; This results in the water volume entering the <i>Aquifer Treatment Zone</i> from the aquifer being calculated as $(x + z)$;
z_p	the negative pressure, Pa, created by the abstraction pump at the infiltration loci;
z_1	Salinity of the irrigation water abstracted from the <i>Aquifer Treatment Zone</i> without recycle—“ <i>Static Strategy</i> ”;
z_g	Reinjection loss ratio = z/y ;
α	solid (crystallized) phase;
α	order of fractional differentiation; $1 < \alpha \leq 2$;
β	solid (crystallized) phase;
β_1	the affinity coefficient of the adsorbate;
δ	differential;
ε	Dubinin-Radushkevich isotherm constant, g.
$\Delta k_{aquifer}$	permeability gradient;
ΔP_r	pressure gradient;
$\Delta Q_{aquifer}$	flow gradient;
Δ	gradient operator;
$\Delta \Phi$	Potential gradient;
φ	Inter-particle or inter-aggregate porosity = $V_o + V_{op}$;
η	fluid viscosity, $N \cdot s^{-1} \cdot m^{-2}$;
Φ	Fluid potential (Pa), e.g., $\Phi = P_A/d_w + gz$;
$\Phi_{Initial (aquifer)}$	Fluid potential (Pa) associated with the aquifer (at a location x m from the abstraction well) prior to the pump associated with the abstraction well being switched on;
$\Phi_{abstraction well}$	Fluid potential (Pa) associated with the aquifer (at a location x m from the abstraction well) after the pump associated with the abstraction well being switched on;
τ	pore tortuosity, e.g., $(L_c/L)^2$;
σ	complexity of pore geometry.

Material and Other Abbreviations

ABS	abacrylonitrile-butadiene-styrene;
Buna-N	abCopolymer of butadiene and acrylonitrile;
BS2846	abBritish Standard BS2846: Part 1, Routine analysis of quantitative data. Issued by the British Standards Institute.
CPVC	abchlorinated polyvinyl chloride;
EC	abelectrical conductivity, $\text{mS}\cdot\text{cm}^{-1}$; $\text{dS}\cdot\text{m}^{-1}$;
Eh	abpotential calculated using the standard hydrogen electrode, mV; At pH 4 in quinhydrone solution $E_h = \text{ORP} + 265.1 \text{ mV}$; at pH 7 in quinhydrone solution $E_h = \text{ORP} + 87.4 \text{ mV}$;
EPDM	abEthylene-propylene-diene monomer;
FEHED	abFront-end hydrological engineering and design;
FPM	abFluoro-carbon elastomer;
GRP	abGlass reinforced plastics;
HDPE	abhigh density polyethylene;
MDPE	abMedium density polyethylene;
MSFD	abmultistage flash distillation;
ORP	aboxidation reduction potential, mV;
C_{red}	abreductant concentration;
PA 11	polyamide 11;
PB	abpolybutylene;
PE	abpolyethylene;
PEX	abcross-linked polyethylene;
PIR	abpolyisocyanurate;
PK	abpolyketone;
PP	abpolypropylene;
PRB	abPermeable Reactive Barrier;
PTFE	abpolytetrafluoroethylene;
PVC	abpolyvinyl chloride;
PVDF	abpoly vinylidene fluoride;
PVP	abpolyvinylpyrrolidone;
RO	abReverse osmosis;
SBR	abstyrene-butadiene;
ZVI	abZero valent iron, Fe^0 . The term is also used in this study to describe manufactured, structured, desalination catalysts, which have been manufactured using Fe^0 as a starting ingredient, e.g., [16].

References

1. Hoogeveen, J.; Faures, J.M.; Peiser, L.; Burke, J.; van de Giesen, N. GlobWat—A global water balance model to assess water usage in irrigated agriculture. *Hydrol. Earth Syst. Sci.* **2015**, *19*, 3829–3844. [[CrossRef](#)]
2. Jaramillo, F.; Destouni, G. Local flow regulation and irrigation raise human water consumption and footprint. *Science* **2015**, *350*, 1248–1251. [[CrossRef](#)] [[PubMed](#)]
3. Wada, Y.; Florke, M.; Hanasaki, N.; Eisner, S.; Fischer, G.; Tramberend, S.; Satoh, Y.; van Vliet, M.T.H.; Yillia, P.; Ringler, C.; et al. Modelling global water use for the 21st Century: The Water Futures and Solutions (WFaS) initiative and its approaches. *Geosci. Model Dev.* **2016**, *9*, 175–222. [[CrossRef](#)]
4. Brauman, K.A.; Richter, B.D.; Postel, S.; Malsy, M.; Florke, M. Water depletion: An improved metric for incorporating seasonal and dry year water scarcity risk into water risk assessments. *Elem. Sci. Anthropocene* **2016**, *83*. [[CrossRef](#)]
5. Jagermeyr, J.; Gerten, D.; Schapoff, S.; Heinke, J.; Lucht, W.; Rockstrom, J. Integrated crop management might sustainably halve the global food gap. *Environ. Res. Lett.* **2016**, *11*, 025002. [[CrossRef](#)]
6. Jagermeyr, J.; Gerten, D.; Heinke, J.; Schaphoff, S.; Kumm, M.; Lucht, W. Water savings potentials of irrigation systems: Global simulation of process and linkages. *Hydrol. Earth Syst. Sci.* **2015**, *19*, 3073–3091. [[CrossRef](#)]
7. Lekakis, E.H.; Antonopoulos, V.Z. Modeling the effects of different irrigation salinity on soil water movement, uptake and multicomponent solute transport. *J. Hydrol.* **2015**, *530*, 431–446. [[CrossRef](#)]
8. Fishman, R.; Devineni, N.; Raman, S. Can improved agricultural water use efficiency save India's groundwater? *Environ. Res. Lett.* **2015**, *10*, 084022. [[CrossRef](#)]
9. OEDC. *Tackling the Challenges of Agricultural Groundwater Use*; Trade and Agriculture Directorate; OECD Publishing: Paris, France, 2016.

10. Kulmatov, R.; Rasulov, A.; Kulmatova, D.; Rozilhodjaev, B.; Groll, M. The modern problems of sustainable use and management of irrigated lands on the example of the Bukhara region (Uzbekistan). *J. Water Res. Protect.* **2015**, *7*, 956–971. [CrossRef]
11. Knapp, K.C.; Baerenklau, K.A. Ground water quantity and quality management: Agricultural production and aquifer salinization over long time scales. *J. Agric. Resour. Econ.* **2006**, *31*, 616–641.
12. FAO. *The State of the World's Land and Water Resources for Food and Agriculture (SOLAW)—Managing Systems at Risk*; Food and Agricultural Organization of the United Nations and Earth Scan: Abingdon, UK, 2011.
13. Amarasinghe, U.A.; Smakhtin, V. *Global Water Demand Projections: Past, Present and Future*; Report 156; International Water Management Institute (IWMI): Colombo, Sri Lanka, 2014.
14. Wada, Y.; Bierkens, M.F.P. Sustainability of global water use: Past reconstruction and future projections. *Environ. Res. Lett.* **2014**, *9*, 104003. [CrossRef]
15. Panta, S.; Flowers, T.; Lane, P.; Doyle, R.; Haros, G.; Shaala, S. Halophyte agriculture: Success stories. *Environ. Exp. Bot.* **2014**, *107*, 71–83. [CrossRef]
16. Antia, D.D.J. Desalination of water using ZVI, Fe⁰. *Water* **2015**, *7*, 3671–3831. [CrossRef]
17. Antia, D.D.J. ZVI (Fe⁰) Desalination: Stability of product water. *Resources* **2016**, *5*, 15. [CrossRef]
18. Potassium Nitrate Association. Effect of Salinity on Crop Yield Potential. PNA, Ternat, Belgium. Available online: <http://www.kno3.org/en/product-features-a-benefits/potassium-nitrate-and-saline-conditions/effect-of-salinity-on-crop-yield-potential-> (accessed on 15 June 2016).
19. Kim, H.; Jeong, H.; Jeon, J.; Bae, S. Effects of irrigation with saline water on crop growth and yield in greenhouse cultivation. *Water* **2016**, *8*, 127. [CrossRef]
20. Ayers, R.S.; Westcot, D.W. *Water Quality for Agriculture*; Irrigation and Drainage Paper No. 29, Rev. 1, Reprinted 1989, 1994; Food and Agriculture Organization of the United Nations: Rome, Italy, 1994.
21. Hill, R.; Koenig, R.T. *Water Salinity and Crop Yield*; Utah Water Quality AG-425.3; Utah State University Co-Operative Extension: Logan, UT, USA, 1999.
22. Grattan, S.R. *Irrigation Water Salinity and Crop Production*; Publication 8066. FWQP Reference Sheet 9.10; University of California, Agriculture and Natural Resources, Farm Water Quality Planning: Oakland, CA, USA, 2002.
23. Munns, R.; Gilliham, M. Salinity tolerance of crops—What is the cost? *New Phytol.* **2015**, *208*, 668–673. [CrossRef] [PubMed]
24. Yao, R.; Yang, J.; Wu, D.; Xie, W.; Gao, P.; Jin, W. Digital mapping of soil salinity and crop yield across a coastal agricultural landscape using repeated electromagnetic induction (EMI) surveys. *PLoS ONE* **2016**, *11*, e015377. [CrossRef] [PubMed]
25. Satir, O.; Berberoglu, S. Crop yield prediction under soil salinity using satellite derived vegetation indices. *Field Crops Res.* **2016**, *192*, 134–143. [CrossRef]
26. Qadir, M.; Quillerou, E.; Nangia, V.; Murtaza, G.; Singh, M.; Thomas, R.J.; Drechsel, P.; Noble, A.D. Economics of salt induced land degradation and restoration. *Nat. Res. Forum* **2014**, *38*, 282–295. [CrossRef]
27. APA Citation: World Losing 2000 Hectares of Farm Soil Daily to Salt Damage. 2014. Available online: <http://phys.org/news/2014-10-world-hectares-farm-soil-daily.html> (accessed on 15 June 2016).
28. Martinez-Alvarez, V.; Martin-Gorrioz, B.; Soto-Garcia, M. Seawater desalination for crop irrigation—A review of current experiences and revealed key issues. *Desalination* **2016**, *381*, 58–70. [CrossRef]
29. Barron, O.; Ali, R.; Hodgson, G.; Smith, D.; Qureshi, E.; McFarlane, D.; Campos, E.; Zarzo, D. Feasibility assessment of desalination application in Australian traditional agriculture. *Desalination* **2015**, *364*, 33–45. [CrossRef]
30. Lee, C.; Herbek, J. *Estimating Soybean Yield*; AGR—188, Cooperative Extension Service; University of Kentucky—College of Agriculture: Frankfort, KY, USA, 2005.
31. Heatherley, L.G. *Soybean Irrigation Guide for Midsouthern US*; Mississippi Soybean Promotion Board: Canton, MS, USA, 2014.
32. Monsanto. *2010 Demonstration Report: Soybean Irrigation Recommendations*; Monsanto Technology Development, The Learning Centre: Gothenburg, NE, USA, 2010.
33. Fronczyk, J.; Pawluk, K.; Michniak, M. Application of permeable reactive barriers near roads for chloride ions removal. *Ann. Wars. Univ. Life Sci.* **2010**, *42*, 249–259. [CrossRef]

34. Fronczyk, J.; Pawluk, K.; Garbulewski, K. Multilayer PRBs—Effective technology for protection of the groundwater environment in traffic infrastructures. *Chem. Eng. Trans.* **2012**, *28*, 67–72.
35. Hwang, Y.; Kim, D.; Shin, H.-S. Inhibition of nitrate reduction by NaCl adsorption on a nano-zero valent iron surface during concentrate treatment for water reuse. *Environ. Technol.* **2015**, *36*, 1178–1187. [[CrossRef](#)] [[PubMed](#)]
36. Antia, D.D.J. Desalination of groundwater and impoundments using nano-zero valent iron, Fe⁰. *Meteor. Hydrol. Water Manag.* **2015**, *3*, 21–38.
37. Antia, D.D.J. Desalination of irrigation water, livestock water, and reject brine using n-ZVM (Fe⁰, Al⁰, Cu⁰). In *Advanced Environmental Analysis: Applications of Nano-Materials*; Advanced Detection Science Series No. 10; Hussain, C.M., Kharisov, B., Eds.; Royal Society Chemistry: Oxford, UK, 2017; pp. 237–272.
38. Antia, D.D.J. Sustainable zero-valent metal (ZVM) water treatment associated with diffusion, infiltration, abstraction and recirculation. *Sustainability* **2010**, *2*, 2988–3073. [[CrossRef](#)]
39. Gupta, D.; Kim, H.; Park, G.; Li, X.; Eom, H.-J.; Ro, C.-U. Hygroscopic properties of NaCl and NaNO₃ mixture particles as reacted inorganic sea-salt aerosol surrogates. *Atmos. Chem. Phys.* **2015**, *15*, 3379–3393. [[CrossRef](#)]
40. Wise, M.E.; Semenuik, T.A.; Bruintjes, R.; Martin, S.T.; Russell, L.M.; Busek, P.R. Hygroscopic behaviour of NaCl bearing natural aerosol particles using environmental transmission electron microscopy. *J. Geophys. Res. Atmos.* **2007**, *112*, D10224. [[CrossRef](#)]
41. Bladh, K.W.; Bideaux, R.A.; Antony-Morton, E.; Nichols, B.G. *Handbook of Mineralogy*; Mineralogical Society of America: Chantilly, VA, USA, 2003.
42. Gribble, C.D.; Hall, A.J. *Optical Mineralogy, Principles and Practice*; George Allen and Unwin: London, UK, 1985.
43. Battey, M.H. *Mineralogy for Students*; Oliver & Boyd: Edinburgh, UK, 1972.
44. Craig, J.R.; Vaughan, D.J. *Ore Microscopy and Ore Petrography*; John Wiley and Sons: New York, NY, USA, 1994.
45. Short, M.N. *Microscopic Determination of the Ore Minerals*; US Geological Survey Bulletin 825; United States Department of the Interior: Washington, DC, USA, 1931.
46. Short, M.N. *Microscopic Determination of the Ore Minerals*; US Geological Survey Bulletin 914; United States Department of the Interior: Washington, DC, USA, 1940.
47. Cooke, S.R.B. *Microscopic Structure and Concentratability of the Important Iron Ores of the United States*; US Bureau of Mines Bull. 391; United States Department of the Interior: Washington, DC, USA, 1936.
48. Stewart, F.H. *Data of Geochemistry. Chapter Y. Marine Evaporites*; Geological Survey Professional Paper 440-Y; US Government Printing Office: Washington, DC, USA, 1963.
49. Kuster, Y.; Leiss, B.; Schramm, M. Structural characteristics of the halite fabric type ‘kristallbrocken’ from the Zechstein Basin with regard to its development. *Int. J. Earth Sci.* **2010**, *99*, 505–526. [[CrossRef](#)]
50. Pourbaix, M. *Atlas of Electrochemical Equilibria in Aqueous Solutions*, 1st ed.; NACE International, Cebelcor: Houston, TX, USA, 1974.
51. Hannington, M.D. The formation of atacamite during weathering of sulphides on the sea floor. *Can. Min.* **1993**, *31*, 945–956.
52. Sharkey, J.B.; Lewin, S.Z. Conditions governing the formation of atacamite and paratacamite. *Am. Min.* **1971**, *56*, 179–192.
53. Getahun, A.; Reed, M.H.; Symonds, R. Mount St Augustine volcano fumarole wall rock alteration: Mineralogy, zoning, composition and numerical models of its formation process. *J. Volcanol. Geotherm. Res.* **1996**, *71*, 73–107. [[CrossRef](#)]
54. Scott, D.A. *Metallography and Microstructure of ANCIENT and Historic Metals*; The Getty Conservation Institute: Marina del Rey, CA, USA, 1991.
55. Rodriguez, L.A.C.; Gonzalez, E.N.A. Nanoadsorbents: Nanoadsorbents for water protection. In *CRC Concise Encyclopedia of Nano-Technology*; Kharisov, B.I., Kharissova, O.V., Ortiz-Mendez, U., Eds.; CRC Press: Boca Raton, FL, USA, 2016; pp. 573–589.
56. Yusan, S.D.; Erenturk, S.A. Sorption behaviours of uranium (VI) ions on α -FeOOH. *Desalination* **2011**, *269*, 58–66. [[CrossRef](#)]

57. Wang, Z.-M.; Shindo, N.; Otake, Y.; Kaneko, K. Enhancement of NO adsorption on pitch-based activated carbon fibers by dispersion of Cu-doped α -FeOOH fine particles. *Carbon* **1994**, *32*, 515–521. [[CrossRef](#)]
58. Yusan, S.D.; Erenturk, S.A. Adsorption equilibrium and kinetics of U(IV) on beta type of akaganeite. *Desalination* **2010**, *263*, 233–239. [[CrossRef](#)]
59. Lan, B.; Wang, Y.; Wang, X.; Zhou, X.; Kang, Y.; Li, L. Aqueous arsenic (As) and antimony (Sb) removal by potassium ferrate. *Chem. Eng. J.* **2016**, *292*, 389–397. [[CrossRef](#)]
60. Kapoor, A.; Ritter, J.A.; Yang, R.T. On the Dubinin-Radushkevich equation for adsorption in microporous solids in the Henry's law region. *Langmuir* **1989**, *5*, 1118–1121. [[CrossRef](#)]
61. Nguyen, C.; Do, D.D. The Dubinin-Radushkevich equation and the underlying microscopic adsorption description. *Carbon* **2001**, *39*, 1327–1336. [[CrossRef](#)]
62. Antia, D.D.J. Formation and control of self-sealing high permeability groundwater mounds in impermeable sediment: Implications for SUDS and sustainable pressure mound management. *Sustainability* **2009**, *1*, 855–923. [[CrossRef](#)]
63. Antia, D.D.J. Interacting Infiltration Devices (Field Analysis, Experimental Observation and Numerical Modeling): Prediction of seepage (overland flow) locations, mechanisms and volumes—Implications for SUDS, groundwater raising projects and carbon sequestration projects. In *Hydraulic Engineering: Structural Applications, Numerical Modeling and Environmental Impacts*, 1st ed.; Hirsch, G., Kappel, B., Eds.; Nova Science Publishers: Hauppauge, NY, USA, 2010; pp. 85–156.
64. Antia, D.D.J. Interpretation of overland flow associated with infiltration devices placed in boulder clay and construction fill. In *Overland Flow and Surface Runoff*; Wong, T.S.W., Ed.; Nova Science Publishers: Hauppauge, NY, USA, 2013; pp. 211–286.
65. Antia, D.D.J. Prediction of overland flow and seepage zones associated with the interaction of multiple Infiltration Devices (Cascading Infiltration Devices). *Hydrol. Process.* **2008**, *21*, 2595–2614. [[CrossRef](#)]
66. Antia, D.D.J. Water remediation—Water remediation using nano-zero-valent metals (n-ZVM). In *CRC Concise Encyclopedia of Nanotechnology*, 1st ed.; Kharisov, B.I., Kharissova, O.V., Ortiz-Mendez, U., Eds.; CRC Press, Taylor & Francis Group: Boca Raton, FL, USA, 2016; pp. 1103–1120.
67. Antia, D.D.J. Modification of aquifer pore water by static diffusion using nano-zero-valent metals. *Water* **2011**, *3*, 79–112. [[CrossRef](#)]
68. Antia, D.D.J. Groundwater water remediation by static diffusion using nano-zero valent metals [ZVM] (Fe^0 , Cu^0 , Al^0), $n\text{-FeH}^{n+}$, $n\text{-Fe(OH)}_x$, $n\text{-FeOOH}$, $n\text{-Fe-[O}_x\text{H}_y]^{(n+/-)}$). In *Nanomaterials for Environmental Protection*, 1st ed.; Kharisov, B.I., Kharissova, O.V., Dias, H.V.R., Eds.; Wiley Inc.: Hoboken, NJ, USA, 2014; pp. 3–25.
69. Kodama, S.; Fukui, K.; Mazume, A. Relation of space velocity and space time yield. *Ind. Eng. Chem.* **1953**, *45*, 1644–1648. [[CrossRef](#)]
70. Winterbottom, J.M.; King, M.B. *Reactor Design for Chemical Engineers*; Stanley Thornes: Cheltenham, UK, 1999.
71. Smith, R. *Chemical Process Design and Integration*; John Wiley: Chichester, UK, 2005.
72. Kent, J.A. *Kent and Riegel's Handbook of Industrial Chemistry and Biotechnology*, 11th ed.; Springer Science: New York, NY, USA, 2007.
73. Ebbing, D.D.; Gammon, S.D. *General Chemistry*, 6th ed.; Houghton Mifflin Co.: Boston, MA, USA, 1999.
74. Wilkin, R.T.; McNeil, M.S. Laboratory evaluation of zero-valent iron to treat water impacted by acid mine drainage. *Chemosphere* **2003**, *53*, 715–725. [[CrossRef](#)]
75. Dake, L.P. *Fundamentals of Reservoir Engineering*; Elsevier: Amsterdam, The Netherlands, 1998.
76. Euzen, J.-P.; Trambouze, P.; Wauquier, J.-P. *Scale up Methodology for Chemical Processes*; Editions Technip: Paris, France, 1993.
77. Zlokarnik, M. *Scale-up in Chemical Engineering*; Wiley: Weinheim, Germany, 2006.
78. Li, J.; Kwauk, M. Exploring complex systems in chemical engineering—the multi-scale methodology. *Chem. Eng. Sci.* **2003**, *59*, 521–535. [[CrossRef](#)]
79. Garurevich, I.A. Foundations of chemical kinetic modeling, reaction models and reactor scale up. *J. Chem. Eng. Process. Technol.* **2016**, *7*, 2.
80. Piccinno, F.; Hischer, R.; Seeger, S.; Som, C. From laboratory to industrial scale: A scale-up framework for chemical processes in life cycle assessment studies. *J. Clean. Prod.* **2016**, *135*, 1085–1097. [[CrossRef](#)]

81. Henderson, A.D.; Demond, A.H. Long-term performance of zero valent iron permeable reactive barriers: A critical review. *Environ. Eng. Sci.* **2007**, *24*, 401–423. [[CrossRef](#)]
82. Araujo, R.; Castro, A.C.M.; Baptista, J.S.; Fluza, A. Nanosized iron based permeable reactive barriers for nitrate removal—Systematic review. *Phys. Chem. Earth* **2016**, *94*, 29–34. [[CrossRef](#)]
83. Ma, L.; Zhang, W.-X. Enhanced biological treatment of industrial wastewater with bimetallic zero-valent iron. *Environ. Sci. Technol.* **2008**, *42*, 5384–5389. [[CrossRef](#)] [[PubMed](#)]
84. Fan, J.-H.; Ma, L.-M. The pre-treatment by the Fe-Cu process for enhancing biological degradability of the mixed waste water. *J. Hazard. Mater.* **2009**, *164*, 1392–1397. [[CrossRef](#)] [[PubMed](#)]
85. Branan, C. *Rules of Thumb for Chemical Engineers*; Elsevier: Amsterdam, The Netherlands, 2005.
86. Tsagkari, M.; Couturier, J.-L.; Kokossis, A.; Dubois, J.-L. Early-stage capital cost estimation of biorefinery processes: A comparative study of heuristic techniques. *ChemSusChem* **2016**, *9*, 2284–2297. [[CrossRef](#)] [[PubMed](#)]
87. Wu, X.; Hu, Y.; Wu, L.; Li, H. Model and design of cogeneration system for different demands of desalination water, heat, and power production. *Chin. J. Chem. Eng.* **2014**, *22*, 330–338. [[CrossRef](#)]
88. Antia, D.D.J. Oil polymerisation and fluid expulsion from low temperature, low maturity, over pressured sediments. *J. Petrol. Geol.* **2008**, *31*, 263–282. [[CrossRef](#)]
89. Antia, D.D.J. Low temperature oil polymerisation and hydrocarbon expulsion from continental shelf and continental slope sediments. *Indian J. Petrol. Geol.* **2009**, *16*, 1–30.
90. Clark, I. *Groundwater Geochemistry and Isotopes*; CRC Press: Boca Raton, FL, USA, 2015.
91. Dahlberg, E.C. *Applied Hydrodynamics in Petroleum Exploration*; Springer: New York, NY, USA, 1982.
92. Brusaert, W. *Hydrology an Introduction*; Cambridge University Press: Cambridge, UK, 2005.
93. Neuman, S.P. Theoretical derivation of Darcy's Law. *Acta Mech.* **1977**, *25*, 153–170. [[CrossRef](#)]
94. Mulder, M. *Basic Principles of Membrane Technology*; Kluwer Academic Publishers: Dordrecht, The Netherlands, 1996.
95. Ye, G.; van Breugel, P.L.K. Modeling of water permeability in cementitious materials. *Mater. Struct.* **2006**, *39*, 877–885. [[CrossRef](#)]
96. Pereira, J.-M.; Arson, C. Retention and permeability properties of damaged porous rocks. *Comp. Geotech.* **2013**, *48*, 272–282. [[CrossRef](#)]
97. Berg, C.F. Permeability description by characteristic length, tortuosity, constriction and porosity. *Trans. Porous Media* **2014**, *103*, 381–400. [[CrossRef](#)]
98. Gudjonsdottir, M.; Palsson, H.; Eliasson, J.; Saevarsdottir, G. Calculation of relative permeabilities of water and steam from laboratory measurements. *Geothermics* **2015**, *53*, 396–405. [[CrossRef](#)]
99. Richards, L.A. The usefulness of capillary potential to soil moisture and plant investigations. *J. Agric. Res.* **1928**, *37*, 719–742.
100. Brusaert, W. A concise parameterization of the hydraulic conductivity of unsaturated soils. *Adv. Water Resour.* **2000**, *23*, 811–815. [[CrossRef](#)]
101. Douglas, J.F.; Gasiorek, J.M.; Swaffield, J.A. *Fluid Mechanics*, 4th ed.; Pearson: Harlow, UK, 2001.
102. Massey, B.; Ward-Smith, J. *Mechanics of Fluids*; Stanley Thornes: Cheltenham, UK, 1998.
103. Amiri, H.A.A.; Hamouda, A.A. Pore-scale modeling of non-isothermal two phase flow in 2D porous media: Influences of viscosity, capillarity, wettability and heterogeneity. *Int. J. Multiph. Flow* **2014**, *61*, 14–27. [[CrossRef](#)]
104. Guo, C.; Xu, J.; Wu, K.; Wei, M.; Liu, S. Study on gas flow through nano pores of shale gas reservoirs. *Fuel* **2015**, *143*, 107–117. [[CrossRef](#)]
105. Brodkey, R.S.; Hershey, H.C. *Transport Phenomena. Vol 1. Part 1- Basic Concepts in Transport Phenomena*; Brodkey Publishing: Columbus, OH, USA, 1988.
106. Childs, E.C.; Collis-George, N. The permeability of porous media. *Proc. R. Soc. Lond. A* **1950**, *201*, 392–405. [[CrossRef](#)]
107. Carmen, P.C. Fluid flow through granular beds. *Trans Inst. Chem. Eng. Lond.* **1937**, *15*, 150–166. [[CrossRef](#)]
108. Carmen, P.C. *Flow of Gases through Porous Media*; Academic Press: New York, NY, USA, 1956.
109. Brooks, R.H.; Corey, A.T. *Hydraulic Properties of Porous Media*; Hydrology Paper 3; Colorado State University: Fort Collins, CO, USA, 1964.

110. Mualem, Y. A new model for predicting the hydraulic conductivity of unsaturated porous media. *Water Resour. Res.* **1976**, *12*, 513–521. [[CrossRef](#)]
111. Mualem, Y. Hydraulic conductivity of unsaturated porous media: Generalized macroscopic approach. *Water Resour. Res.* **1978**, *14*, 325–334. [[CrossRef](#)]
112. Burdine, N.T. Relative permeability calculations from pore-size distribution data. *Pet. Trans. Am. Inst. Min. Metal. Pet. Eng.* **1953**, *198*, 71–78. [[CrossRef](#)]
113. Alexander, L.R.; Skaggs, R.W. Predicting unsaturated hydraulic conductivity from the soil water retention curve. *Trans. Am. Soc. Agric. Eng.* **1986**, *29*, 176–184. [[CrossRef](#)]
114. Van Genuchten, M.T.V. A closed form equation for predicting the hydraulic conductivity of unsaturated soils. *Soil. Sci. Soc. Am. J.* **1980**, *44*, 892–898. [[CrossRef](#)]
115. Leong, E.C.; Rahardjo, H. Permeability function for unsaturated soils. *J. Geotech. Geoenviron. Eng.* **1997**, *123*, 1118–1126. [[CrossRef](#)]
116. Fredlund, D.G.; Rahardjo, H.; Fredlund, M.D. *Unsaturated Soil Mechanics in Engineering Practice*; Wiley: New York, NY, USA, 2012.
117. Yang, Z.; Mohanty, B.P. Effective parameterizations of three nonwetting phase relative permeability models. *Water Resour. Res.* **2015**, *51*, 6520–6531. [[CrossRef](#)]
118. Iden, S.C.; Peters, A.; Dumer, W. Improving prediction of hydraulic conductivity by constraining capillary bundle models to a maximum pore size. *Adv. Water Res.* **2015**, *85*, 86–92. [[CrossRef](#)]
119. Malama, B.; Kuhlman, K.L. Unsaturated hydraulic conductivity models based on truncated lognormal pore-size distributions. *Groundwater* **2015**, *53*, 498–502. [[CrossRef](#)] [[PubMed](#)]
120. White, J.; Zardava, K.; Nayagum, D.; Powrie, W. Functional relationships for the estimation of van Genuchten parameter values in landfill processes models. *Waste Manag.* **2015**, *38*, 222–231. [[CrossRef](#)] [[PubMed](#)]
121. Oh, S.; Kim, Y.K.; Kim, J.-W. A modified van Genuchten-Mualem Model of hydraulic conductivity in Korean Residual Soils. *Water* **2015**, *7*, 5487–5502. [[CrossRef](#)]
122. Seki, K.; Ackerer, P.; Lehmann, F. Sequential estimation of hydraulic parameters in layered soil using limited parameters. *Geoderma* **2015**, *247–248*, 117–128. [[CrossRef](#)]
123. Zhai, Q.; Rahardjo, H. Estimation of permeability function from the soil-water characteristic curve. *Eng. Geol.* **2015**, *199*, 148–155. [[CrossRef](#)]
124. Bevington, J.; Piragnolo, D.; Teatini, P.; Vellidis, G.; Morari, F. On the spatial variability of soil hydraulic properties in a Holocene coastal farmland. *Geoderma* **2016**, *262*, 294–305. [[CrossRef](#)]
125. Gilberg, M.R.; Seeley, N.J. The identity of compounds containing chloride ions in marine iron corrosion products: A critical review. *Stud. Conserv.* **1981**, *26*, 50–56. [[CrossRef](#)]
126. Sarin, P.; Snoeyink, V.; Lytie, D.; Kriven, W. Iron corrosion scales: Model for scale growth, iron release and coloured water formation. *J. Environ. Eng.* **2004**, *130*, 364–373. [[CrossRef](#)]
127. Foley, R.T. Role of chloride ion in iron corrosion. *Corrosion* **1970**, *26*, 58–70. [[CrossRef](#)]
128. Larroumet, D.; Greenfield, D. Raman spectroscopic studies of the corrosion of model iron electrodes in sodium chloride solution. *J. Raman Spectrosc.* **2007**, *38*, 1577–1585. [[CrossRef](#)]
129. Wang, Y.; Cheng, G.; Wu, W.; Qiao, Q.; Li, Y.; Li, X. Effect of pH and chloride on the micro-mechanism of pitting corrosion for high strength pipeline steel in aerated NaCl solutions. *Appl. Surf. Sci.* **2015**, *349*, 746–756. [[CrossRef](#)]
130. Nestic, S. Key issues related to the internal corrosion of oil and gas pipelines—A review. *Corros. Sci.* **2007**, *49*, 4308–4338. [[CrossRef](#)]
131. Perez, F.R.; Barrero, C.A.; Walker, A.R.H.; Garcia, K.E.; Nomura, K. Effects of chloride concentration, immersion time and steel composition on the spinel phase formation. *Mater. Chem. Phys.* **2009**, *117*, 214–223. [[CrossRef](#)]
132. Ray, R.I.; Lee, J.S.; Little, B.J. *Iron-Oxidizing Bacteria: A Review of Corrosion Mechanisms in Fresh Water and Marine Environment*; Paper 10218, NACE Corrosion 2010 Conference and Expo; Naval Research Laboratory, Office of Naval Research: Arlington, VA, USA, 2010.
133. Lide, D.R. *CRC Handbook of Chemistry and Physics 89th Edition 2008–2009*; CRC Press: Boca Raton, FL, USA, 2008.
134. Noubactep, C. Aqueous contaminant removal by metallic iron: Is the paradigm shifting? *Water SA* **2011**, *37*, 419–426. [[CrossRef](#)]

135. Noubactep, C. Designing metallic iron packed-beds for water treatment: A critical review. *Clean-Soil Air Water* **2016**, *44*, 411–421. [[CrossRef](#)]
136. Noubactep, C. Predicting the hydraulic conductivity of metallic iron filters: Modeling gone astray. *Water* **2016**, *8*, 162. [[CrossRef](#)]
137. Luo, P.; Bailey, E.H.; Mooney, S.J. Quantification of changes in zero valent iron morphology using X-ray computed tomography. *J. Environ. Sci.* **2013**, *25*, 2344–2351. [[CrossRef](#)]
138. Domga, R.; Togue-Kamga, F.; Noubactep, C.; Tchatchueng, J.-B. Discussing porosity loss of Fe⁰ packed water filters at ground level. *Chem. Eng. J.* **2015**, *263*, 127–134. [[CrossRef](#)]
139. Li, L.; Benson, C.H.; Lawson, E.M. Modelling porosity reductions caused by mineral fouling in continuous wall permeable reactive barriers. *J. Contam. Hydrol.* **2006**, *83*, 89–121. [[CrossRef](#)] [[PubMed](#)]
140. Btateku-K, B.D.; Olvera-Vargas, H.; Tchatchueng, J.B.; Noubactep, C.; Care, S. Determining the optimum Fe⁰ ratio for sustainable granular Fe⁰/sand water filters. *Chem. Eng. J.* **2014**, *247*, 265–274. [[CrossRef](#)]
141. Guan, X.; Sun, Y.; Qin, H.; Li, J.; Lo, I.M.C.; He, D.; Dong, H. The limitations of applying zero valent iron technology in contaminants sequestration and the corresponding countermeasures: The development in zero-valent iron technology in the last two decades (1994–2014). *Water Res.* **2015**, *75*, 224–248. [[CrossRef](#)] [[PubMed](#)]
142. Wilkin, R.T.; Puls, R.W.; Sewell, G.W. Long-term performance of permeable reactive barriers using zero valent iron: Geochemical and microbiological effects. *Groundwater* **2003**, *41*, 493–503. [[CrossRef](#)]
143. Slip, W.P.; England, M.H. The control of polar haloclines by along-Isopycnal diffusion in climate models. *J. Clim.* **2009**, *22*, 486–498.
144. Neuman, S.P.; Tartakovsky, D.M. Perspectives on theories of non-Fickian transport in heterogeneous media. *Adv. Water Resour.* **2009**, *32*, 670–680. [[CrossRef](#)]
145. Mackenzie, P.D.; Horney, D.P.; Sivavec, T.M. Mineral precipitation and porosity losses in granular iron columns. *J. Hazard. Mater.* **1999**, *68*, 1–17. [[CrossRef](#)]
146. Li, L.; Benson, C.H.; Lawson, E.M. Impact of mineral fouling on hydraulic behavior of permeable reactive barriers. *Groundwater* **2005**, *43*, 582–596. [[CrossRef](#)] [[PubMed](#)]
147. Chen, K.-F.; Li, S.; Zhang, W.-X. Renewable hydrogen generation by bimetallic zero valent iron nanoparticles. *Chem. Eng. J.* **2011**, *170*, 562–567. [[CrossRef](#)]
148. Bouniol, P. Influence of iron on water radiolysis in cement based materials. *J. Nucl. Mat.* **2010**, *403*, 167–183. [[CrossRef](#)]
149. Ruhl, A.S.; Jekel, M. Degassing, gas retention and release in Fe(0) permeable reactive barriers. *J. Cont. Hydrol.* **2014**, *159*, 11–19. [[CrossRef](#)] [[PubMed](#)]
150. Reardon, E.J. Capture and storage of hydrogen gas by zero valent iron. *J. Cont. Hydrol.* **2014**, *157*, 117–124. [[CrossRef](#)] [[PubMed](#)]
151. Da Silva, M.L.B.; Johnson, R.L.; Alvarez, P.J.J. Microbial characterization of groundwater undergoing treatment with a permeable reactive barrier. *Environ. Eng. Sci.* **2007**, *24*, 1122–1127. [[CrossRef](#)]
152. Xie, Y.; Dong, H.; Zeng, G.; Tang, L.; Jiang, Z.; Zhang, C.; Deng, J.; Zhang, L.; Zhang, Y. The interactions between nanoscale zero-valent iron and microbes in the subsurface environment: A review. *J. Hazard. Mater.* **2017**, *321*, 390–407. [[CrossRef](#)] [[PubMed](#)]
153. Lefere, E.; Bossa, N.; Wiesener, M.R.; Gunsch, C.K. A review of the environmental implications of in situ remediation by nanoscale zero valent iron (nZVI): Behavior, transport and impacts on microbial communities. *Sci. Total Environ.* **2016**, *565*, 889–901. [[CrossRef](#)] [[PubMed](#)]
154. Avillera, A.; Cid, M.; Petit, M.C. Anodic reaction of iron in transpassive range. *J. Electroanal. Chem.* **1979**, *105*, 149–160. [[CrossRef](#)]
155. Xia, L.; Zheng, X.; Shao, H.; Xin, J.; Sun, Z.; Wang, L. Effects of bacterial cells and two types of extracellular polymers on bioclogging of sand columns. *J. Hydrol.* **2016**, *535*, 293–300. [[CrossRef](#)]
156. SPE. *Guidelines for the Evaluation of Petroleum Reserves and Resources*; Society Petroleum Engineers: Richardson, TX, USA, 2001.
157. SPE. *Guidelines for Application of the Petroleum Resources Management System*; Society Petroleum Engineers: Richardson, TX, USA, 2011.

158. Etherington, J.; Pollen, T.; Zuccolo, L. Oil and Gas Reserves Committee (OGRC) Mapping subcommittee final report—December 2005. In *Comparison of Selected Reserves and Resource Classifications and Associated Definitions*; Society Petroleum Engineers: Richardson, TX, USA, 2005.
159. Lerche, I. *Oil Exploration Basin Analysis and Economics*; Academic Press: San Diego, CA, USA, 1992.
160. Gavaskar, A.; Tatar, L.; Condit, W. *Cost and Performance Report: Nanoscale Zero-Valent Iron Technologies for Source Remediation*; Contract Report CR-05-007-ENV; NAVFAC Naval Facilities Engineering Command, US Navy Engineering Services Center: Port Hueneme, CA, USA, 2005.
161. Gavaskar, A.; Bhargava, M.; Condit, W. *Cost and Performance Report for a Zero Valent Iron (ZVI) Treatability Study at Naval Air Station North Island*; Technical report TR-2307-ENV; NAVFAC Naval Facilities Engineering Command, US Navy Engineering Services Center: Port Hueneme, CA, USA, 2008.
162. Tosco, T.; Papini, M.P.; Viggì, C.C.; Sethi, R. Nanoscale zero valent iron particles for groundwater remediation: A review. *J. Clean. Prod.* **2014**, *77*, 10–21. [[CrossRef](#)]
163. Chowdhury, A.I.A.; Krol, M.M.; Kocur, C.M.; Boparai, H.K.; Weber, K.P.; Sleep, B.E.; O'Carroll, D.M. nZVI injection into variably saturated soils: Field and modeling study. *J. Contam. Hydrol.* **2015**, *183*, 16–28. [[CrossRef](#)] [[PubMed](#)]
164. Nemecek, J.; Pokomy, P.; Lacinova, L.; Cernik, M.; Masopustova, Z.; Lhotsky, O.; Filipova, A.; Cajthami, T. Combined abiotic and biotic in situ reduction of hexavalent chromium in groundwater using n-ZVI and whey: A remedial pilot test. *J. Hazard. Mater.* **2015**, *300*, 670–679. [[CrossRef](#)] [[PubMed](#)]
165. Kocur, C.M.D.; Lomheim, L.; Boparai, H.K.; Chowdhury, A.I.A.; Weber, K.P.; Austrins, L.M.; Edwards, E.A.; Sleep, B.E.; O'Carroll, D.M. Contributions of abiotic and biotic dechlorination following carboxymethyl cellulose stabilized nanoscale zero valent iron injection. *Environ. Sci. Technol.* **2015**, *49*, 8648–8656. [[CrossRef](#)] [[PubMed](#)]
166. Hatfield, K.; Klammer, H. The problem of flow bypass at permeable reactive barriers. *WIT Trans. Built Environ.* **2008**, *100*, 15–24.
167. Klammer, H.; Hatfield, K.; Kacimov, A. Analytical solutions for flow fields near drain and gate reactive barriers. *Ground Water* **2010**, *48*, 427–437.
168. Wanner, C.; Zink, S.; Eggenberger, U.; Mader, U. Unraveling the partial failure of a permeable reactive barrier using a multi-tracer experiment and Cr isotope measurements. *Appl. Geochem.* **2013**, *37*, 125–133. [[CrossRef](#)]
169. Field, R. *Chemical Engineering*; Macmillan: London, UK, 1988.
170. Carberry, J.J. *Chemical and Catalytic Reaction Engineering*; Dover: New York, NY, USA, 2001.
171. Misstear, B.; Banks, D.; Clark, L. *Water Wells and Boreholes*; John Wiley & Sons Ltd.: Chichester, UK, 2006.
172. Hill, C.G. *An Introduction to Chemical Engineering Kinetics & Reactor Design*; John Wiley and Sons: New York, NY, USA, 1977.
173. Hill, C.G.; Root, T.W. *An Introduction to Chemical Engineering Kinetics & Reactor Design*, 2nd ed.; John Wiley and Sons: New York, NY, USA, 2014.
174. Thakur, G.C.; Satter, A. *Integrated Waterflood Asset Management*; Penwell Books: Tulsa, OK, USA, 1998.
175. Baker, R. Reservoir management for waterfloods—Part II. *J. Can. Petrol. Technol.* **1998**, *37*, 12–17. [[CrossRef](#)]
176. Roldin, M.; Locatelli, L.; Mark, O.; Mikkelsen, P.S.; Binning, P.J. A simplified model of soakaway infiltration interaction with a shallow groundwater table. *J. Hydrol.* **2013**, *497*, 165–175. [[CrossRef](#)]
177. Roldin, M.; Fryd, O.; Jeppesen, J.; Mark, O.; Binning, P.J.; Mikkelsen, P.J.; Jensen, M.B. Modelling the impact of soakaway retrofits on combined sewage overflows in a 3 km² urban catchment in Copenhagen, Denmark. *J. Hydrol.* **2012**, *452–453*, 64–74. [[CrossRef](#)]
178. Roldin, M.; Mark, O.; Kuczera, G.; Mikkelsen, P.S.; Binning, P.J. Representing soakaways in a physically distributed urban drainage model—Upscaling individual allotments to an aggregated scale. *J. Hydrol.* **2012**, *414–415*, 530–538. [[CrossRef](#)]
179. Locatelli, L.; Gabriel, S.; Mark, O.; Mikkelsen, P.S.; Arbjerg-Nielsen, K.; Taylor, H.; Brockhorn, B.; Larsen, H.; Kjelby, M.J.; Blicher, A.S.; et al. Modelling the impact of retention-detention units on sewer surcharge and peak and annual runoff reduction. *Water Sci. Technol.* **2015**, *71*, 898–903. [[CrossRef](#)] [[PubMed](#)]
180. Roldin, M. *Distributed Models Coupling Soakaways, Urban Drainage and Groundwater*. Ph.D. Thesis, Technical University Denmark, Lyngby, Denmark, 2012.

181. Locatelli, L.; Mark, O.; Mikkelsen, P.S.; Arbjerg-Nielsen, K.; Wong, T.; Binning, P.J. Determining the extent of groundwater interference on the performance of infiltration trenches. *J. Hydrol.* **2015**, *529*, 1360–1372. [[CrossRef](#)]
182. Stumpp, C.; Ekdal, A.; Gonenc, I.E.; Maloszewski, P. Hydrological dynamics of water sources in a Mediterranean lagoon. *Hydrol. Earth Syst. Sci.* **2014**, *18*, 4825–4837. [[CrossRef](#)]
183. Strauch, G.; Oyarzun, J.; Fiebig-Wittmaack, M.; Gonzalez, E.; Weise, S.M. Contributions of the different water sources to the Elqui river runoff (northern Chile) evaluated by H/O isotopes. *Isotopes Environ. Health Stud.* **2006**, *42*, 303–322. [[CrossRef](#)] [[PubMed](#)]
184. Dinar, A.; Zilberman, D. *Economics of Water Resources: The Contributions of Dan Yaron*; Springer Science + Business Media: New York, NY, USA, 2002.
185. BGS and PHE. *Arsenic Contamination of Groundwater in Bangladesh; Phase 2, Groundwater flow Modeling*; Kinniburgh, D.G., Smedley, P.L., Eds.; British Geological Survey Technical Report WC/00/19; British Geological Survey: Keyworth, UK, 2001.



© 2016 by the author; licensee MDPI, Basel, Switzerland. This article is an open access article distributed under the terms and conditions of the Creative Commons Attribution (CC-BY) license (<http://creativecommons.org/licenses/by/4.0/>).